# Experimental Analysis of Scour Depth Around Eccentric Circular Piers Under Constant Flow Conditions

*A thesis submitted towards partial fulfilment of the requirements for the degree of*

**Master of Engineering**

*in*

**Water Resources and Hydraulic Engineering**

*Submitted by*


## BINOY BANIK

**Exam. Roll No. – M4WRE24004**

**Registration No. – 163857 of 2022-23**


***Under the guidance of***


**Dr. RAJIB DAS**

**Assistant Professor**

**School of Water Resources Engineering, Jadavpur University**

**&**

**Dr. SUBHASISH DAS**

**Associate Professor and Joint Director**

**School of Water Resources Engineering, Jadavpur University**



**School of Water Resources Engineering**

*M.E. (Water Resources & Hydraulic Engineering)*

*Course affiliated to **Faculty Council of Engineering & Technology***

**Jadavpur University**

Kolkata-700032, West Bengal, India

**2024**

## Declaration of Originality and Compliance of Academic Ethics

I hereby declare that this thesis contains a literature survey and original research work by the undersigned candidate, as part of my **Master of Engineering** in **Water Resources and Hydraulic Engineering** in the Faculty Council of Interdisciplinary Studies, Law & Management, Jadavpur University during the academic session 2023-24.

All information in this document have been obtained and presented in accordance with academic rules and ethical conduct.

I also declare that, as required by these rules and conduct, I have fully cited and referenced all material and results that are not original to this work.

| | | |
|---|---|---|
| **Name** | : | **BINOY BANIK** |
| **Exam Roll Number** | : | **M4WRE24004** |
| **Thesis Title** | : | **Experimental Analysis of Scour Depth Around Eccentric Circular Piers Under Constant Flow Conditions** |
| **Signature with Date** | : | |

**M.E. (Water Resources & Hydraulic Engg.) course affiliated to**
**Faculty Council of Engineering & Technology**
**Jadavpur University**
Kolkata, India

# *Certificate of Recommendation*

This is to certify that the thesis entitled "***Experimental Analysis of Scour Depth Around Eccentric Circular Piers Under Constant Flow Conditions***" is a bonafide work carried out by **Shri. Binoy Banik** under our supervision and guidance for partial fulfilment of the requirement for the Post Graduate Degree of Master of Engineering in Water Resources and Hydraulic Engineering during the academic session 2023-24.

**THESIS ADVISOR**
**Dr. Rajib Das**
**Assistant Professor**
**School of Water Resources Engineering**
**Jadavpur University**

**THESIS ADVISOR**
**Dr. Subhasish Das**
**Associate Professor and Joint Director**
**School of Water Resources Engineering**
**Jadavpur University**

**DIRECTOR**
**Prof. (Dr.) Asis Mazumdar**
**School of Water Resources Engineering**
**Jadavpur University**

**DEAN**
**Prof. (Dr.) Joydeep Mukherjee**
**Faculty Council of Interdisciplinary Studies, Law & Management**
**Jadavpur University**

**M.E. (Water Resources & Hydraulic Engg.) course affiliated to**
**Faculty Council of Engineering & Technology**
**Jadavpur University**
Kolkata, India

## CERTIFICATE OF APPROVAL **

This foregoing thesis is hereby approved as a credible study of an engineering subject carried out and presented in a manner satisfactory to warrant its acceptance as a prerequisite to the degree for which it has been submitted. It is understood that by this approval the undersigned do not endorse or approve any statement made or opinion expressed or conclusion drawn therein but approve the thesis only for the purpose for which it has been submitted.

**Committee of**
**Final Examination**
**for the evaluation**
**of the thesis**

** Only in case the thesis is approved.

# ACKNOWLEDGEMENTS

*I express my sincere gratitude to my supervisors,* ***Dr. Rajib Das****, Assistant Professor, and* ***Dr. Subhasish Das****, Associate Professor and Joint Director, School of Water Resources Engineering, Jadavpur University, under whose supervision and guidance this work has been carried out. It would have been impossible to carry out this thesis work with confidence without their wholehearted involvement, advice, support and constant encouragement throughout. They have not only helped me in carrying out my thesis but also have given me valuable advice to proceed further in my life.*

*I would also express my sincere gratitude to* ***Prof. (Dr.) Asis Mazumdar****, Director,* ***Prof. (Dr.) Arunabha Majumder****, Emeritus Professor;* ***Prof. (Dr). Pankaj Kumar Roy*** *and* ***Dr. Gourab Banerjee,*** *Faculty members of the School of Water Resources Engineering, Jadavpur University for their continuous encouragement and valuable suggestions.*

*I also express my sincere thanks to* ***Mr. Buddhadev Nandi, Mr. Plabon Sen, Mr. Tanmoy Das and Mr. Saikat Mondal*** *Research Scholar; of the School of Water Resources Engineering, Jadavpur University for their unconditional support and affection during my work. Also, thanks to my classmates* ***Ms. Tryasa Roy, Ms. Shubhashree Laha, Ms. Purbi Ali,*** *and* ***Ms. Tania Sultana*** *for their help.*

*Thanks, are also due to all staff of the School of Water Resources Engineering and the* ***Regional -cum-Facilitation Centre (RCFC), NMPB, Jadavpur University*** *for their help and support.*

**Date : 30 August, 2024**

**Place : Jadavpur University**

**Mr. Binoy Banik**
**(Exam. Roll No: M4WRE24004)**

# ABSTRACT

Scouring by the flow of water in rivers and streams has the greatest impact on alluvial materials beds, but solid rock can also be vulnerable in some cases in mountains stretches of the river. Bridge collapses are a widespread occurrence that causes fatalities, property damage, and halts transportation due to this hydraulic phenomenon called scour. As a result, bridge designers and technician must increasingly understand how soil, water flow, and bridge structures interact. Mostly in the growing cities around the world, traffic load increases, rapidly and more bridges are needed beside the existing one to connect roads and manage traffic. In recent years, researchers have been also studying how to use the natural process of scour to their advantage. They have explored the idea of dredging, which is a method that allows water to naturally move sediments to the sides of channels, without using machines. This process can reduce costs and environmental impact, while still helping to maintain water channels. This study looks into how bridge piers can affect the way water flows and causes erosion around them, especially when the piers are placed in different positions. Understanding how deep the water can dig around these piers, called scour depth, is important to keep bridges safe. The research focuses on how different pier layouts affect the movement of water and erosion. In a controlled environment, we studied how the water erodes and deposits sediment around both front piers and eccentric center piers over time. A total of 24 experiments were carried out using two identical circular bridge piers, each 7 cm in diameter. The distance between the upstream and off-center piers was kept the same, set at 5.185 times the diameter of pier. During the experiments, a steady water flow rate of 30 liters per second was maintained to ensure clear water conditions. The experiments lasted between 2.5 to 10 hours, depending on the specific setup, to observe how the scour changed over time. Various measurements, including the depth, width, length, area, and volume of the scour, were carefully calculated using the data from the experiments. The results were then carefully analysed to determine the most optimal eccentricity arrangement, which is an important issue for bridge designers and dredging professionals looking to improve their procedures. In conclusion, this study investigates the complex dynamics of scouring in connection to bridge design and sediment control. It highlights the potential benefits of using natural scouring processes to relocate sediments gives valuable insights for specialists in this field. Through experimental methods and in-depth research allow for a better understanding of how bridge structures interact with their aquatic environments, resulting in the development of more durable and sustainable infrastructure solutions.

# CONTENT


| Chapter No. | Topics | Page No. |
|---|---|---|
| | Declaration | iii |
| | Certificate of Recommendation | v |
| | CERTIFICATE OF APPROVAL | vii |
| | ACKNOWLEDGEMENTS | ix |
| | ABSTRACT | xi |
| | CONTENT | xiii-xiv |
| | NOTATIONS | xv-xvi |
| **Chapter 1** | | |
| | 1.1 Introduction | 1-2 |
| | 1.2 Scouring around piers | 2 |
| | 1.3 Classification of scour | 2-3 |
| | 1.4 Local scour | 3-4 |
| **Chapter 2** | | |
| | 2.1 Literature Review | 5-11 |
| **Chapter 3** | | |
| | 3.1 Local scour mechanism | 12 |
| | 3.2 Horseshoe vortex and downflow | 12-13 |
| | 3.3 Wake vortex | 13-14 |
| | 3.4 Classification of scour parameters | 14-16 |
| | 3.4.1 Flow intensity | 14 |
| | 3.4.2 Flow depth | 14 |
| | 3.4.3 Pier width | 14-15 |
| | 3.4.4 Pier Shape | 15 |
| | 3.4.5 Sediment Size | 15-16 |
| | 3.4.6 Flow Froude Number | 16 |
| | 3.5 Angle of repose | 16-17 |
| **Chapter 4** | | |
| | 4.1 Objectives | 18 |
| | 4.2 Methodology | 19-20 |
| **Chapter 5** | | |
| | 5.1 Experimental setup | 21-24 |
| | 5.1.1 Tilting Flume | 21-22 |
| | 5.1.2 Pump | 22 |
| | 5.1.3 Pier | 22-23 |
| | 5.1.4 Sand Bed | 23-24 |
| | 5.2 Experimental procedure | 24-25 |
| **Chapter 6** | | |
| | 6.1 Results and Discussion | 26-49 |
| | 6.1.1 Experiment No. 1 | 27 |
| | 6.1.2 Experiment No. 2 | 28 |
| | 6.1.3 Experiment No. 3 | 28-29 |
| | 6.1.4 Experiment No. 4 | 29-30 |
| | 6.1.5 Experiment No. 5 | 30-31 |
| | 6.1.6 Experiment No. 6 | 31 |
| | 6.1.7 Experiment No. 7 | 31-32 |
| | 6.1.8 Experiment No. 8 | 32-33 |
| | 6.1.9 Experiment No. 9 | 33-34 |

6.1.10 Experiment No. 10 34-35
6.1.11 Experiment No. 11 35
6.1.12 Experiment No. 12 35-36
6.1.13 Experiment No. 13 36-37
6.1.14 Experiment No. 14 37-38
6.1.15 Experiment No. 15 38
6.1.16 Experiment No. 16 38-39
6.1.17 Experiment No. 17 39-40
6.1.18 Experiment No. 18 40-41
6.1.19 Experiment No. 19 41
6.1.20 Experiment No. 20 41-42
6.1.21 Experiment No. 21 42-43
6.1.22 Experiment No. 22 43-44
6.1.23 Experiment No. 23 44
6.1.24 Experiment No. 24 44-45
6.1.25 Experimental outcomes 45-46
6.1.26 Comparison of maximum scour depths 46
6.1.27 Temporal evolution of scour depth 47
6.1.28 Comparison of surface area with eccentricity 47-48
6.1.29 Comparison of volume with eccentricity 48
6.1.30 Comparison of width with eccentricity 48-49
6.1.31 Comparison of length with eccentricity 49

**Chapter 7**

7.1 Conclusions 50
7.2 Future scope of the study 51

**References** 52-55

# NOTATIONS

The following symbols are used in this dissertation work:

| | | |
|---|---|---|
| $A$ | = | ($hB$) Cross-sectional area of flow [$L^2$]; |
| $a_{ps}$ | = | Planar area of scour [$L^2$]; |
| $a_{ss}$ | = | Surface area of scour [$L^2$]; |
| $a_s$ | = | Scour area [$L^2$]; |
| $b$ | = | Pier diameter [L]; |
| $B$ | = | Width of the tilting flume [L]; |
| $d_e$ | = | Eccentric pier scour depth [L]; |
| $d_{sf}$ | = | Scour depth at front pier [L]: |
| $d_{se}$ | = | Scour depth at eccentric pier [L]; |
| $d_{16}$ | = | 16% finer sand diameter [L]; |
| $d_{50}$ | = | Median diameter of sand [L]; |
| $d_{84}$ | = | 84% finer sand diameter [L]; |
| $d_{90}$ | = | 90% finer sand diameter [L]; |
| $F_r$ | = | Froude number of flow [—]; |
| $g$ | = | Gravitational acceleration [$LT^{-2}$]; |
| $h$ | = | Approaching flow depth [L]; |
| $l_s$ | = | Scour length [L]; |
| $n$ | = | Manning's coefficient of roughness [—]; |
| $Q$ | = | Inlet discharge [$L^3T^{-1}$]; |
| $R_e$ | = | $\left(\frac{UH}{\nu}\right)$ Flow Reynolds number [—]; |
| $R_{e_c}$ | = | $\left(\frac{u_{*_c}R}{\nu}\right)$ Critical shear flow Reynolds number [—]; |
| $R_p$ | = | $\left(\frac{Ub}{\nu}\right)$ Pier Reynolds number [—]; |
| $e$ | = | Eccentricity [L]; |
| $S_0$ | = | Bed slope [—]; |
| $u$ | = | Depth-averaged approaching flow velocity [$LT^{-1}$]; |
| $u_c$ | = | Critical velocity [$LT^{-1}$]; |
| $u_*$ | = | Shear velocity [$LT^{-1}$]; |
| $u_{*_c}$ | = | Critical shear velocity [$LT^{-1}$]; |
| $V_s$ | = | Volume of scour [$L^3$]; |
| $w_s$ | = | Scour width [L]; |

| | | |
|---|---|---|
| $\rho_f$ | = | Mass density of fluid [$ML^{-3}$]; |
| $\rho_s$ | = | Mass density of sand [$ML^{-3}$]; |
| $\gamma_f$ | = | Specific weight of fluid [$ML^{-2}T^{-2}$]; |
| $\tau_o$ | = | Average bed shear stress [$ML^{-1}T^{-2}$]; |
| $\tau_{oc}$ | = | Critical bed shear stress [$ML^{-1}T^{-2}$]; |
| $\sigma_g$ | = | Geometric standard deviation [—]; |
| $\nu$ | = | Kinematic viscosity [$L^2T^{-1}$]; |
| $\varphi_r$ | = | Dynamic angle of repose [—]; |
| $\Theta_c$ | = | Critical Shields parameter [—]; |
| $t$ | = | Time [T]; |

# Chapter 1

## 1.1 Introduction

Scour is a natural phenomenon generated by rushing water's erosive impact on the beds and banks of alluvial rivers. Scour, in other terms, is the erosion of streambed silt around a barrier in a flow field. Cheremisinoff *et al.* (1987) defined scour as the lowering of the river bed due to water erosion, which has the potential to expose the foundations of structures such as bridges. Scour was characterized by Breusers *et al.* (1977) as a natural phenomenon created by the movement of water in rivers and streams. The scouring mechanism may endanger the structural integrity of hydraulic structures including bridges. When the foundation of the structures is compromised, this might lead to ultimate failure. A succession of bridge failures during floods caused by pier scour has highlighted the significance of developing better methods of protecting bridges from the ravages of scour. Bridge construction in alluvial channels causes the waterway at the bridge site to constrict. The waterway's shrinking could produce substantial scour at that location. According to Hoffmans and Verheij (1997), local scour around bridge piers and foundations caused by flood flows is the leading cause of bridge failure. Among those who have worked on pier scour are Raudkivi and Ettema (1983), Ahmed and Rajaratnam (1998), Chiew and Melville (1987), and Breusers *et al.* (1977). In their laboratory investigation on flow past cylindrical piers set on smooth, bumpy, and movable beds, Ahmed and Rajaratnam (1998) evaluated the flow around bridge piers. Jia *et al.* (2002) performed a numerical modelling study to simulate the time-dependent scour development around a cylindrical pier built on a loose substrate in an open channel. Link and Zanke (2004) investigated the time-dependent development of scour-hole volume at a circular pier in uniform coarse sand and produced a mathematical link between the scour volume and the maximum scour depth for water depth to pier diameter ratios ranging from one to two. However, just as scour depth is crucial in scour research, so is the time taken to reach a specific scour depth because scour holes take time to form. As a result, it is vital to comprehend the evolution of the local scour hole over time.

Every year, numerous bridges fail, resulting in the loss of lives and property as well as some uncomfortable circumstances for transportation systems. The potential losses from bridge failures, as well as the necessity to protect against them, have encouraged a greater knowledge of the scour process, as well as improved scour prediction methods and equations. Under-prediction of pier scour depth can result in bridge failure, whereas over-prediction results in excessive resource spending in terms of building expenses. Because of this, bridge designers are increasingly considering the flow-soil-structure interaction. Achieving the safest design in light of local and regional characteristics is the most crucial factor to take into account at this stage. This is typically based on calculations of the maximum scour depth at bridge structural components and the geometrical features of the scour hole surrounding them.

The flow conditions, sediment characteristics, structure characteristics, and scouring duration are the main factors affecting the scour and deposition around the structure. As the number of structures in a river increases, the interaction between the structures will have a

stronger impact on the surrounding bed profile. Local scour can be classified as "clear-water scour" or "live-bed scour." In clear water scour, bed materials are removed from the scour hole but not replenished by the approach flow, whereas in live-bed scour, the scour hole is constantly supplied with sediment by the approach flow and an equilibrium is reached when the average amount of sediment transported into the scour hole by the approach flow equals the average amount of sediment removed from the scour hole over time. Under these conditions, the local scour depth changes around a mean value on a regular basis. The interplay of flow around a bridge pier and the erodible sediment substrate surrounding is quite complex.

In this study, the scour characteristics around two circular piers- placed eccentrically to each other were investigated. All the experiments were carried out in an experimental channel at the Fluvial Hydraulics Laboratory of the School of Water Resources Engineering, Jadavpur University. The study was confined to uniform cohesion less material and clear-water flow conditions.

## 1.2 Scouring around piers

Scouring is a natural phenomenon generated by the passage of water in a river or stream. It is most noticeable in alluvial materials, but the severely worn rock can also be vulnerable under specific conditions. It is caused by the erosive action of flowing water, which dissolves and erodes material from the stream bed and banks, as well as the vicinity of bridge piers and abutments. Scouring happens naturally as a result of river morphology changes and as a result of man-made structures. The following are the primary causes of scour:

(1) Depth of flow
(2) Pier width
(3) Velocity
(4) Froude number
(5) Bed materials

One of the primary reasons for bridge failure is scour. The scour destroys the bed materials around the bridge's foundation, exposing the foundation and jeopardizing the bridge's stability.

## 1.3 Classification of scour

Regardless of whether a structure is present, general scour happens in a river or stream as a result of natural processes. Man-made buildings or any other hazard may also induce scour in the river bed. Scour is divided into two types: (a) widespread scour and (b) localized scour. In addition, further sub-divisions of scour are depicted in Fig. 1.1.

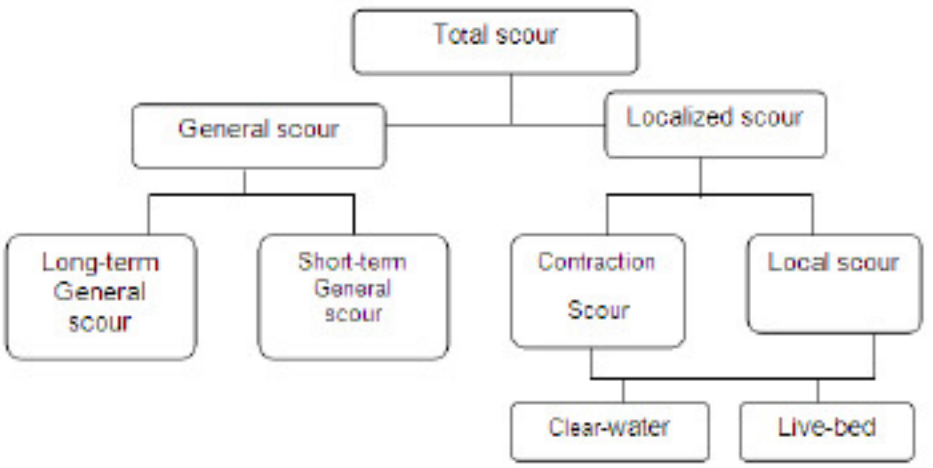



**Fig. 1.1** Types of scour

## 1.4 Local scour

Local scour is the erosion that takes place close to a pier, an abutment, an erosion control device, or another obstruction to the flow. These impediments speed up the flow and produce vortices that sweep the surrounding sediments away. Local scour depths are typically ten times greater than general or contraction scour depths in most cases. Local scour can cause failures by impairing the stability of riprap revetments and other structures. The following variables influence local scour:

[1] Width of the obstruction.
[2] Projection length of the obstruction into the flow.
[3] Length of the obstruction.
[4] Angle of the approach flow
[5] Velocity of the approach flow
[6] Size of the bed material.
[7] Depth of flow.
[8] Shape of the obstruction.
[9] Bed configuration.

The depth of the scour is directly dependent on the width of the obstruction. Thus, the wider the obstruction, the deeper is the scour. Though not addressed by most empirical relations, the ratio of obstruction width to channel width is probably a better measure of scour potential than is the obstruction width alone. The projected length of obstruction into the stream affects the depth of the scour. With an increase in the projected length of an abutment into the flow, there is an increase in scour.



**Fig. 1.2** Local scour around two eccentric piers.

The depth of the scour can increase with length, but only to a certain point. When the ratio of the projected length of the stream to the depth of the approaching flow is approximately 30 l/s. For straight sections, a structure's streamwise length has no discernible impact on the scour depth; however, when the structure is at an angle to the flow, the length has a significant impact. When a structure's length is doubled, the scour depth rises by as much as 33% at the same angle of attack. Some equations incorporate the length factor by using the ratio of the structure's length to the flow's depth or width as well as the flow's angle of attack on the structure. Others incorporate flow in their equations using the projected area of the structure.

The scour depth can rise by a factor of 2 or more with an increase in flow depth. Depending on the shape of the abutment, the increase for bridge abutments ranges from 1.1 to 2.15. Along with the approach flow's velocity, scour depth also rises. Although the effect is typically a function of the time exposed to erosive flows, the size of the bed material affects scour depth. In other words, only the time it takes to reach the maximum or ultimate scour may be impacted by sediment size. Large particles in the bed material, like boulders or cobbles, may armour the scour hole's plate.

Local scour is greatly influenced by the shape of the structure as well as the flow's angle of attack on an obstruction. Structures that are angled to cause flow convergence tend to increase scour, whereas structures that are angled to cause flow divergence tend to reduce scour. Streamlined structures effectively lower ultimate scour depths by weakening the horseshoe and wake vortices. The shape of the bed (bed configuration) in streams with sand beds influences the flow velocity and turbulence, which in turn influences the depth of the scour. Both the local and global (contraction) scour can be accelerated by ice and debris. The extent of the growth is still largely unknown.

# Chapter 2

## 2.1 Literature Review

The depth of the channel bed that is scouring by flowing water in a steady condition when the rate of sediment deposition and transport is equal is referred to as the "equilibrium scour depth". The flow velocity, the kind of sediment, and the channel design are some of the factors that determine the scour depth that the channel bed reaches. We will examine a few studies that examined the time it takes for equilibrium to establish in relation to scour depth in this review of the literature.

Many experimental studies have been conducted by researchers to better understand the scour process at bridge piers and abutments since the 1950s. To anticipate scour, a great deal of research has been done, and a great deal of researchers have generated a great number of equations, including Das et al. (2014), Das et al. (2014), Das et al. (2015a), Das et al. (2016), Das and Mazumdar (2015), Das et al. (2015b), Kuila et al (2020) etc.

**Melville (1975)** [also see Melville and Raudkivi (1977)] was the pioneer to measure the turbulent flow field within a scour hole at a circular pier with the aid of the DISA Hot-Film Anemometer. The flow patterns were traced using the hydrogen-bubble method. He measured the flow field in the upstream axis of symmetry and the near-bed turbulence intensity for the case of a flat bed, intermediate, and equilibrium scour hole. He also estimated the bed-shear stresses from the measured near-bed velocities. A design method for the estimation of scour at cylindrical piers was presented by Melville *et al.* (1987). The method was based upon envelope curves drawn to experimental data derived mostly from laboratory experiments.

**Melville and Sutherland (1988)** presented a design method for the estimation of equilibrium depths of local scour at bridge piers. The method was based upon envelope curves drawn to experimental data derived mostly from laboratory experiments. The laboratory data included wide variations in flow velocity and depth, sediment size and gradation, and pier size, shape, and alignment. Local scour depth estimation was based upon the largest possible scour depth that can occur at a cylindrical pier, which was $2.4b$, where $b$ is the pier width. According to the method, this depth was reduced using multiplying factors where clear-water scour conditions exist, the flow depth was relatively shallow, and the sediment size was relatively coarse. In the case of nonrectangular piers, additional multiplying factors to account for pier shape and alignment were applied. The method of estimation of local scour depth was summarized in a flow chart.

**Dargahi (1990)** presented an extensive study containing the temporal evolution of the main flow features around circular bridge piers placed in a fixed sediment bed. He also visualized the flow field using air bubbles. Additionally, the bed shear stresses were measured with a Preston tube. Dargahi observed the simultaneous presence of various horseshoe vortices upstream of the leading pier front.

Breusers and Raudkivi (1991) found that reduction of scour depth due to a foundation located at an appropriate level below the initial bed level, should not be reposed on unless: Definite foretelling of bed level is possible, because the level of the river bed can go down extraordinarily during a flood in a particular spread of the river, or the place of the pier may correspond with that of a moving stream channel in the cross-section.

**Kothyari et al. (1992a, b)** discussed in a paper about scour depth. Since the scour depth was needed for the economical design of the pier foundation and determination of design scour depth was mainly based on the use of relationships for maximum scour depth in steady flow along with the design discharge. The time taken by the design discharge to scour to its full potential was generally larger than the time for which it runs. Hence, the computation of temporal variation of scour depth should form the basis of the design. Experiments were conducted on temporal variation of scour around circular bridge piers placed in uniform, non-uniform, and stratified beds under steady and unsteady clear-water flows. Considering the primary vortex in front of the pier to be the prime agent causing scour, a procedure was developed for computing the temporal variation of scour depth under these conditions. Since the maximum scour depth was the scour depth at a large time, the procedure was logically extended to obtain an expression for the same. Sediment nonuniformity and stratification were shown to have a significant effect on scour depth. The effect of these elements as well as that of unsteadiness of flow on scour depth are studied and taken into account in the proposed method of scour calculations.

**Melville and Chiew (1999)** conducted laboratory studies to determine how long it takes for a scour hole to establish equilibrium around circular piers under different flow conditions. The study found that the time scale of scour was related to the square of the pier diameter and sediment size, but inversely proportional to flow velocity and sediment density. The authors' theoretical model, based on the balance of forces acting on sediment particles, was shown to be consistent with experimental observations. Melville and Chiew (1999), Ettema (1980), and Graf (1995) proposed an equation based on 84 datasets from several flume studies. Predictions of equilibrium time by this formula result in values of Mean Absolute Percent Errors (MAPE) 231%.

**Mia and Nago (2003)** suggested an approach that considers sediment movement and flow conditions over time, which are key elements in the formation of local scour. The suggested design method accurately predicted time dependent scour depth around circular piers, as proven by experimental data. The suggested method outperformed existing design methods, particularly in predicting longterm scour depth. The suggested method outperformed existing design methods, particularly in predicting long-term scour depth.

**Barbhuiya and Dey (2004)** obtained similar results from a semicircular pier arrangement placed at the channel sidewall. The vortex size, vortex velocity and vortex strength were determined in terms of the relevant hydraulic and geometric parameters and the temporal scour hole evolution. These flow features govern the scour advance. In contrast to most other studies, a generalized approach was selected to determine the velocity distribution. The knowledge of these coherent plane flow structures allows for estimating the acting bed-shear stresses, a topic dealt with in a forthcoming study.

**Marsh et al. (2004)** presented a comparison of four methods for predicting the incipient motion conditions of a uniform sand bed. The four methods are (1) the Shields diagram, (2) an empirical approach, (3) a method derived from the resolution of rotational forces and (4) a simplified resolution of rotational forces with a variable lift force coefficient. The four methods were used to predict the incipient motion conditions for 97 experimental runs taken from seven independent experimental flume studies. The effectiveness of predicting depth averaged incipient motion velocity for each of the four methods was compared. The simplified resolution of the rotational forces model and Shields method were most successful in predicting the incipient motion velocity. The slope of the line of best fit for plots illustrating predicted versus measured incipient motion velocity was similar (slope = 0.63, 0.65, respectively), illustrating that both methods provide a similarly justifiable prediction of depth averaged incipient motion. The empirical method was the least successful at predicting the measured incipient motion conditions.

**Dey and Barbhuiya (2005)** stated a semi empirical model that presented to compute the time variation of scour depth in an evolving scour hole at short abutments (abutment length/flow depth ≤1), namely the vertical wall, 45° wing wall, and semicircular, in uniform and non-uniform sediments under clear water scour condition based on the concept of the conservation of the mass of sediment, considering the primary vortex system as the main agent of scouring, and assuming a layer-by-layer scouring process. Experiments were conducted for time variation and equilibrium scour depths at different sizes of vertical walls, 45° wing walls and semicircular abutments in uniform and no uniform sediments under limiting clear water scour conditions.

**Dey and Raikar (2005)** derived an expression to estimate clear-water scour depth at circular and square piers, embedded in a sand bed overlain by a thin armour layer of gravel, which was experimentally studied. Depending on the pier width, flow depth, armour gravel, and bed-sand sizes, three cases of scour holes at piers in armoured beds were recognized. A comparison of the experimental data shows that the scour depth at a pier with an armour layer under limiting the stability of the surface particles was greater than that without an armour layer for the same bed sediments if the secondary armouring formed within the scour hole is scattered. The equations of maximum equilibrium scour depths at piers in armoured beds for these cases were proposed. On the other hand, the scour depth with an armour layer was less than that without an armour layer for the same bed sediments when the scour hole was shielded by the compact secondary armour layer.

**Das et al. (2014)** conducted experiment about the flow pattern and characteristics of a local equilibrium scour around two identically shaped equilateral triangular piers facing the approaching flow. The piers were placed longitudinally with an eccentricity (transverse distance).

**MALIK and SETIA (2014)** ran an experiment about an experimental study on the behaviour of closely placed bridge and pier models. The study was done on a mobile bed with average sediment size ($d_{50}$ = 0.18mm) and pier models of diameter 50mm apiece. The piers

were tested in two orientations: side by side and tandem. Bridge piers in close proximity can interfere with one other's scour behaviour, regardless of orientation. In tandem arrangements, the two pier models can affect each other up to eight times the pier's circumference. The study found that when the pier spacing is 1.5D, the models behave independently in a side-by-side pattern. The presence of one pier does not impact the scour of the other. In tandem arrangement, piers can cause scouring up to eight times their diameter.

**Da et al (2015)** also conducted an experimental investigation on the flow pattern and characteristics of a local equilibrium scour around a series of identical circular piers arranged eccentrically. In the equilibrium condition of a single pier, the eccentricity and longitudinal spacing were three times the pier width and 0.5 times the scour-affected length, respectively. The maximum scour depth at the eccentric back pier was approximately 44% larger than in the single pier instance. In addition, the maximum depth of the scour hole upstream of the inline front pier was approximately 29% more than that of the single pier scenario.

**Das and Mazumdar (2015)** conducted an experimental study to examine the horse-shoe vortex and flow characteristics in a local equilibrium scour hole around two identical cylindrical piers positioned eccentrically along the flow. They concluded that the formation of a greater scour depth at the eccentric rear pier is significantly influenced by the eccentric arrangement of the piers.

**Da et al (2016)** conducted 19 clear water scour experiments to find the equilibrium scour geometry of two circular, square, and equilateral triangle piers arranged in-line front and eccentric rear. The eccentricity was kept constant while the longitudinal spacing (l) varied from 0.25 to 0.75 times the maximum equilibrium scour-affected length for a single-pier test (L). At l = 0.75L, the maximum scour depth at the eccentric rear pier is approximately 45-60% more than that in the single-pier scenario. Furthermore, the maximum depth of the scour hole upstream of the in-line front pier is approximately 35% greater than in the single-pier situation. This could be due to the reinforcement of the scour mechanism. The eccentric pier was found to have a higher diversion angle and deposition rate.

**Das et al. (2016)** conducted 19 clear water scour experiments to find the equilibrium scour geometry of two circulars, square, and equilateral triangle piers arranged in-line front and eccentric rear. The eccentricity was kept constant while the longitudinal spacing (l) varied from 0.25 to 0.75 times the maximum equilibrium scour-affected length for a single-pier test (L). At l = 0.75L, the maximum scour depth at the eccentric rear pier is approximately 45-60% more than that in the single-pier scenario. Furthermore, the maximum depth of the scour hole upstream of the in-line front pier is approximately 35% greater than in the single-pier situation. This could be due to the reinforcement of the scour mechanism. The eccentric pier was found to have a higher diversion angle and deposition rate.

**Wang et al (2016)** laboratory investigations were conducted to assess local scouring around twin cylindrical piers in open-channel flows. Experiments with clear-water scouring around twin piers revealed that the scour hole generated around the upstream pier at varying

pier spacings was nearly identical to that around an isolated pier. The study revealed experimental findings on local scouring around twin piers in open-channel flows. The scour depth around the upstream pier was comparable to that around a single pier under the same flow conditions. Scouring depth surrounding the downstream pier might grow in two stages over time. The downstream pier's scour depth varied with flow speed, resulting in four distinct regions: no-scour, synchronous-scouring, transition, and radical divergence.

**Jaman et al. (2017a, b)** conducted experiments at a clear water equilibrium scour condition to measure flow formations in local scour holes around three identical circular shaped piers arranged inline and eccentrically in staggering manners. Two inline piers were positioned toward flow, and an eccentric one was placed in the middle region of the two inline piers. The experiments were done for an approach flow depth of 0.125 m on the uniform bed of sand particles having a 0.825 mm median diameter. The hydrodynamic consequences of the three-pier arrangement on scour were investigated here. The contour profiles of the scour were well addressed around the piers. The maximum equilibrium depth of all scour holes gauged for inline front, eccentric-middle and inline-rear piers were about 40, 61 and 15% larger than the depth for one single-pier experiment. Also, these depths at inline-front, eccentric-middle and inline rear piers were more than two pier cases with the inline front eccentric rear arrangement. The dune formation was found more on the side of the eccentric pier (away from the line of symmetry). The diversion angle for sediment shifting was found to be more on the side of the eccentric pier.

**Khaple et al. (2017)** presented three kinds of pier arrangement - (i) two piers in tandem, (ii) two piers in a staggered arrangement, and (iii) three piers in symmetrically staggered arrangements. In the arrangement of two piers in tandem, the equilibrium scour depth at the downstream pier decreased with an increase in the downstream distance up to approximately eight times the pier diameter and then increased with a further increase in downstream distance. However, the scour depth at the downstream pier was always smaller than that at the upstream pier. In the arrangement of two staggered piers, the scour depth at the downstream pier for $e/b = 4$, where $e$ is the offset distance and $b$ is the pier diameter, was the same as that of the upstream pier at $S = 8b$, where $S$ is the stream-wise spacing or distance between piers. Further, for three piers in a staggered arrangement, as the lateral spacing between downstream piers increased, the equilibrium scour depth at the downstream pier decreased.

**Yilmaz et al. (2017)** conduct experiment about clear-water scour evolution at dual bridge piers. A semi-empirical model is used to predict the temporal fluctuation of clear-water scour depth at two identical cylindrical uniform piers in tandem configuration. Experiments are conducted with varying pier sizes, spacing, and flow intensities. The model is developed utilizing a sediment continuity technique and a volumetric sediment transport rate from the scour hole via a sediment pickup function. The model findings are presented as design charts that show the relationship between dimensionless scour depth and time for practical applications. The proposed model's results align well with the experimental results within the tested range. The studies were conducted using uniformly graded bed material with a median

size of 0.88 mm. The studies used piers with diameters of 7.5, 6.3, and 4.0 cm and spacing ratios of 0.50, 0.33, and 0.25, respectively. Experiments revealed that the shape of the scour hole at the front pier remained relatively stable over time. Design charts were created to illustrate the relationship between dimensionless scour depth and time. The predicted scour depths closely matched the experimental results within the tested range. The selected pier diameter to pier spacing ratios resulted in decreased scour depth as the spacing between piers decreased.

**Das et al. (2019)** examined the relative scour situation around three pier groups. Scour geometries were seen when two tandem piers were aligned and a third pier was positioned eccentrically in the middle. Experiments were carried out on a laboratory scale by gradually changing the intermediate longitudinal gap between tandem piers. Following each experimental run, the scour formation surrounding the pier group and dune formation downstream of the pier group are analyzed.

**Malik and Setia (2019)** conducted experiment about interference between pier (a group of piers) models and its effects on scour depth. An experimental investigation was done in a 15 m long, 0.4 m wide, and 0.6 m high recirculating water fume, which contained homogenous sediment with a mean size of 0.30 mm. Experiments on 42 mm cylindrical pier models were conducted at 0.89 times the critical velocity ($u_c$). Three different arrangements (Tandem, Side by Side, and Staggered) were employed to study the impact of spacing and direction on scour. Initial investigations indicate that in Tandem arrangements with pier separation of 16 times the diameter or greater, both piers exhibit autonomous behaviour. If the distance between bridge piers is 0D, they behave like a single pier, resulting in a 41% higher scour depth. When the clear separation exceeded 1.5 times for side by side or 2.5 times for staggered arrangement, the piers acted independently.

**Kuila et al (2020)** conducted experiment about computing equilibrium flow structures at three interfering squire piers causing relative scour. An analysis was conducted using experiments to determine the hydrodynamic flow pattern around three identical square piers that were spaced apart and under a clear-water equilibrium scouring condition. Two piers were arranged in a line, and the third was positioned eccentrically in the middle of the square-shaped line. Every pier had a side face that faced the flow perpendicularly. The moment the equilibrium scour was reached, the precise 3-D velocities were recorded. Five distinct vertical azimuth sections and two horizontal sections (near bed and middle depth) were used to take readings. They concluded that the maximum equilibrium scour-depth measured at the square front pier, square rear pier, and square eccentrically positioned pier is approximately 1.5, 3.1, and 1.4 times more than the max-equilibrium scour-depth measured at a single pier. Furthermore, three piers' maximum depths are greater than those of two piers' experiments with in-line, eccentric placing. The dune creation was situated further away from the symmetry line, more on the eccentric square-pier side. On the square eccentric-pier side, the sediment diversion was more noticeable. Further downstream, shifted sediment was deposited with a slant toward the square eccentric pier side. The maximum values of u for eccentric pier and rear pier are determined to be 117% and 244% of the maximum values on

0° for square front pier, respectively. When the azimuth-angle α rises, u also rises and becomes finite. The square front pier and square rear pier have comparable max-w values of 105% and 189% of max-w on 0°, respectively, in the upstream region of the square eccentric pier.

**Malik and Setia (2021)** conducted experiment about local scour around closely placed bridge piers. an experimental study was conducted using round and oblong piers with a diameter(D) of 6.2 cm in tandem, side by side, and staggered patterns. The experiment was conducted in a recirculating flume of 12 meters in length, 0.6 meters in width, and 0.7 meters in height. The sediment was uniformly sized with an average diameter of ($d_{50}$) = 0.23 mm. The experiments were conducted at a velocity equivalent to 0.93 times the critical velocity, $u_c$. Piers separated by one diameter had maximum scour depths of 1.06, 1.51, and 1.53 for tandem, side by side, and staggered layouts, compared to single piers. Experiments reveal that when the separation between bridge piers is 16 times the diameter, they behave independently in tandem arrangements. The scour depth of the next pier is unaffected by the previous one. In a side-by-side design with 2.5D space between bridge piers, they behave independently. In a staggered arrangement, the front pier has a higher scour depth than rare piers and a lower scour depth slope, similar to the rear pier. When the spacing between the bridge piers is 5D, the three piers in staggered arrangement behave independently. When two piers of different forms are put in tandem, the circular pier has a higher scour depth than the oblong pier. However, both piers exhibit decreased scour depth. When the space between piers is 8D, they behave independently. When piers are arranged side-by-side and separated by four times their diameter (4D), they behave independently.

**Nandi et al. (2023)** established the isolated pier equation using metadata analysis. The study uses a comprehensive dataset spanning 57 years to conduct a comparative examination of temporal scour depth prediction algorithms, with a specific focus on circular piers in clearwater conditions. Sediment coarseness, flow shallowness, constriction ratio, Threshold-Froude number, sediment uniformity relative density, and duration are all taken into account. Using influential statistical criteria, 11 literature formulas are evaluated alongside a newly established one. Equal weightage and CRITIC techniques are used to establish the weightage for each influential element. Compromise programming is used to determine formula rankings. The study's overall result emphasises that when equilibrium scour depth and equilibrium time are known, the NCHRP (2011) method remains the most trustworthy for temporal scour depth prediction.

# Chapter 3

## 3.1 Local scour mechanism

The boundary layer flow past a cylindrical pier undergoes a three-dimensional separation. This separated shear layer rolls up along the obstruction to form a vortex system in front of the element which is swept downstream by the river flow. Viewed from the top, this vortex system has the characteristic shape of a horseshoe and is thus called a horseshoe vortex (Fig. 3.1), The formation of the horseshoe vortex and the associated down flow around the cylindrical pier results in increased shear stress and hence a local increase in sediment transport capacity of the flow. This leads to the development of a deep hole (scour hole) around the cylindrical pier, which in turn, changes the flow pattern causing a reduction in shear stress by the flow thus reducing its sediment transport capacity. The temporal variation of scour and the maximum depth of scour at bridge elements therefore mainly depend on the characteristics of flow, pier and river-bed material. The formation of the horseshoe vortex and the associated down flow cause scour at the cylindrical pier, abutment and spur dike.

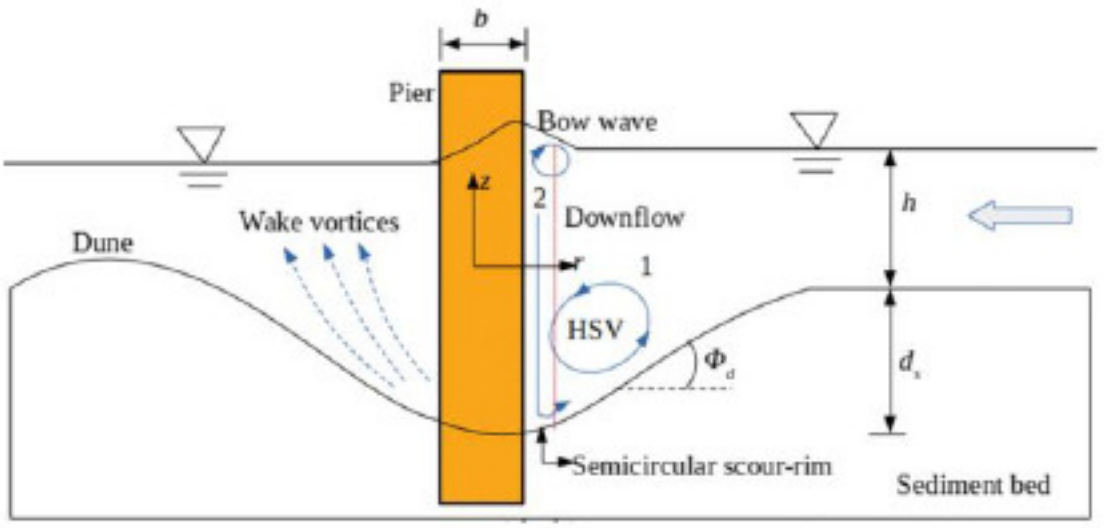



**Fig. 3.1** Scour mechanism at the cylindrical pier

The mechanism of scour around bridge piers was studied by Kothyari et al. (1992a, b) whereas studies on the mechanism of scour around abutments and spur dikes are available in Kothyari and Ranga Raju (2001).

## 3.2 Horseshoe vortex and downflow

The flow deflected by sediment embedded bridge piers causes scour at its foundations. Scour may endanger the stability of the complete bridge structure. In bridge hydraulics, circular-shaped pier foundations are commonly used. Due to the similar flow structures of airflow around circular bodies in wind tunnels, the basic research concerns flow visualization in aerodynamics. The main flow features involve a vertically deflected flow along the cylinder front, a horseshoe vortex system upstream of the cylinder, a flow separation beside the cylinder and a wake zone downstream of it shown in Fig. 3.2, For all flow conditions a horseshoe vortex system consisting of at least two vortices.

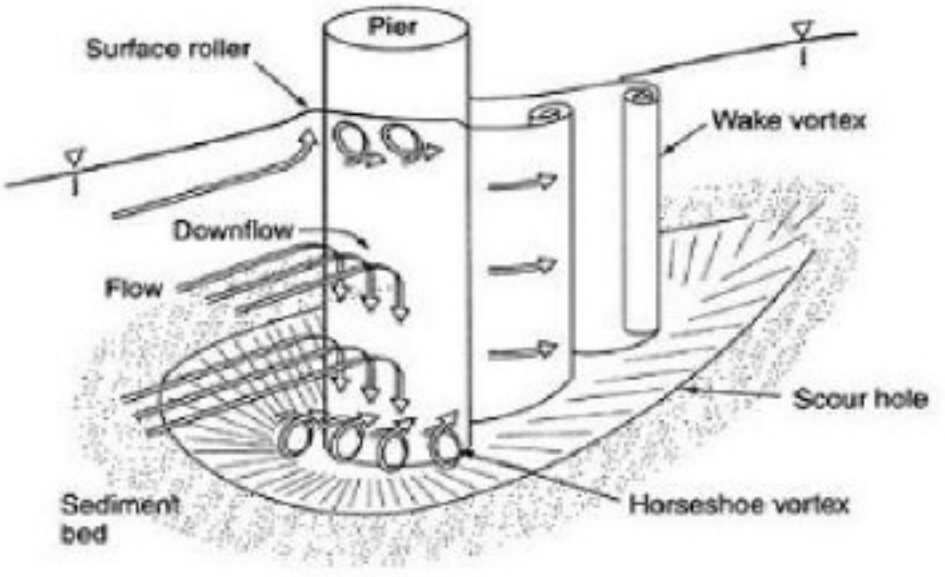



**Fig. 3.2** Mechanism of horseshoe vortex

The horseshoe vortex in front of the pier is the prime agent causing scour as said by Kothyari et al. (1992) assuming a layer-by-layer scouring process as said by Dey (1999). Tseng et al. (1999) said near the upstream face of the pier there exists a downflow which joins the separated flow to form the horseshoe vortex stretched around the pier.

## 3.3 Wake vortex

Wake vortices form at the downstream side of piers and are the result of flow separation at the sides of the pier. Called cast-off vortices by Raudkivi (1986), these have vertical axes. One vortex develops on one side, sheds away, and is convicted downstream. Immediately, other forms on the other side, finally shedding also. The wake vortices dissipate as they move downstream. The frequency of vortex shedding is directly proportional to the approach velocity and inversely proportional to the pier diameter.

Information on wake vortex scour at bridge piers is particularly scanty. As wake vortex scour occurs at the downstream of the pier, it has little or no destructive potential. Because the horseshoe vortex scour occurs at the face of the pier and threatens to undermine the pier, this type of scour has been given considerable theoretical thought by Bruesers *et al.* (1977) and is well-documented with model studies by Raudkivi (1986).

Knowledge about wake vortex scour due to bridge piers has come mainly from a few laboratories' experiments Melville (1975). To describe the scouring action, Melville wrote "each of the concentrated vortices acts with its low-pressure centre as a vacuum cleaner", picking up material from the bed, which is then transported downstream.

At most bridges, wake vortex scour is insignificant and confluence scour does not exist. In clear-water Rivers flowing on fine sand, these two forms of local scour can be very large. The deep scour holes downstream from the large circular piers (10 and 15 m in diameter) at the Tahrir and Imbaba Bridges over the Nile River in Cairo, Egypt was produced by the conflicting velocity fields at the intersection of the wake vortex streams from adjacent piers. The depths of scour due to these wake vortices are now 8 to 11 m where the normal depth of flow is approximately 8 m. Confluence scour where the main and side channel join upstream

from the Imbaba Bridge was 9 m in 1981 and 1987 and was aligned with the bisector of the intersection angle of the two channels. These depths of scour can be considered nearly clear-water scour as the bridges are in the backwater of the Delta Barrages, the velocity was less than 1 m/s and sediment transport was very low. There is concern that the holes may enlarge or move upstream endangering the piers and the bridges. We have made observations in the vicinity of the scour holes and have come to the conclusion that, in each case, the scour was caused by two streams of wake vortices from adjacent piers intersecting downstream. The vortices that result from the two conflicting velocity fields create local scour. At one bridge, the scour is enhanced by the vortices that occur at the confluence of the main channel and its side channel. This is known as confluence scour.

## 3.4 Classification of scour parameters

### 3.4.1 Flow intensity

Flow intensity is defined as the ratio of the shear velocity ($u_*$) to the critical shear velocity ($u_{*c}$) or the ratio of the approach mean velocity to the critical mean velocity [Melville and Chiew (1999)]. Under the clear-water condition, the local scour depth in uniformly-graded sediment increases almost linearly with velocity to a maximum at the threshold velocity [Melville and Coleman (2000)]. The maximum scour depth is reached when the ratio $u_*/u_{*c} = 1$ and the corresponding maximum scour depth is called the threshold peak. As the velocity exceeds the threshold velocity, the local scour depth in uniform sediment first decreases and then increases again to a second peak, but the threshold peak is not exceeded provided the sediment is uniform.

### 3.4.2 Flow depth

The influence of flow depth on the scour depth has been discussed by many authors [e.g., Breusers and Raudkivi (1991); Melville and Coleman (2000)]. The presence of the pier in the channel causes a surface roller around the pier and a horseshoe vortex at the base of the pier. Flow depth affects local scour depth when the horseshoe vortex is affected by the formation of the surface roller (or bow wave) that forms at the leading edge of the pier. The two rollers, (i.e., the bow wave and the horseshoe vortex) rotate in opposite directions. In principle, as long as there is no interference between the two rollers, the local scour depth does not depend on the flow depth but depends only on the pier diameter.

In such an instance, often called deep flow, the local scour is said to occur at narrow piers. As the flow depth decreases, the surface roller becomes relatively more dominant and causes the horseshoe vortex to be less capable of entraining sediment. Therefore, for shallower flows, the local scour depth is reduced. Subsequently, in a very shallow flow, the local scour is dependent on the flow depth and the local scour is said to occur at a wide pier.

### 3.4.3 Pier width

Experiments have clearly shown that it is possible to relate the scour depth to the size of the pier (Breusers et al., 1977). This observation can be explained physically by the fact that

scouring is due to the horseshoe vortex system whose dimension is a function of the diameter of the pier. It has also been observed that the horseshoe vortex, being one of the main scouring agents, is proportional to the pier Reynolds number ($R_e$), which in turn is a function of the pier diameter.

For the same value of mean approach flow velocity, therefore, the scour depth is proportional to the pier width. The influence of pier size on the local scour depth is of interest when data from the laboratory are interpreted for field use (Breusers and Raudkivi, 1991).

Under clear-water conditions, pier size influences the time taken to reach the ultimate scour depth but not its relative magnitude $y_s/b$, if the influence of relative depth, $h/b$, and relative grain size $b/d_{50}$ on the local scour depth are excluded (Breusers and Raudkivi, 1991). They also concluded that the volume of the local scour hole formed around the upstream half of the perimeter of the pier is proportional to the cube of the pier diameter (or the projected width of the pier). The larger the pier the larger the scour hole volume and also the longer is the time taken for the development of the scour hole for a given shear stress ratio.

### 3.4.4 Pier Shape

Piers are constructed of various shapes. The most common shapes used are circular, rectangular, square, rectangular with chamfered end, oblong, lenticular and Joukowski. The effect of pier shape has been reported by many researchers [e.g., Breusers (1977), Breusers and Raudkivi (1991), Melville and Coleman (2000)].

The blunter the pier, the deeper the local scour has been a general conclusion. The shape of the downstream end of the pier is concluded to be of little significance to the maximum scour depth. The pier shape is often accounted for by using a shape factor. Melville and Chiew (1999) discussed shape factors for uniform piers which are piers having constant sections throughout their depth, which was proposed. The local scour depths for a variety of different pier shapes all have the same projected width (140 mm). From his results, a circular pier produced the least scour while a rectangular pier having blunt ends produced the most scour.

For piers tapered on the upstream and downstream faces, the slope, in elevation, of the leading edge of the pier affects the local scour depth. Downward-tapered piers induce deeper scour than does a circular pier of the same width.

### 3.4.5 Sediment Size

The effects of the grain size and the density of the sediment material are often expressed as a function of the critical flow velocity for the initiation of sediment motion. Breusers and Raudkivi (1991) reported on the work of Raudkivi and Ettema (1977) in which the effect of sediment size on the local depth of scour at a bridge pier was studied. The experiments were conducted under clear-water conditions and using a pier of diameter 7 cm and a flume 1.5 m in width. It was observed that a sediment size of $d_{50} \leq 0.7$ mm leads to the formation of ripples, whereas a sediment size of $d_{50} \geq 0.7$ mm does not cause ripples. It was further stated that the results for grain sizes which lead to the formation of ripples ($d_{50} \leq 0.7$ mm) were different from those for larger grain sizes for which ripples do not form ($d_{50} \geq 0.7$ mm).

According to Raudkivi and Ettema (1996), for non-ripple forming sediments ($d_{50} \geq 0.7$ mm), experiments can be run successfully with a flow condition, $u_* \sim 0.95^{u_{*c}}$, without the upstream bed being disturbed by the approach flow, whereas with finer sands ($d_{50} < 0.7$ mm) a flatbed cannot be maintained for the same flow condition. Therefore, if the sediment is uniform sand with grain size $d_{50} < 0.7$ mm, a flatbed cannot be maintained near the threshold shear stress condition because ripples will develop, with a small amount of general sediment transport taking place so as to replenish some of the sand scoured at the pier. Thus, true clear-water scour conditions cannot be maintained for this case.

### 3.4.6 Flow Froude Number

The Froude number is a dimensionless number comparing inertia and gravitational forces. It may be used to quantify the resistance of an object moving through water and compare objects of different sizes. Named after William Froude, the Froude number is based on the speed/length ratio as defined by him.

$$F_r = \frac{u}{\sqrt{gh}} \tag{3.1}$$

where, $u$ is a characteristic velocity and For rectangular cross-sections with uniform depth $h$, For $F_r < 1$ the flow is called a subcritical flow, further for $F_r > 1$ the flow is characterized as supercritical flow. When $F_r \approx 1$ the flow is denoted as critical flow.

## 3.5 Angle of repose

The angle of repose also referred to as the angle of friction, is an engineering property of granular materials. The angle of repose is the maximum angle of a stable slope determined by friction, cohesion and the shapes of the particles. When bulk granular materials are poured on a horizontal surface, a conical pile will form. The internal angle between the surface of the pile and the horizontal surface is known as the angle of repose and is related to the density, surface area, and coefficient of friction of the material. Material with a low angle of repose forms flatter piles than material with a high angle of repose. In other words, the angle of repose is the angle a pile forms with the ground.

The angle of repose is the steepest angle that the surface of a mass of loose particulate matter makes with the ground. The angle of repose is affected by the size, mass, angularity, and dampness of the particles and by the force of downward acceleration, but it is consistent for a given material. Knowing the angle of repose of material in various circumstances is vital for engineers and landscapers, for example.

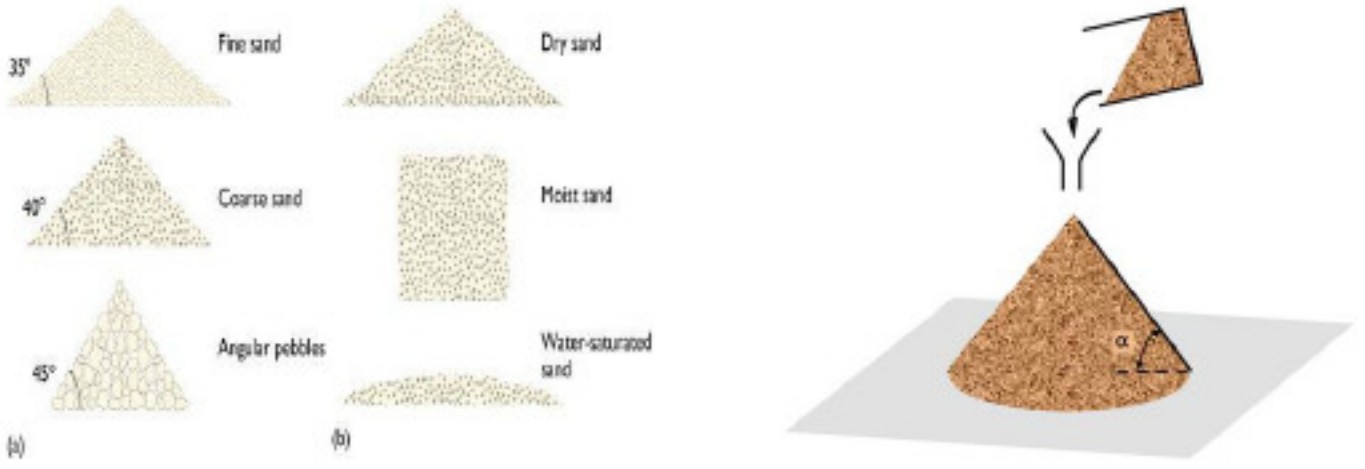



**Fig. 3.3** Angle of repose

The way in which most people are familiar with the angle of repose is sand castles. Dry sand generally has an angle of repose of about 30°, so piled dry sand forms shallow inverted cones. When sand is dampened, the surface tension of the water binds the grains together, and the angle of repose is increased to more than vertical so that walls and towers and sea caves can be made. When sand is too wet, however, the water lubricates the grains instead of sticking them together, and the angle of repose is decreased to nearly zero. This should be required knowledge for anyone who is thinking of buying a house built on a sandbar.

# Chapter 4

## 4.1 Objectives

The primary purpose of this research is to conduct tests to show how clear water scour varies around two eccentrically positioned circular piers at various eccentricities and flow depths.

- The current study attempted to observe the nature of the scour depth that develops around circular piers over time by altering the eccentricity of the piers as well as the approach flow depth.
- To analyse experimental data in order to determine the optimal pier layout that maximizes scouring.
- To calculate and analyse the volume and area for scour and deposition for each experimental run.

The experimental procedure followed is as under in Table 4.1.

**Table 4.1** Series of experiments conducted

| Pier diameter ($b$) cm | Flow shallow-ness ($h/b$) | Flow depth ($h$) m | Discharge ($Q$) l/s | Flow velocity ($u$) m/s | Flow intensity ($u/u_c$) | Froude No ($F_r$) | Longitudinal spacing ($l$) | Eccentricity ($e$) | Run No |
|---|---|---|---|---|---|---|---|---|---|
| 7 | 1.8 | 0.126 | 30 | 0.29 | 0.872 | 0.26 | 5.185$b$ | 2$b$ | 1 |
| 7 | 1.957 | 0.137 | 30 | 0.27 | 0.805 | 0.23 | 5.185$b$ | 2$b$ | 2 |
| 7 | 2.1 | 0.1465 | 30 | 0.25 | 0.748 | 0.21 | 5.185$b$ | 2$b$ | 3 |
| 7 | 2.25 | 0.1575 | 30 | 0.24 | 0.698 | 0.19 | 5.185$b$ | 2$b$ | 4 |
| 7 | 1.8 | 0.126 | 30 | 0.29 | 0.872 | 0.26 | 5.185$b$ | 2.25$b$ | 5 |
| 7 | 1.957 | 0.137 | 30 | 0.27 | 0.805 | 0.23 | 5.185$b$ | 2.25$b$ | 6 |
| 7 | 2.1 | 0.1465 | 30 | 0.25 | 0.748 | 0.21 | 5.185$b$ | 2.25$b$ | 7 |
| 7 | 2.25 | 0.1575 | 30 | 0.24 | 0.698 | 0.19 | 5.185$b$ | 2.25$b$ | 8 |
| 7 | 1.8 | 0.126 | 30 | 0.29 | 0.872 | 0.26 | 5.185$b$ | 2.5$b$ | 9 |
| 7 | 1.957 | 0.137 | 30 | 0.27 | 0.805 | 0.23 | 5.185$b$ | 2.5$b$ | 10 |
| 7 | 2.1 | 0.1465 | 30 | 0.25 | 0.748 | 0.21 | 5.185$b$ | 2.5$b$ | 11 |
| 7 | 2.25 | 0.1575 | 30 | 0.24 | 0.698 | 0.19 | 5.185$b$ | 2.5$b$ | 12 |
| 7 | 1.8 | 0.126 | 30 | 0.29 | 0.872 | 0.26 | 5.185$b$ | 2.75$b$ | 13 |
| 7 | 1.957 | 0.137 | 30 | 0.27 | 0.805 | 0.23 | 5.185$b$ | 2.75$b$ | 14 |
| 7 | 2.1 | 0.1465 | 30 | 0.25 | 0.748 | 0.21 | 5.185$b$ | 2.75$b$ | 15 |
| 7 | 2.25 | 0.1575 | 30 | 0.24 | 0.698 | 0.19 | 5.185$b$ | 2.75$b$ | 16 |
| 7 | 1.8 | 0.126 | 30 | 0.29 | 0.872 | 0.26 | 5.185$b$ | 3b | 17 |
| 7 | 1.957 | 0.137 | 30 | 0.27 | 0.805 | 0.23 | 5.185$b$ | 3$b$ | 18 |
| 7 | 2.1 | 0.1465 | 30 | 0.25 | 0.748 | 0.21 | 5.185$b$ | 3$b$ | 19 |
| 7 | 2.25 | 0.1575 | 30 | 0.24 | 0.698 | 0.19 | 5.185$b$ | 3b | 20 |
| 7 | 1.8 | 0.126 | 30 | 0.29 | 0.872 | 0.26 | 5.185$b$ | 3.5b | 21 |
| 7 | 1.957 | 0.137 | 30 | 0.27 | 0.805 | 0.23 | 5.185$b$ | 3.5$b$ | 22 |
| 7 | 2.1 | 0.1465 | 30 | 0.25 | 0.748 | 0.21 | 5.185$b$ | 3.5$b$ | 23 |
| 7 | 2.25 | 0.1575 | 30 | 0.24 | 0.698 | 0.19 | 5.185$b$ | 3.5$b$ | 24 |

## 4.2 Methodology

1) The flow depth in the flume was adjusted by a tailgate. The approaching flow depth ($h$) was varied from 12.6 cm to 15.75 cm for all experimental runs. The bed slope $S_0$ (=1:2400) was kept constant throughout all the experiments.
2) The critical condition of the bed was examined before the experiment run using steps 2 to 6. The depth-averaged approaching flow velocity ($u$) was estimated using Manning's equation$\left(u = \frac{1}{n} R^{\frac{2}{3}} S^{\frac{1}{2}}\right)$. Here, the coefficient of roughness ($n$) was determined by using Strickler's formula $\left(n = \frac{1}{24} d_{50}^{\frac{1}{6}}\right)$. From the sieve analysis experiment, the median diameter of sand ($d_{50}$) was determined as 0.805 cm from Fig. 4.1.

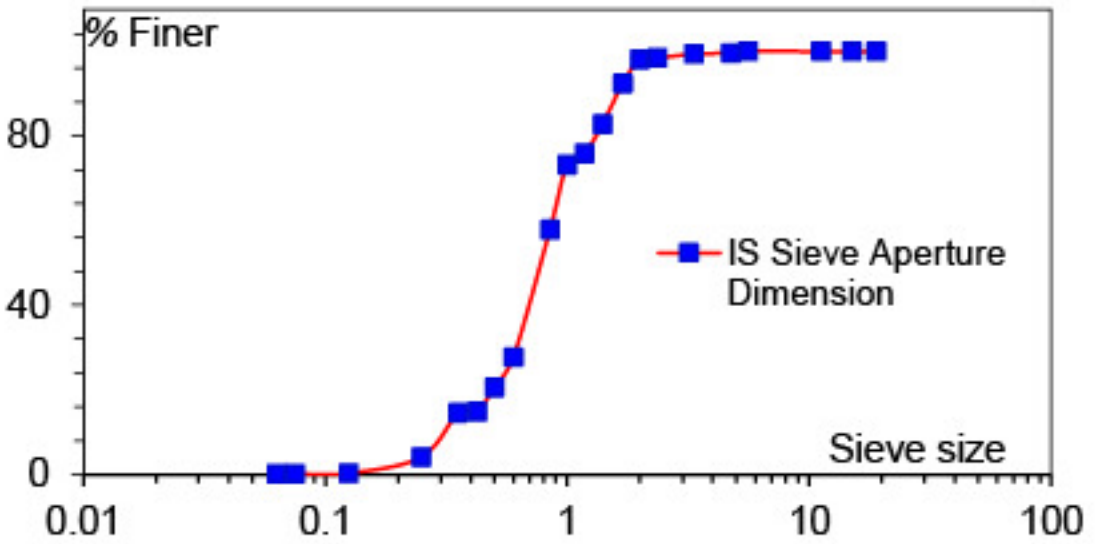



**Fig. 4.1** Grading curve

3) The critical bed shear stress ($\tau_{0c}$) was determined by using the expression for the critical Shields parameter, $\Theta_c \left(= \frac{\tau_{0c}}{\Delta \rho_f g d}\right)$ which was developed by van Rijn (1984). From van Rijn's (1984) empirical equations of the Shields curve the value of the critical Shields parameter was calculated where the particle parameter, $D_* \left(= d \left(\frac{\Delta g}{\nu^2}\right)^{\frac{1}{3}}\right) = 20.06$. Then the equation of critical bed shear stress becomes as $\tau_{0c} = 0.0315 \Delta \rho_f g d$ (=0. 0.3983 N/m$^2$).
5) Then critical shear velocity ($u_{*c}$) was calculated using $u_{*c} = \sqrt{\frac{\tau_0}{\rho_f}} = 0.01997$. Therefore $u_c$ can be calculated from $\frac{u_c}{u_{*c}} = 5.75 \, log \, log \left(\frac{h}{2 d_{50}}\right) + 6$ where $u_{*c}$, $h$, $d_{50}$ are already known. $u_c$ calculate is 0.34 m/s.
6) Critical shear flow Reynolds number $R_{*c} \left(= \frac{u_{*c} R}{\nu}\right)$ was determined at the 20°C temperature of the water where $R$ is the hydraulic radius. The Shields' experimental results which relate critical Shields parameter ($\Theta$) and ($R_{*c}$) is known as the Shields

diagram (1936). The threshold of sediment motion occurs when $\Theta > \Theta_c$ or $\tau_0 > \tau_{0c}$ or $u_* > u_{*c}$. It is clear that the discharge during each experiment run was lower than the minimum discharge required for the incipient motion or threshold conditions of the bed particles. Therefore, it can be said that all the experiments were carried out under clear water scour conditions.

7) The depth-averaged approaching flow velocity ($u$) was varied from 69.8% to 87.2% for varying depths from 12.6 cm to 15.75 cm, and the critical velocity ($u_c$) of the uniform sand bed considering side-wall effect to satisfy the clear water condition i.e. the present research considered only clear water approach flow conditions described by a threshold/critical Froude number of $F_t$ (= $u/u_c$) less than 1 (Dey and Raikar, 2007; Oliveto and Hager, 2002). The depth-averaged approaching flow velocity was determined from the measured vertical profile of the approaching flow velocity at 2 m upstream of the pier where the presence of the pier did not affect the approaching flow. Also, to satisfy clear water scour conditions, average bed shear stress ($\tau_0$) must be less than or equal to critical bed shear stress ($\tau_{0c}$). It was determined using the method proposed by Dey (2003).

8) Das et al. (2015) conducted experimental studies on local equilibrium scour around a set of two identical piers of different shapes placed at a varying eccentricity ($e$ = 2$b$-3.5$b$) to analyze the nature of scour evolved due to the effect of mutual interference of one pier on another, varying the longitudinal spacing between them. It was observed that maximum scour development was taken place at a longitudinal spacing of 5.185$b$. Therefore, based on this concept, the current study was conducted to analyze the effect of eccentricity along with the constant longitudinal distance of 5.185$b$ to find the maximum and minimum scour by varying the eccentricity.

# Chapter 5

## 5.1 Experimental setup

The experimental arrangement, data acquisition system and variables measured in the model study are described. Typical investigation of scour depth development around two eccentric piers has been carried out through various experiments. The experimental setup and conditions of the work are described in detail. All the experiments were conducted in the Fluvial Hydraulics Laboratory (Fig. 5.1) of the School of Water Resources Engineering at Jadavpur University, Kolkata.



**Fig. 5.1** Tilting flume used during the experimentation

### 5.1.1 Tilting Flume

The experiments are carried out in a recirculating flume 11 m long, 0.81 m wide, and 0.60 m deep (Figs. 5.1-5.2). The working section of the flume is filled with sand to a uniform thickness of 0.20 m. The length of the sand bed is 7 m and the width is 0.81 m. The sand bed is located 2.9 m upstream from the flume inlet. The working section of the flume is made up of a steel bottom and Plexiglas side walls along two sides for most of its length to facilitate visual observations. The recirculating flow system is served by a centrifugal pump located at the upstream end of the flume.

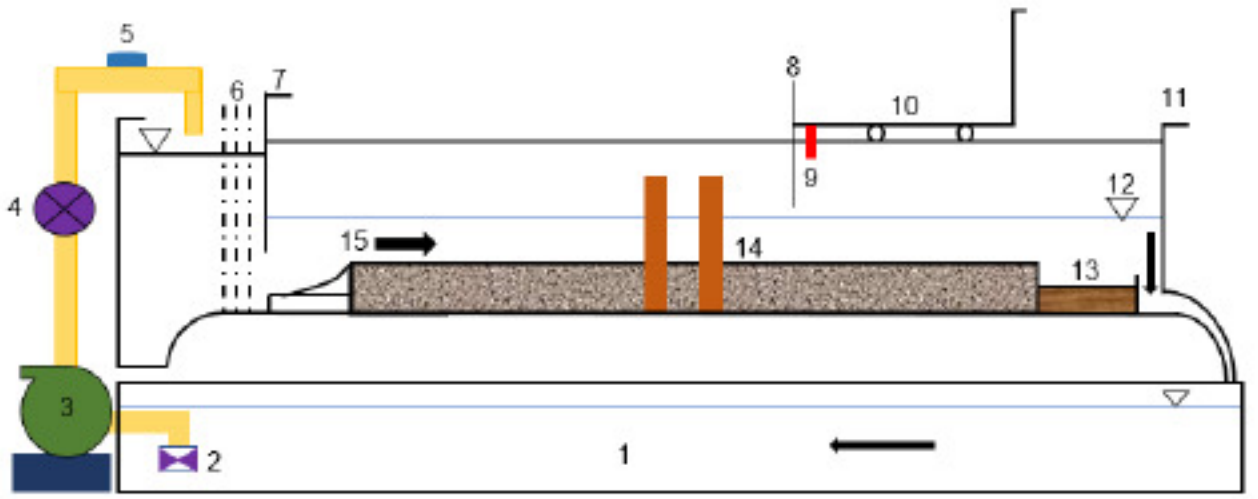



**Fig. 5.2** Schematic diagram of tilting flume: 1. Reservoir, 2. Check Valve or Foot valve, 3. 10 hp Pump, 4. Control Valve, 5. Flow meter, 6. Baffle plate. 7. Inlet gate, 8. Point gauge, 9. LDS (Laser distance meter), 10. Movable trolley, 11. Outlet gate, 12. Water level, 13. Collector, 14. Pier (eccentrically arranged two piers), 15. Flow direction. (Barman, 2023).

### 5.1.2 Pump

The hydraulic machines which convert the mechanical energy into hydraulic energy are called pumps. Hydraulic energy is in the form of pressure energy. The recirculating flow system is served with a 10 hp, variable speed, centrifugal pump located at the upstream end of the flume (Fig. 5.3). Water flows through a 200 mm diameter pipe line which runs directly into the flume. The rpm of the pump is 1430; power is 7.5 kW, and maximum discharge is 30 l/s. There are two pumps for alternative use. To measure the discharge, water flows through a flow meter.



**Fig. 5.3** Pump used to recirculate the flow

### 5.1.3 Pier

In the present study, all two piers models were constructed using Perspex sheets. Two circular bridge piers models of diameter 7 cm have been used in the present study (Fig. 5.4). The height of the piers is 45.6 cm. During the experiment, it is kept in mind that the width of the experimental flume is more than eight times the pier diameter to avoid the wall friction factor.

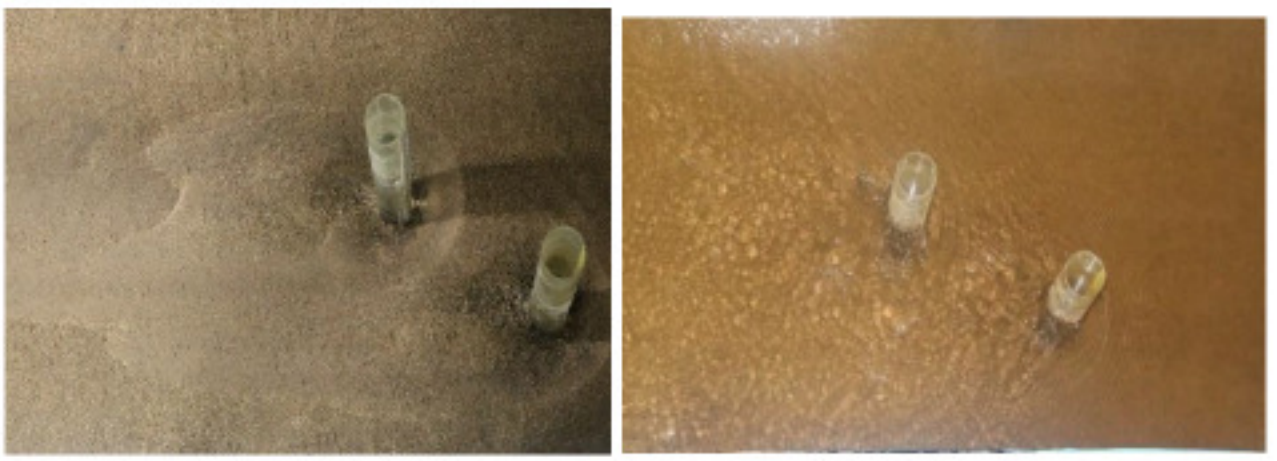


**Fig. 5.4** Piers placed at the working section of the flume

### 5.1.4 Sand Bed

The shields diagram remains the most effective way of determining threshold conditions for uniform sediments. For given fluid density and viscosity and sediment density, the shields diagram can be used to obtain a plot of shear velocity $u_{*c}$ against grain size $d_{50}$. The determination of threshold conditions for non-uniform sediment is not so clear-cut. The effects of particle size distribution may be important and thus $u_c$ would depend on both the median grain size $d_{50}$ and the geometric standard deviation, $\sigma_g=(d_{84}/d_{16})^{0.5}$ with non-uniform sediments, a flow can disturb the grain, removing some but simply rearranging others into a stable pattern that develops into an armoured bed and stabilizes. Such flow is considered here in to be above the threshold. Values of $u_c$ are found using a suggestion first made by Weill that many of the intermediate sizes will move when flow conditions based on $d_{50}$ exceed the shields criterion.

A series of experiments are carried out on the sand bed material (Fig. 5.5). In the laboratory we measured the vibrating sieve analysis and specific gravity Sand particle sizes $d_{50}$ is 0.805 mm, $d_{16}$ is 0.44 mm, $d_{84}$ is 1.458 mm and $d_{90}$ is 1.65 mm. The geometric standard deviation of sediment size ($\sigma_g$) is 1.82. The density of the sand is 2.58. We have measured the sand particle size from the graph. Here we plot the grain size distribution and percent finer.

Small triangular sand waves with a long gradual upstream slope (approximately 6°) and short steep downstream slope (approximately 32°) are called ripples. In the case of fine sediments ($d_{50} < 0.7$ mm), ripples are formed, while coarse sediments usually form dunes. The wave lengths of ripples are usually shorter than 300 mm or approximately equaling $150d_{50}$. It is assumed that ripples are formed if the viscous sub-layer is present when the threshold shear stress is just suppressed, while dunes are formed if the bed is hydraulically rough. The length of the ripples depends on the sediment size and the flow velocity but is essentially independent of the flow depth. Ripples may be superposed upon the upstream side of dunes.

Dunes are the bed –forms larger than ripples, whose profile is out of phase with the free surface profile. The stream-wise profile of a dune is roughly triangular with a mild upstream slope and a downstream slope approximately equal to the angle of repose. Dunes are formed in coarse sediment ($d_{50} > 0.6$ mm).

Above this, a zone of high turbulence exists, where a large production (and dissipation) of turbulent energy takes place. Near the zone of reattachment, the sediment particles are transported by turbulence, even when the local bed shear stress is below its threshold value.

On the upstream side of the dune, the bed shear stress drives sediment particles uphill until they pass over the crest and eventually are buried in the bed for a period. As sediment is transported from the upstream side and deposited on the lee side of a dune, the result is a slow continuous downstream migration of the dunes.

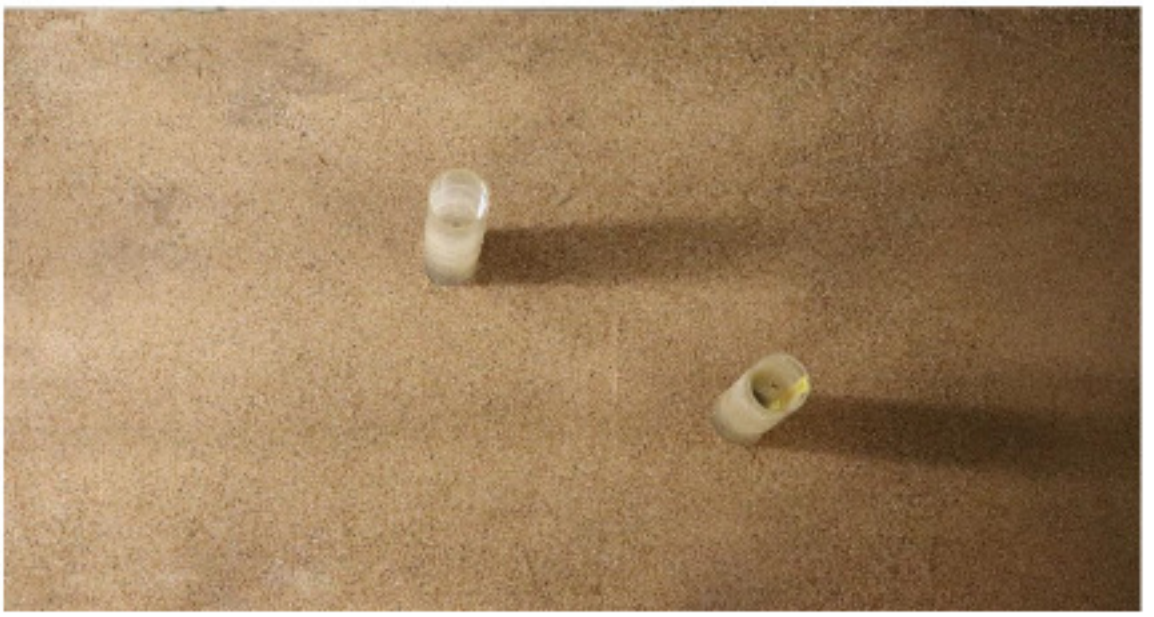


**Fig. 5.5** Experimental sand bed

After placing the piers in the proper position with proper alignment properly flat sand bed was prepared. A very good experiment requires a properly prepared flat sand bed which is essential for attaining good experimental results. A 3 m long and 0.81 m wide flat sand bed was prepared and the flatness of the sand bed was checked with a spirit level. The sand bed preparation was done for every new setup of piers arrangement.

## 5.2 Experimental procedure

The average bed shear stress was 0.3824 Pa and the angle of repose of bed sand and critical bed shear stress were estimated 34° and 0.3983 Pa respectively. The flow depth in the flume was adjusted by operating a tailgate. The depth-averaged approaching flow velocity was found from the measured vertical profile of the approaching flow velocity at 2 m upstream of the pier where the presence of the pier did not affect the approaching flow. Froude number ($F_r$) varies from 0.19 and 0.26.

The pier is first installed in the flume at the desired location. Before each experiment, care is taken to level the sand bed throughout the entire length of the flume and perpendicular to the pier structure. First of all, we have to produce a sand bed having a smooth, uniform surface, so we used a spirit level to check the uniformity of the bed surface. The uneven bed surface is levelled using a hand trowel. After that, we have to measure the bed level by point gauge randomly and check the levelling of the flume. The sand bed preparation is very key as for as the experiment is concerned. Unevenness or defect in the channel bed can cause damage to the experiment. Piers are constructed eccentrically with different conditions with the help of total scour length around the single pier.

During the experiment, it was kept in mind that the width of the experimental flume was more than seven times the pier width to avoid the wall friction factor. The minimum value

of the ratio between flume width and pier width is 6.25, as proposed by Raudkivi and Ettema (1983) which could be used without a measurable effect from the side walls on the local scour at the pier.

To start the experiment, the flume is slowly filled with water to the required depth from downstream. It should be noted that extra care is required when filling the flume with water, especially for an experiment of this nature where no sediment movement is allowed. Any deformity in the bed surface may develop ripples or dunes and general movement of the sand if the shear stress on the smooth bed is close to the critical shear stress. The pump is then turned on and the desired flow rate has been achieved by controlling the control valve and a bypass valve.

Concurrent with getting the pump up to speed, the tailgate is adjusted so as to maintain the correct depth for all the experiments of flow in the flume. Throughout the experiment period, the location and magnitude of the point of maximum scour depth are around the upstream of the pier. The frequency of the scour depth varied throughout the experiment period. The rate of scouring is maximum in the period of 1 to 4 hours and then less frequently thereafter. Here we have used the fibre transferring pier model. The run duration for the experiments are varies from 2.5 to 10 hours. After that, the pump is stopped to allow the flume to slowly drain without disturbing the scour topography.

# Chapter 6

## 6.1 Results and discussion

A study of local erosion around two eccentric circular piers in clearwater conditions was carried out. After conducting all the experiments for the scour hole geometrical parameters like maximum scour depth, length of sediment shifted to the downstream, max-width of scouring deposition, hole surface area and the total volume of scouring deposited and scour volume were analyzed. Here experiments were run for a duration varies from of 2.5 to 10 hours. The scour depth was measured with the help of a laser distance meter and the data obtained was analyzed with the help of surfer software to generate contour maps.

In this present study, the hydrodynamic consequences of different eccentric arrangements on scouring were investigated. Erosion and deposition patterns were studied around the front and eccentric piers at different time intervals along the flume. A total of 24 experiments were carried out with the same experimental conditions such as discharge and bed material. The width of each pier was taken 7 cm.

Each experiment was started with a flattened bed. While the outlet valve was closed, the flume was filled with water very slowly without disturbing the bed material, until the desired flow depth was reached. Then the inflow valve was adjusted to the desired discharge in the flume and the outlet valve was partially opened. The experiments were carried out for constant discharge of 30 l/s and various flow depths are 12.6 cm, 13.65 cm, 14.70 cm, and 15.75 cm. Knowing that scour depth evolves rapidly at the beginning of the experiments and gets slower towards the end, the scour depth measurements are recorded more frequently at the beginning.

In order to plot the contour profile, the water in the flume was drained after the completion of experiments and the sediment deposition was investigated by taking the depth at the scoured region with the help of a laser distance meter. This procedure is repeated for the aforementioned experiment durations and experiments. The experimental outcomes are discussed below.

**Table 6.1:** The parameters kept constant throughout the series of experiments

| Parameters | Values |
|---|---|
| Discharge ($Q$) | 30 l/s |
| Pier width ($b$) | 7 cm |
| Longitudinal distance ($l$) | 5.185$b$ |
| Experimental duration ($t$) | 2.5 to10 hours |

### 6.1.1 Experiment No. 1

This experiment was conducted for an eccentricity of $2b$ for 4 hours. Here, for Fig 1, the sub figures (a), (b), and (c) denotes level bed before starting the experiment, scour bed after drying the bed and the contour plot respectively, the same has been applied for following all figure.

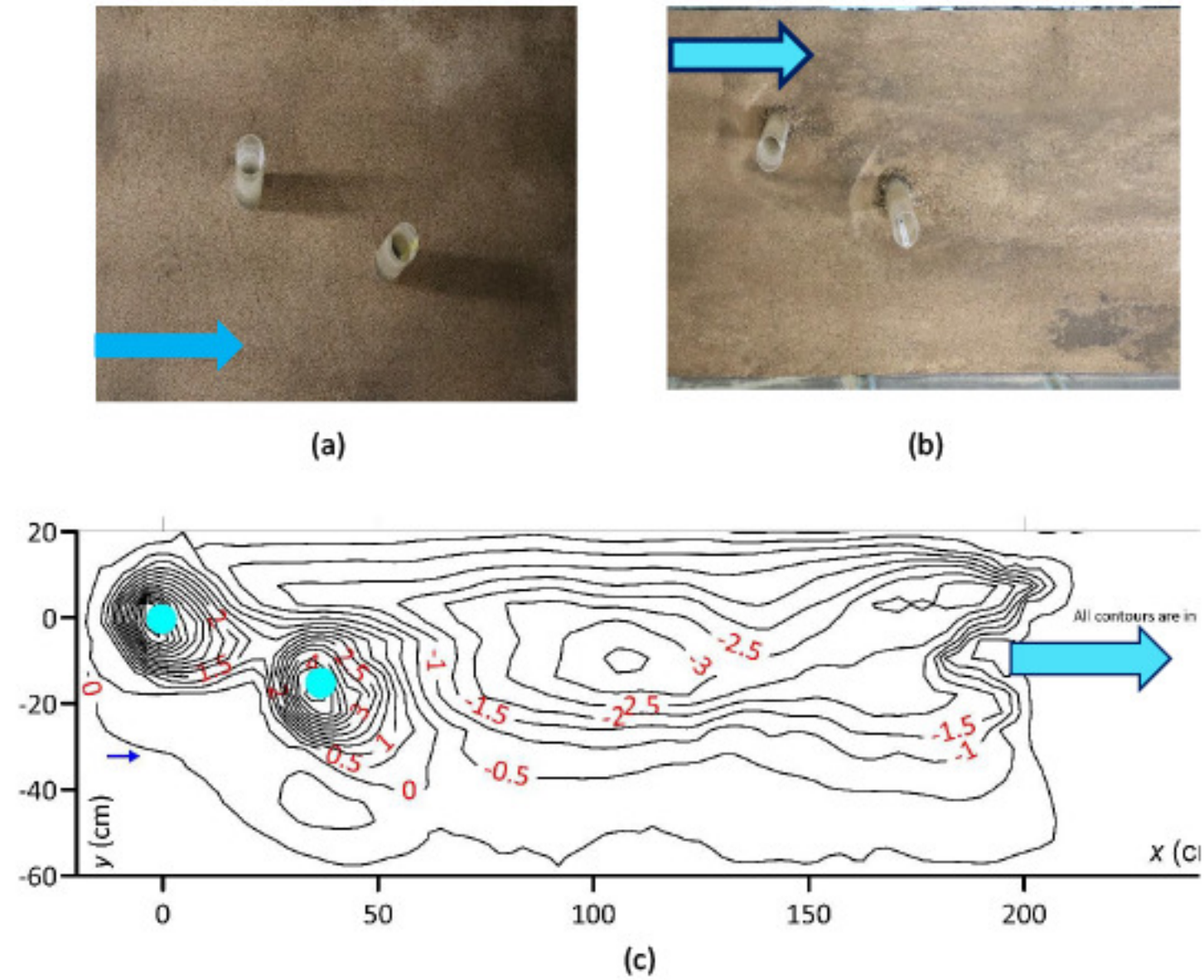



**Fig. 6.1** Experimental condition for experiment 1, $e = 2\,b$, (a) Level bed, (b) Scour bed and (c) Contour Map

The values of subsequent scour depths were recorded with the help of the laser distance meter. The frequency of recording the scour depths was increased with the passing of each hour. It was observed that the scour depth for both the piers, in this case, was maximum among the series of experiments conducted. The scour depth observed at the front pier was **6.65 cm** and that at the eccentric pier was **6.41cm** m, after the completion of the experiment. The contour map was generated using surfer software. All the relevant results are given in Table 3.

### 6.1.2 Experiment No. 2

This experiment was conducted for an eccentricity of $2b$ for 9 hours. The values of subsequent scour depths were recorded with the help of the laser distance meter.

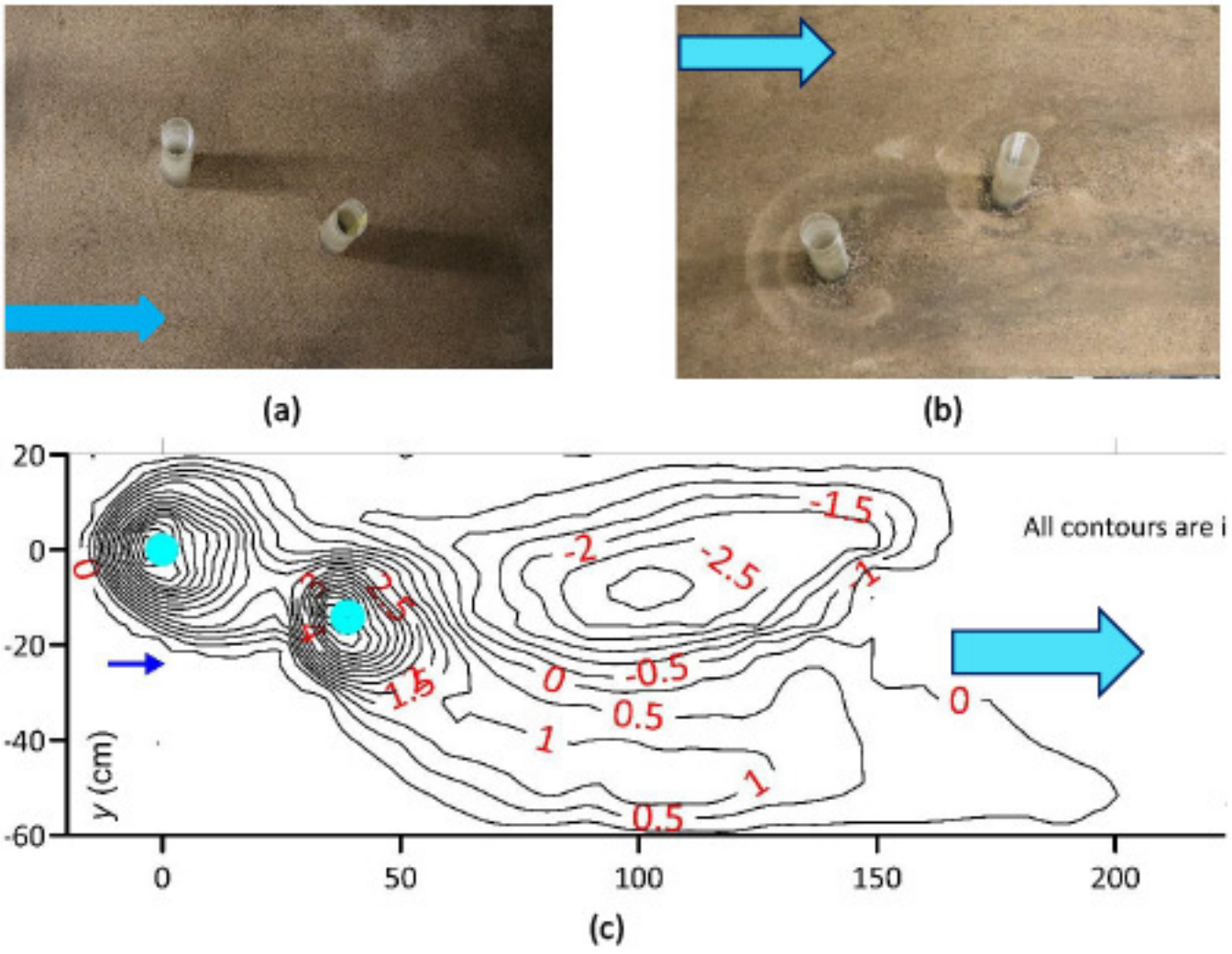



**Fig. 6.2** Experimental condition for experiment 2, $e = 2\,b$, (a) Level bed, (b) Scour bed and (c) Contour Map

The frequency of recording the scour depths was increased with the passing of each hour. The scour depth observed at the front pier was **7.44 cm** and that at the eccentric pier was **6.66 cm**, after the completion of the experiment surfer software was used to generate contour maps.

### 6.1.3 Experiment No. 3

This experiment was conducted for an eccentricity of $2b$ for 9 hours. The values of subsequent scour depths were recorded with the help of the laser distance meter.

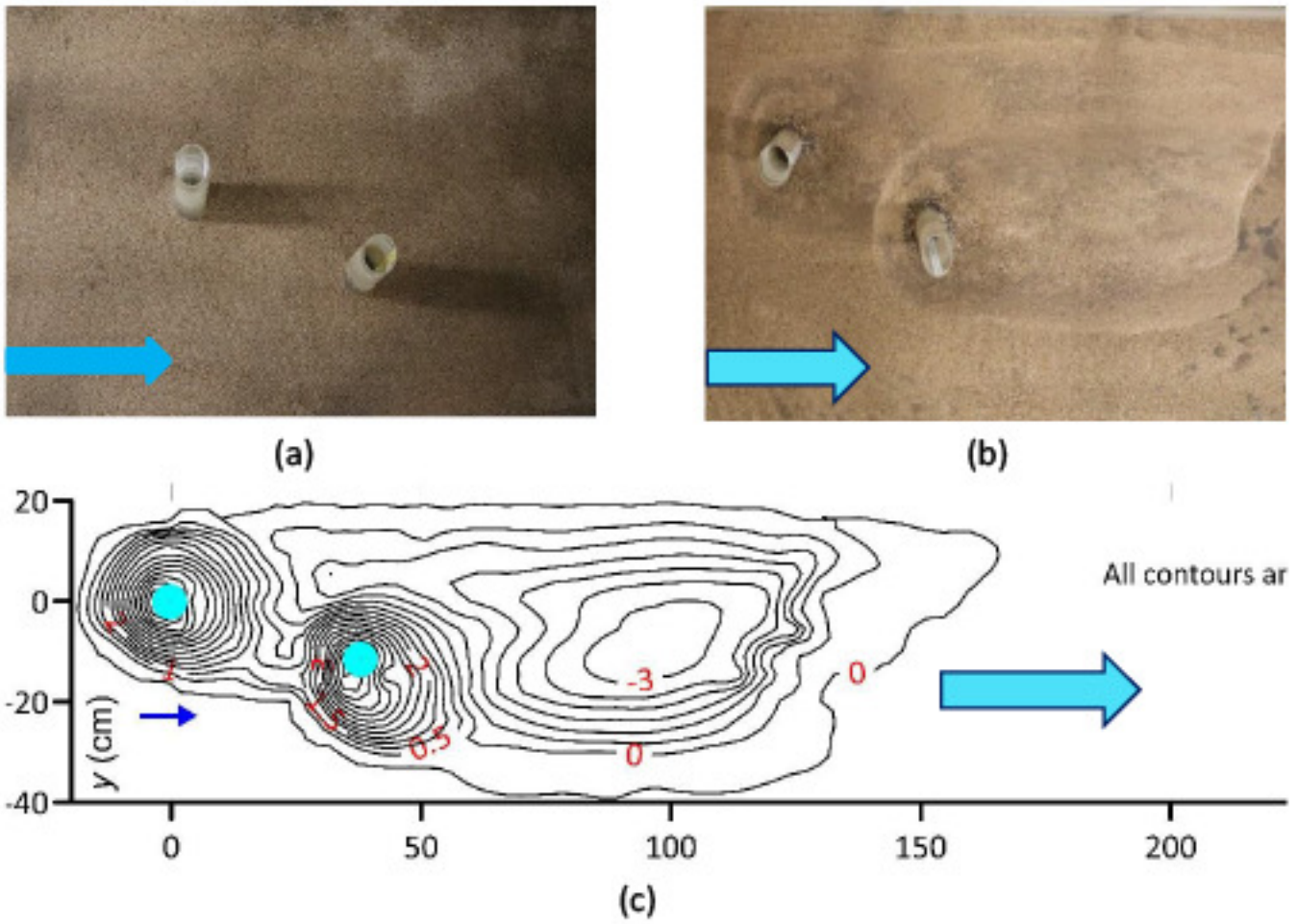
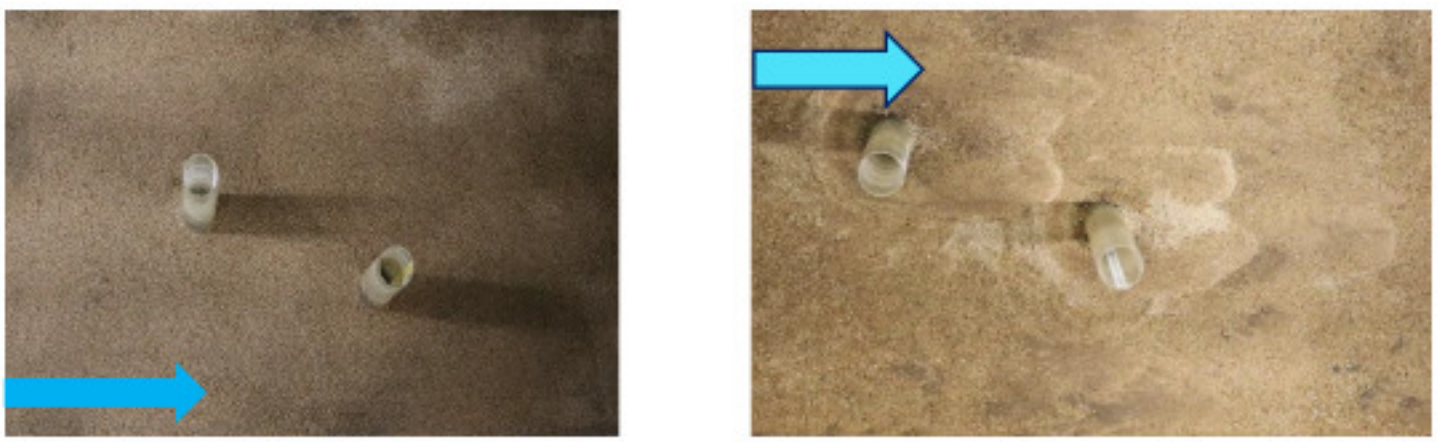



**Fig. 6.3** Experimental condition for experiment 3, $e = 2b$ b (a) Level bed, (b) Scour bed, (c) Contour Map.

The frequency of recording the scour depths was increased with the passing of each hour. It was observed that the maximum scour depth in this experiment was very close to the previous experiment i.e., $e = 2\,b$. The scour depth observed at the front pier was **7.03 cm** and that at the eccentric pier was **6.78 cm**, after the completion of the experiment.

### 6.1.4 Experiment No. 4

This experiment was conducted for an eccentricity of $2b$ for 9 hours. The values of subsequent scour depths were recorded with the help of the laser distance meter.



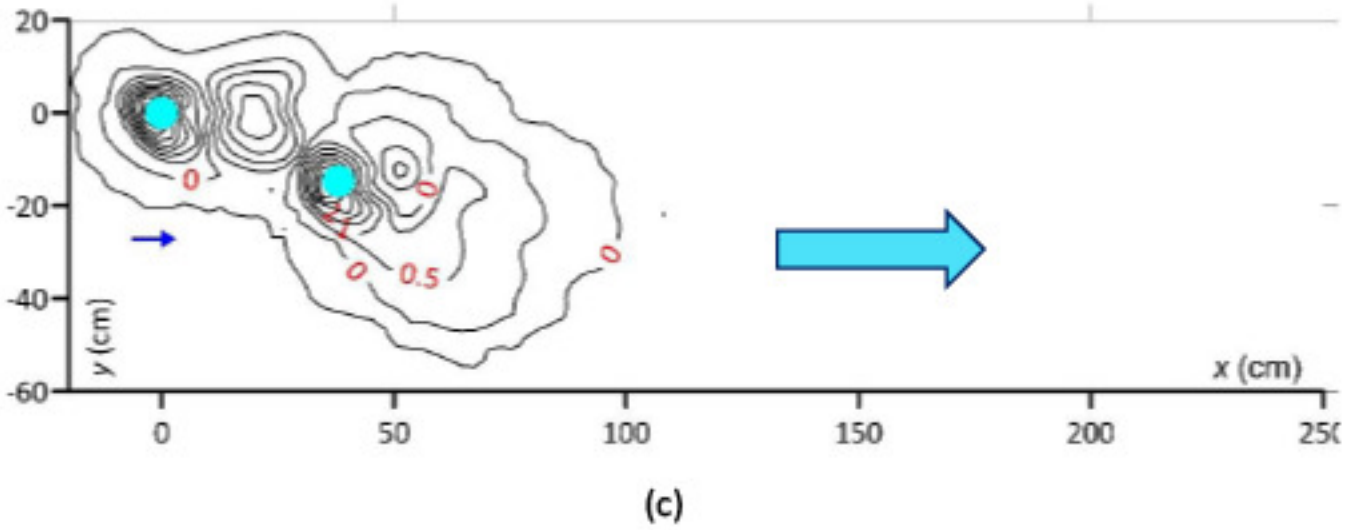



**Fig. 6.4** Experimental condition for experiment 4, $e = 2b$ b (a) Level bed, (b) Scour bed, (c) Contour Map.

The frequency of recording the scour depths was increased with the passing of each hour. The scour depth observed at the front pier was **3.91 cm** and that at the eccentric pier was **3.37cm**, after the completion of the experiment.

### 6.1.5 Experiment No. 5

This experiment was conducted for an eccentricity of $2b$ for 4 hours. The values of subsequent scour depths were recorded with the help of the laser distance meter. The frequency of recording the scour depths was increased with the passing of each hour.

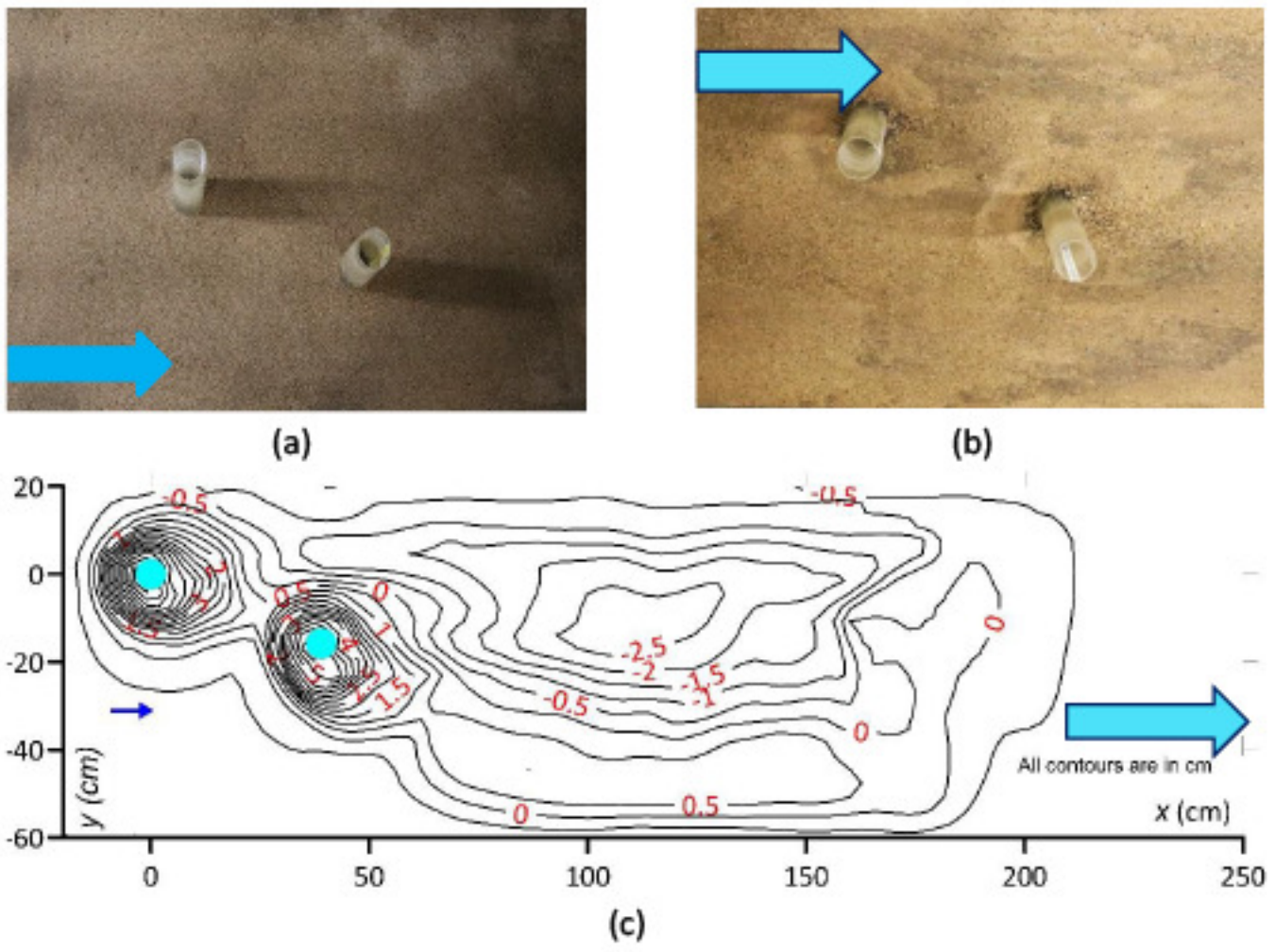



**Fig. 6.5** Experimental condition for experiment 5, $e = 2.25b$ b (a) Level bed, (b) Scour bed, (c) Contour Map.

The maximum scour depth observed at the front pier was **6.7 cm** and that at the eccentric pier was **6.71 cm**, after the completion of the experiment.

### 6.1.6 Experiment No. 6

This experiment was conducted for an eccentricity of $2.25b$ for 9 hours. The values of subsequent scour depths were recorded with the help of the laser distance meter.

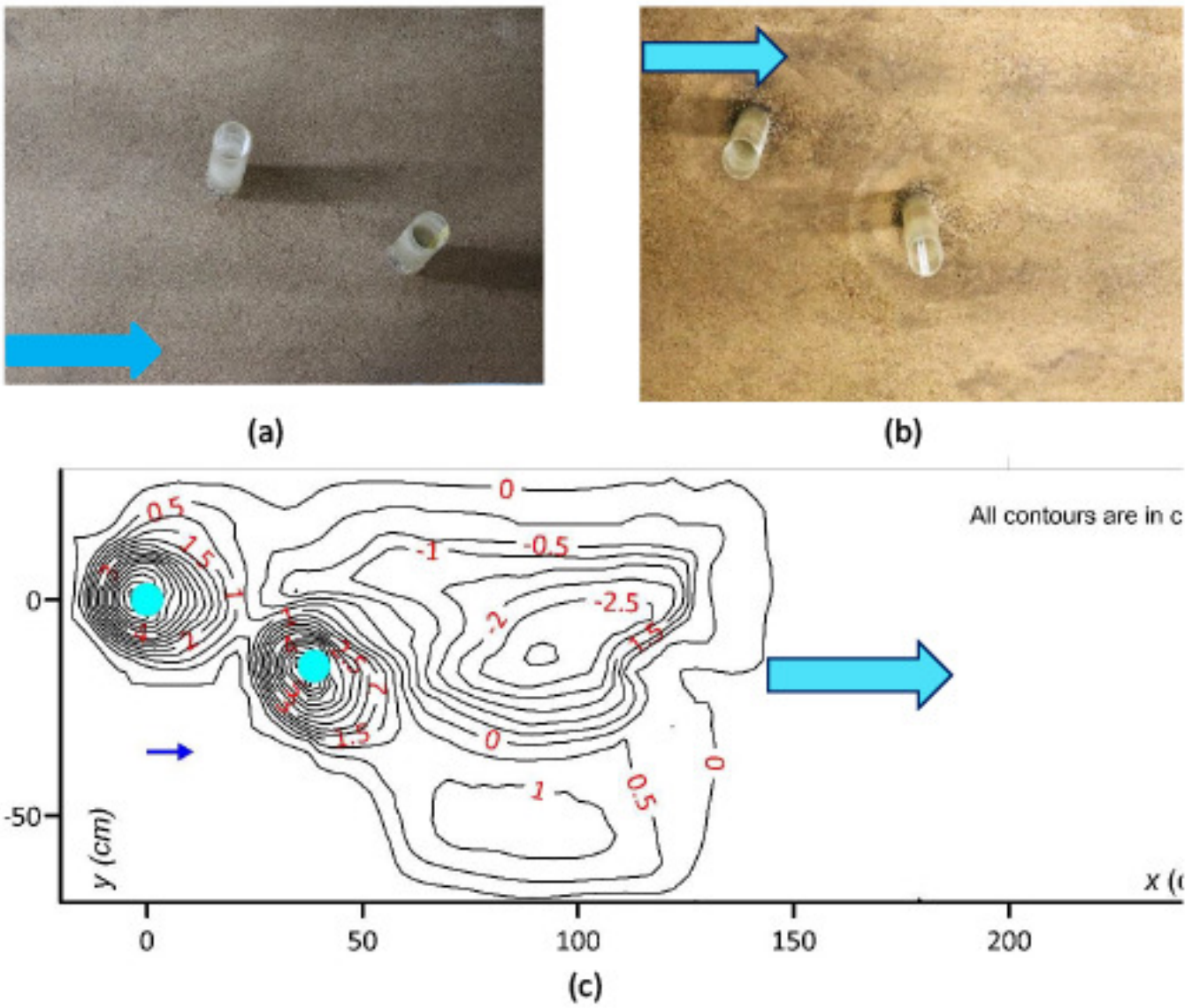



**Fig. 6.6** Experimental condition for experiment 6, $e = 2.25b$, (a) Level bed, (b) Scour bed, (c) Contour Map.

The frequency of recording the scour depths was increased with the passing of each hour. The maximum scour depth observed at the front pier was **6.92 cm** and that at the eccentric pier was **6.74 cm**, after the completion of the experiment.

### 6.1.7 Experiment No. 7

This experiment was conducted for an eccentricity of $2.25b$ for 9 hours. The values of subsequent scour depths were recorded with the help of the laser distance meter.

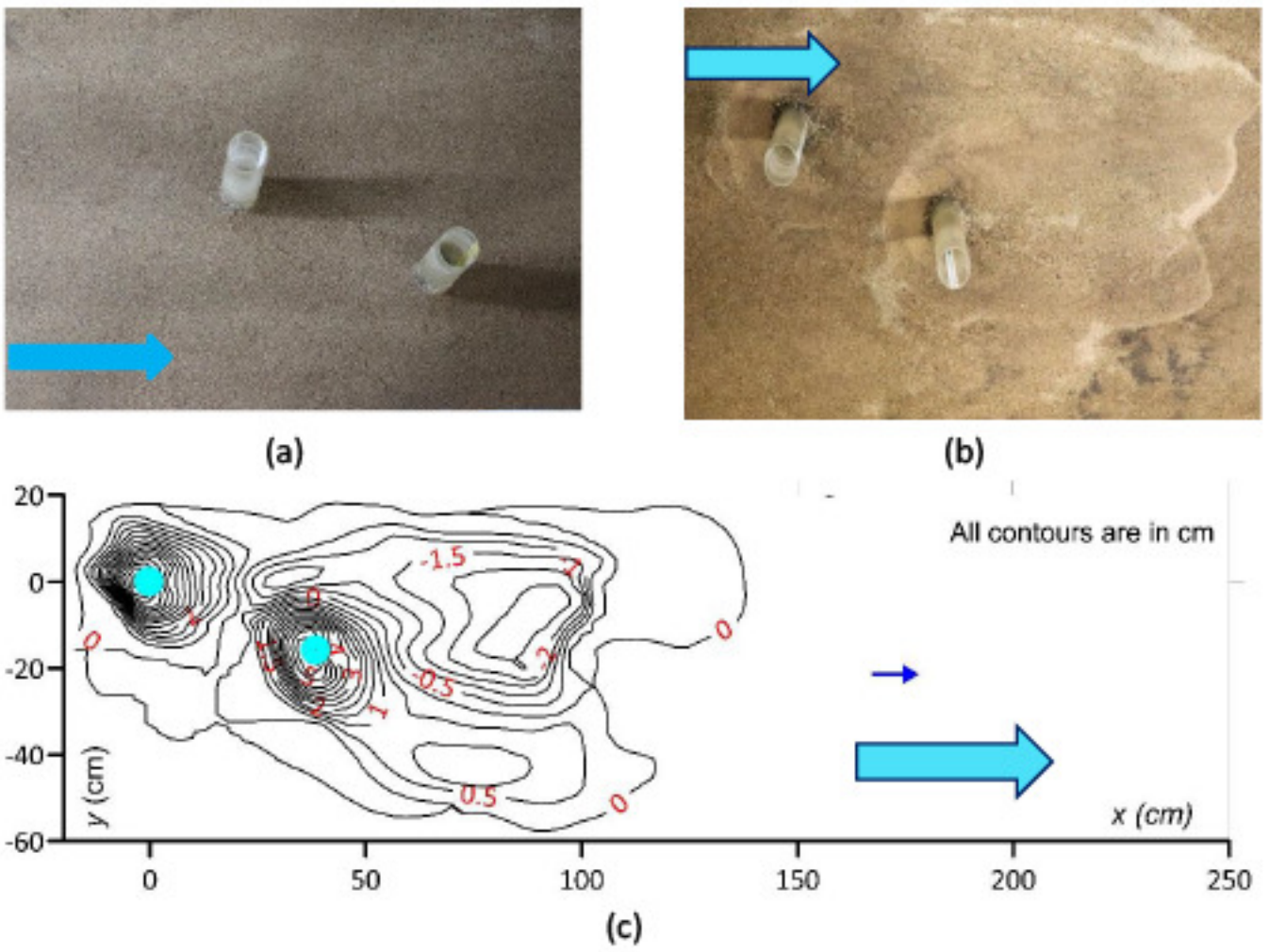



**Fig. 6.7** Experimental condition for experiment 7, $e = 2.25b$, (a) Level bed, (b) Scour bed, (c) Contour Map.

The values of subsequent scour depths were recorded with the help of the laser distance meter. The frequency of recording the scour depths was increased with the passing of each hour. It was observed that the scour depth for both the piers, in this case, was maximum among the series of experiments conducted. The scour depth observed at the front pier was **7.12 cm** and that at the eccentric pier was **6.4 cm**, after the completion of the experiment. The contour map was generated using surfer software. All the relevant results are given in Table 3.

### 6.1.8 Experiment No. 8

This experiment was conducted for an eccentricity of $2.25b$ for 6 hours. The values of subsequent scour depths were recorded with the help of the laser distance meter. The frequency of recording the scour depths was increased with the passing of each hour.

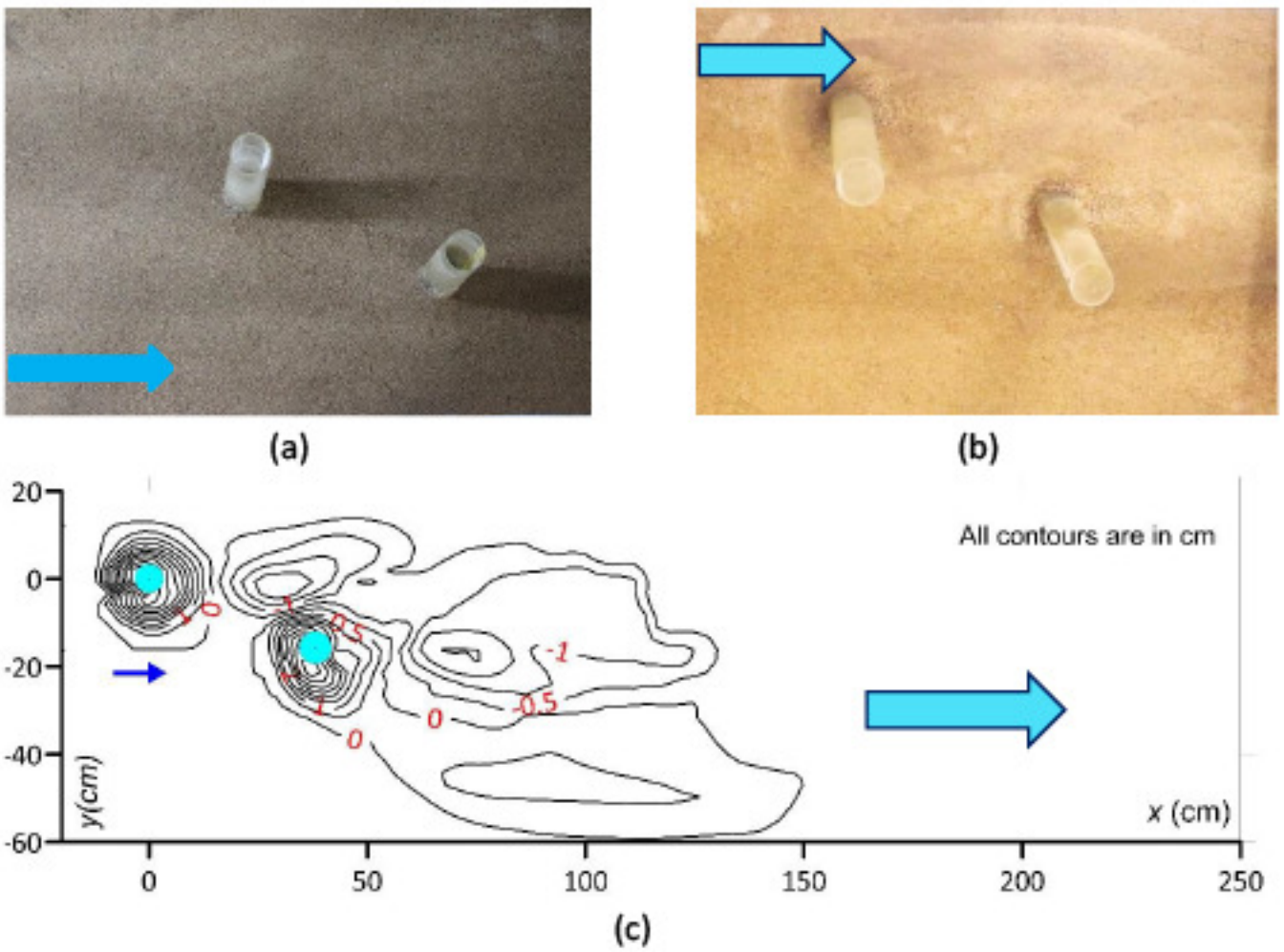
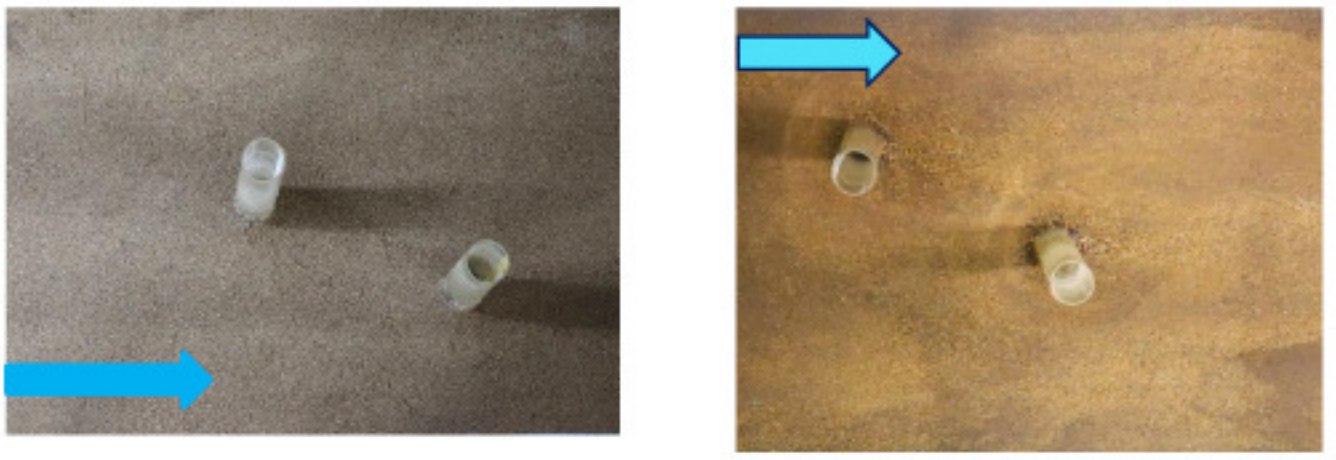



**Fig. 6.8** Experimental condition for experiment 8, $e = 2.25b$, (a) Level bed, (b) Scour bed, (c) Contour Map.

The scour depth observed at the front pier was **4.84 cm** and that at the eccentric pier was **4.65 cm**, after the completion of the experiment surfer software was used to generate contour maps.

### 6.1.9 Experiment No. 9

This experiment was conducted for an eccentricity of $2.5b$ for 6 hours. The values of subsequent scour depths were recorded with the help of the laser distance meter. The frequency of recording the scour depths was increased with the passing of each hour. It was observed that the maximum scour depth in this experiment was very close to the previous experiment i.e., $e = 2.5\ b$.



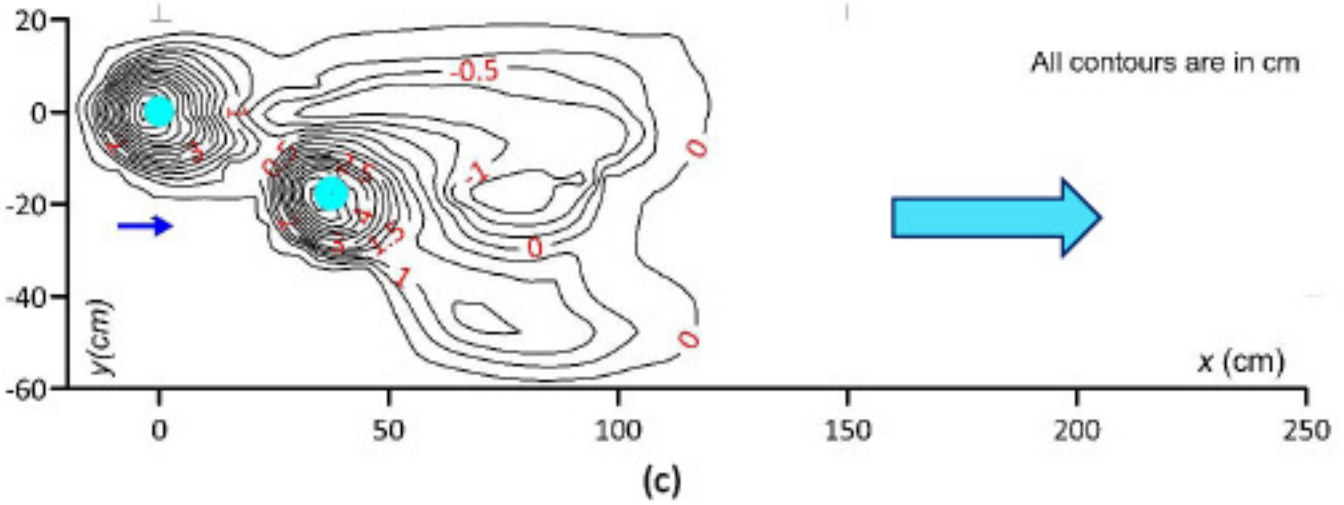



**Fig. 6.9** Experimental condition for experiment 9, $e = 2.25b$, (a) Level bed, (b) Scour bed, (c) Contour Map.

The scour depth observed at the front pier was **6.48 cm** and that at the eccentric pier was **6.37 cm**, after the completion of the experiment.

### 6.1.10 Experiment No. 10

This experiment was conducted for an eccentricity of $2.5b$ for 8 hours. The values of subsequent scour depths were recorded with the help of the laser distance meter.

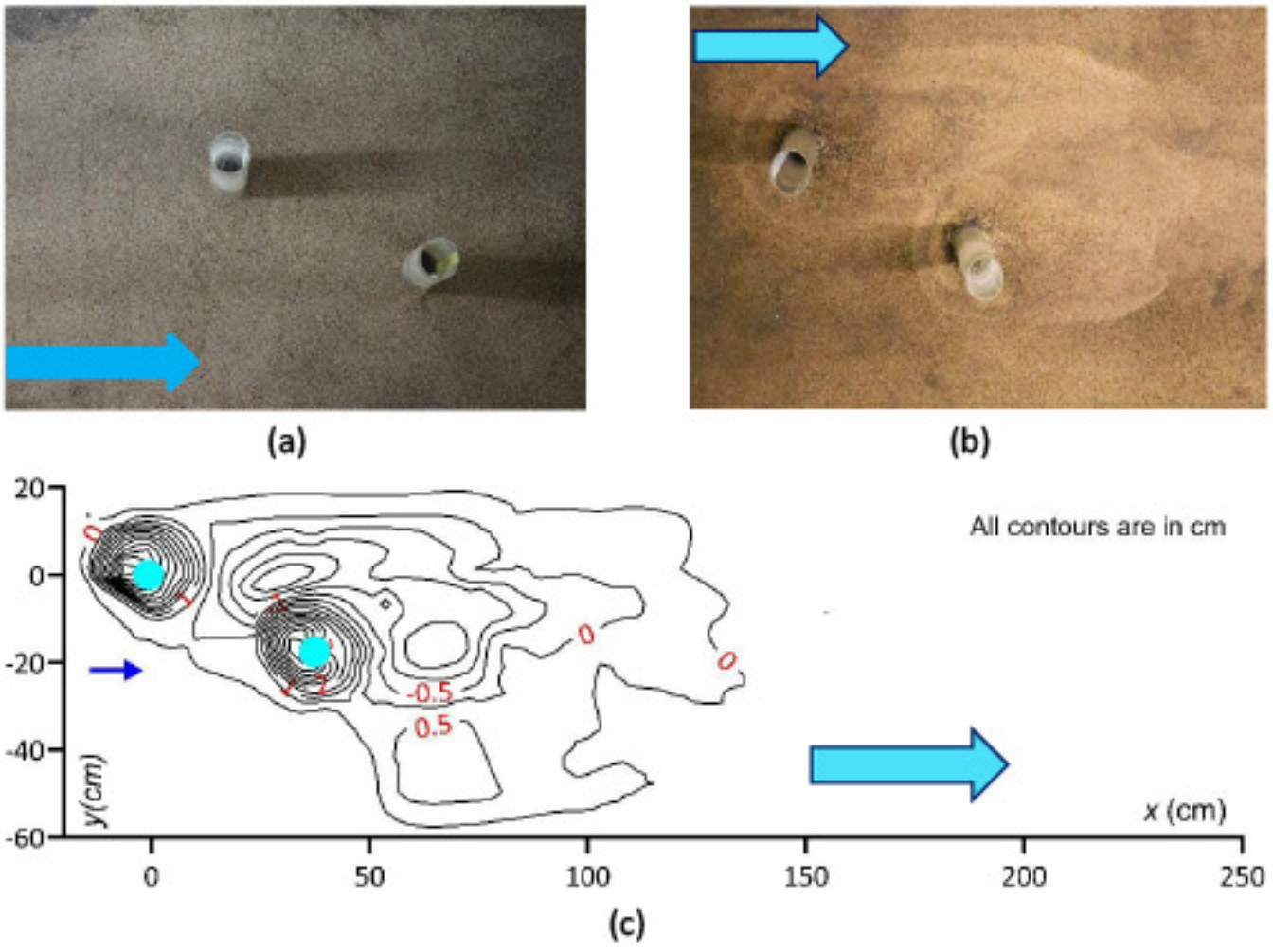



**Fig. 6.10** Experimental condition for experiment 10, $e = 2.5b$, (a) Level bed, (b) Scour bed, (c) Contour Map.

The frequency of recording the scour depths was increased with the passing of each hour. The scour depth observed at the front pier was **5.38 cm** and that at the eccentric pier was **4.72 cm**, after the completion of the experiment.

### 6.1.11 Experiment No. 11

This experiment was conducted for an eccentricity of 2.5*b* for 8 hours. The values of subsequent scour depths were recorded with the help of the laser distance meter.

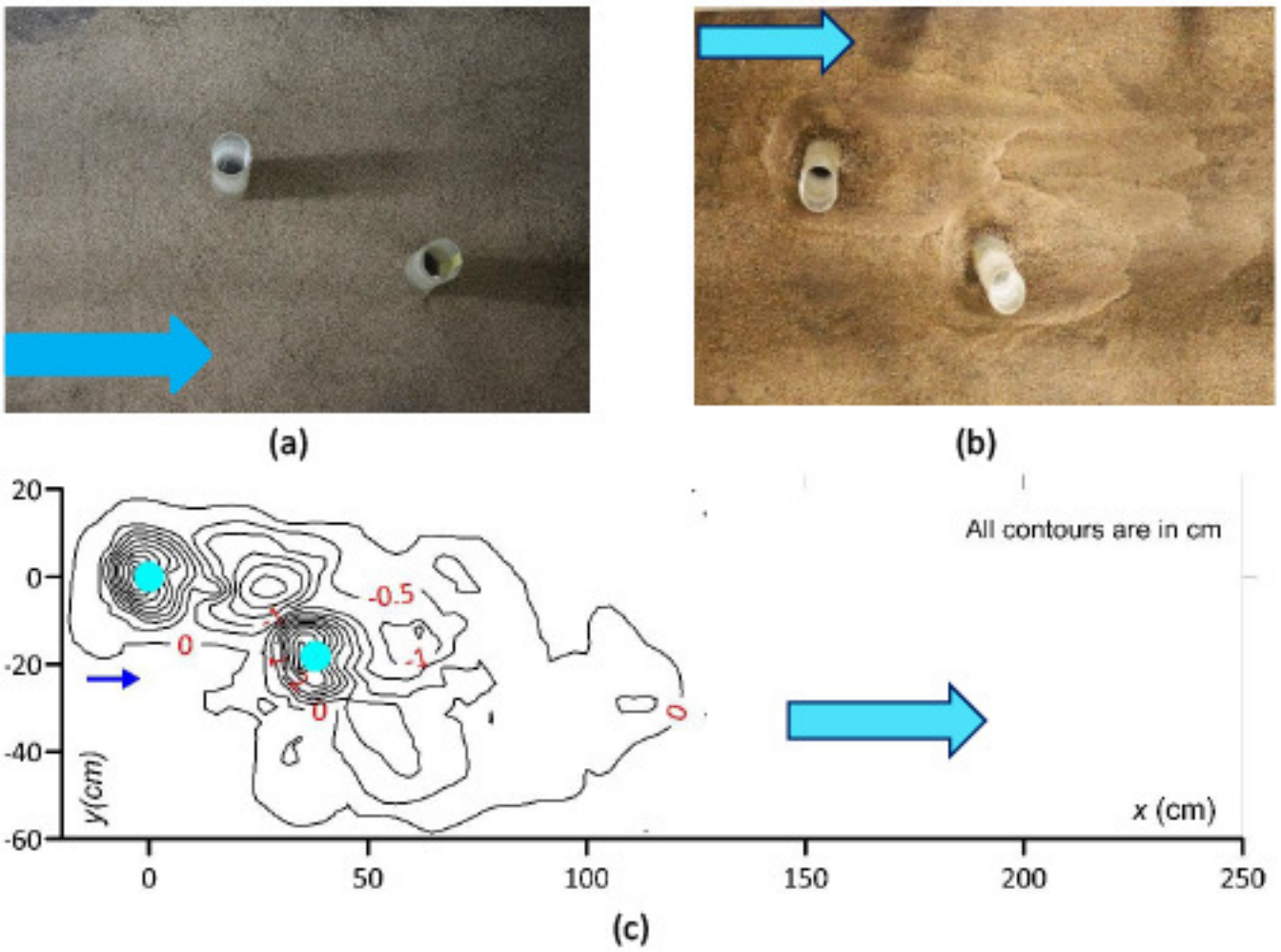



**Fig. 6.11** Experimental condition for experiment 11, $e = 2.5b$, (a) Level bed, (b) Scour bed, (c) Contour Map.

The frequency of recording the scour depths was increased with the passing of each hour. The scour depth observed at the front pier was **4.14 cm** and that at the eccentric pier was **3.16 cm**, after the completion of the experiment.

### 6.1.12 Experiment No. 12

This experiment was conducted for an eccentricity of 2.5*b* for 10 hours. The values of subsequent scour depths were recorded with the help of the laser distance meter.

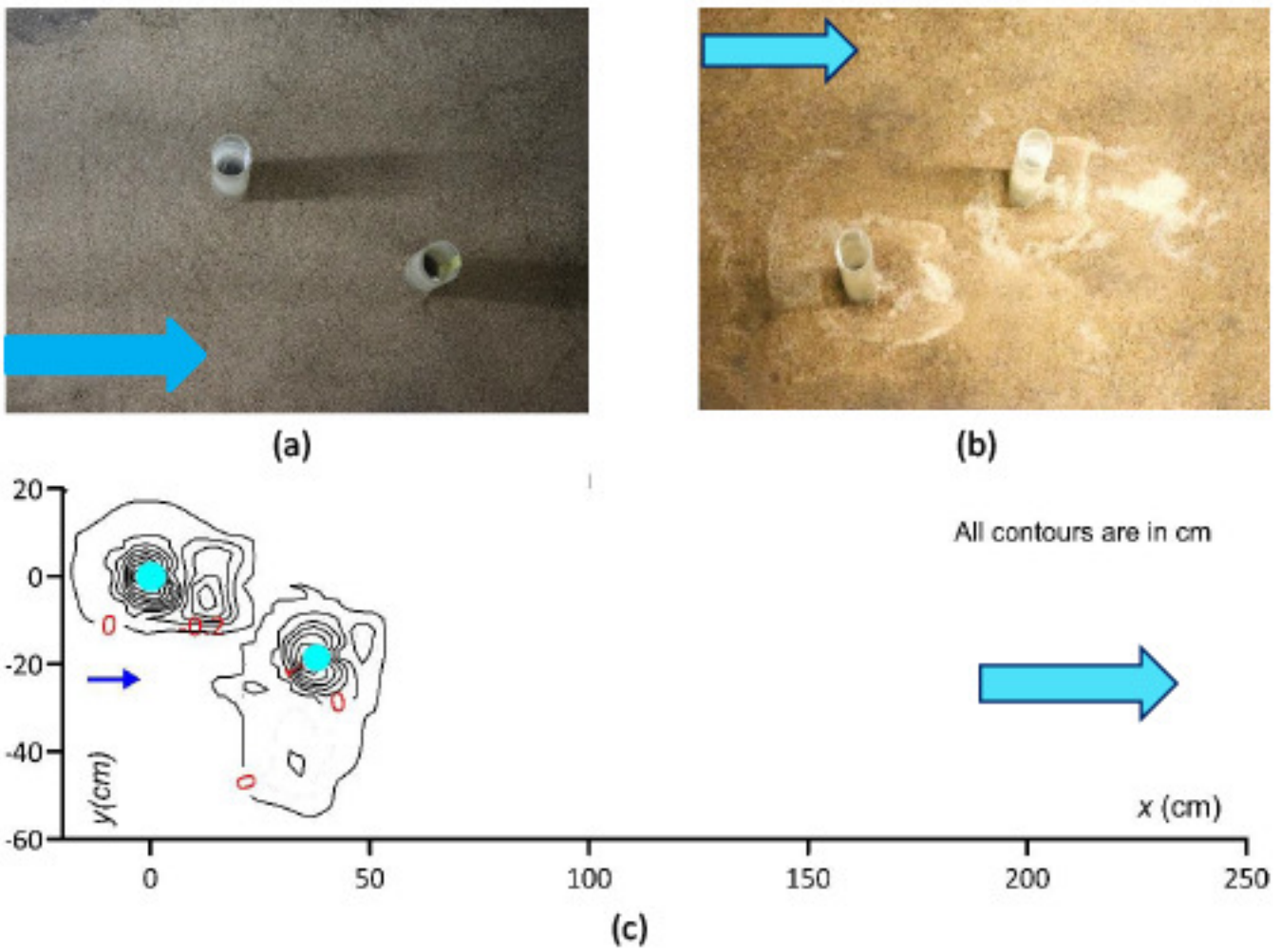
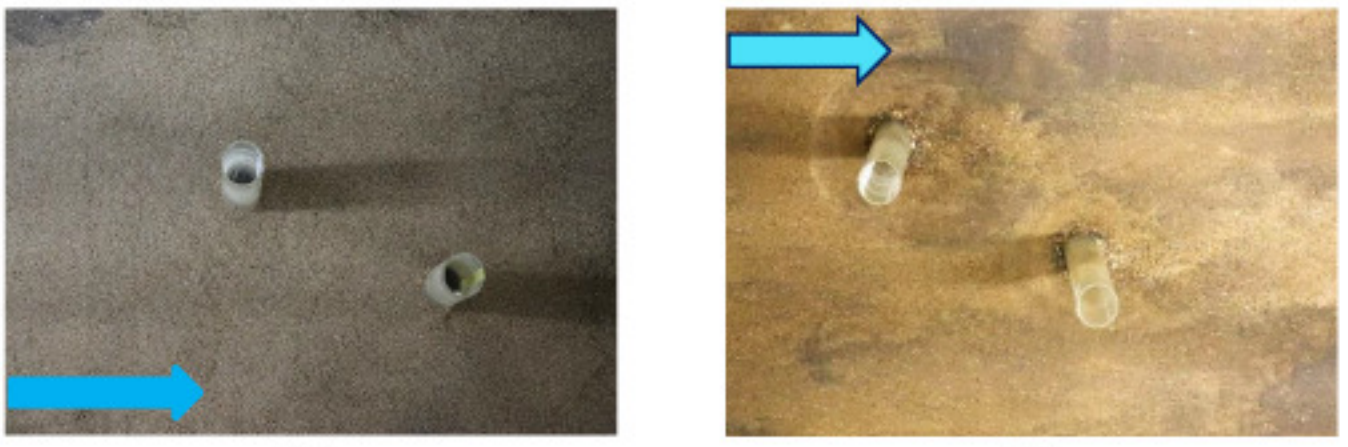



**Fig. 6.12** Experimental condition for experiment 12, $e = 2.5b$, (a) Level bed, (b) Scour bed, (c) Contour Map.

The frequency of recording the scour depths was increased with the passing of each hour. The scour depth observed at the front pier was **2.22 cm** and that at the eccentric pier was **2.39 cm**, after the completion of the experiment.

### 6.1.13 Experiment No. 13

This experiment was conducted for an eccentricity of $2.75b$ for 2.5 hours. The values of subsequent scour depths were recorded with the help of the laser distance meter.



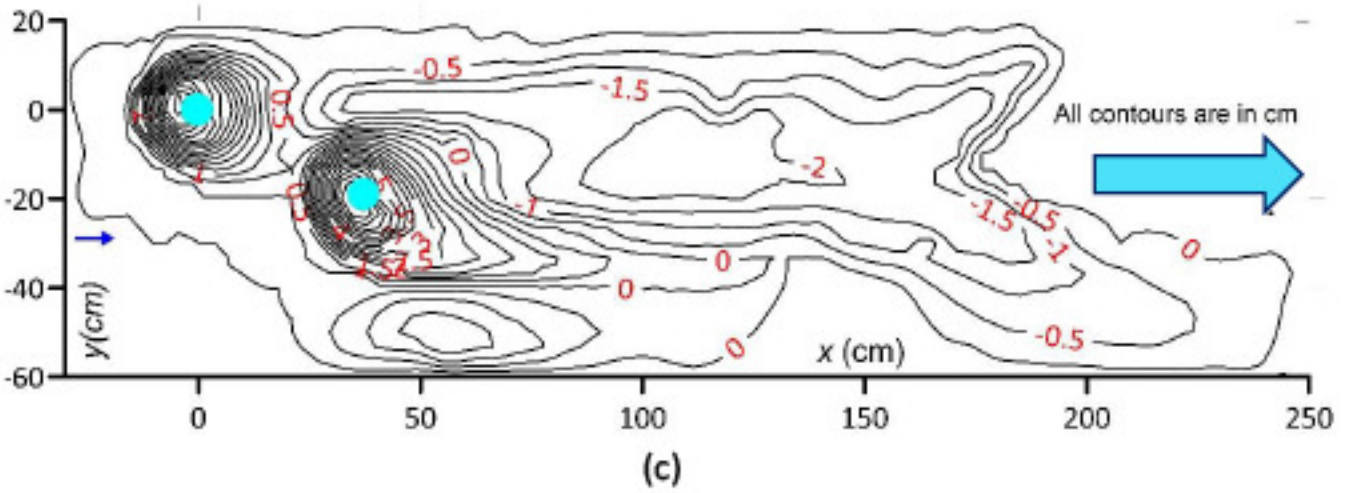



**Fig. 6.13** Experimental condition for experiment 13, $e = 2.75b$, (a) Level bed, (b) Scour bed, (c) Contour Map.

The frequency of recording the scour depths was increased with the passing of each hour. The scour depth observed at the front pier was **7.17 cm** and that at the eccentric pier was **7.71 cm**, after the completion of the experiment.

### 6.1.14 Experiment No. 14

This experiment was conducted for an eccentricity of $2.75b$ for 6 hours. The values of subsequent scour depths were recorded with the help of the laser distance meter.

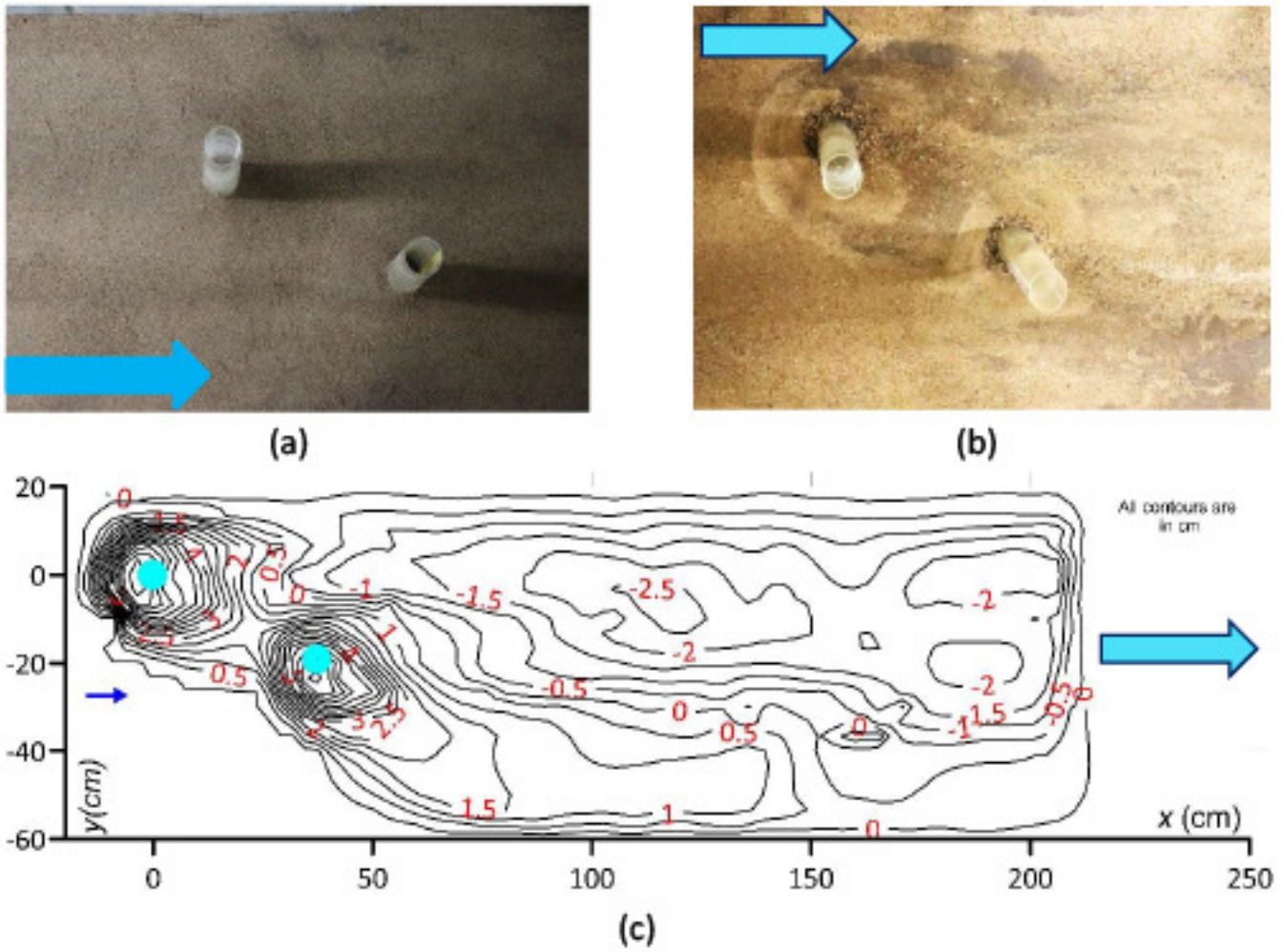



**Fig. 6.14** Experimental condition for experiment 14, $e = 2.75b$, (a) Level bed, (b) Scour bed, (c) Contour Map.

The frequency of recording the scour depths was increased with the passing of each hour. The scour depth observed at the front pier was **7.81 cm** and that at the eccentric pier was **7.12 cm**, after the completion of the experiment.

### 6.1.12 Experiment No. 15

This experiment was conducted for an eccentricity of 3.5*b* for 7 hours. The values of subsequent scour depths were recorded with the help of the laser distance meter.

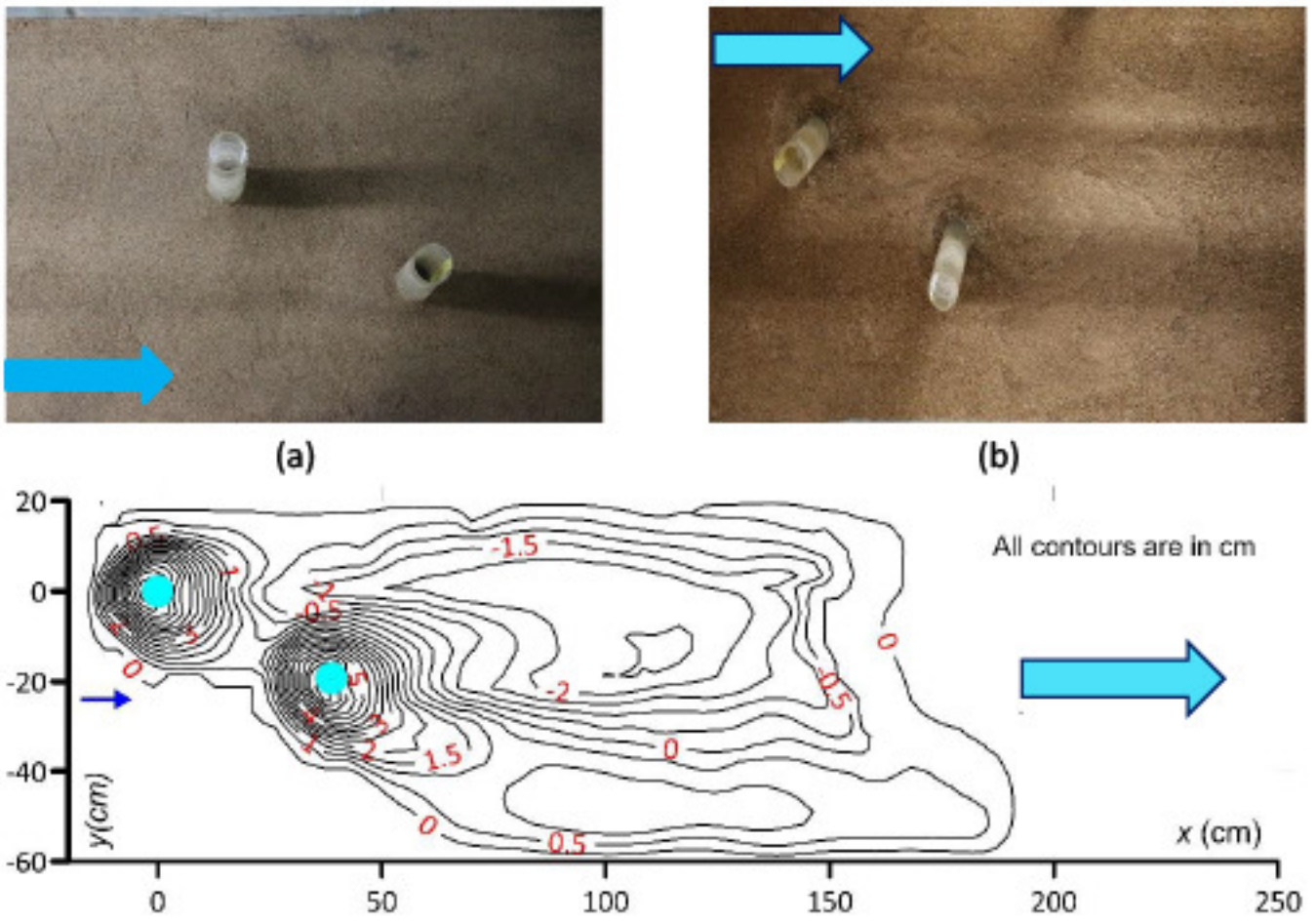



**Fig. 6.15** Experimental condition for experiment 15, $e = 2.75b$, (a) Level bed, (b) Scour bed, (c) Contour Map.

The frequency of recording the scour depths was increased with the passing of each hour. The scour depth observed at the front pier was **7.34 cm** and that at the eccentric pier was **7.86 cm**, after the completion of the experiment.

### 6.1.16 Experiment No. 16

This experiment was conducted for an eccentricity of 2.75*b* for 7 hours. The values of subsequent scour depths were recorded with the help of the laser distance meter.

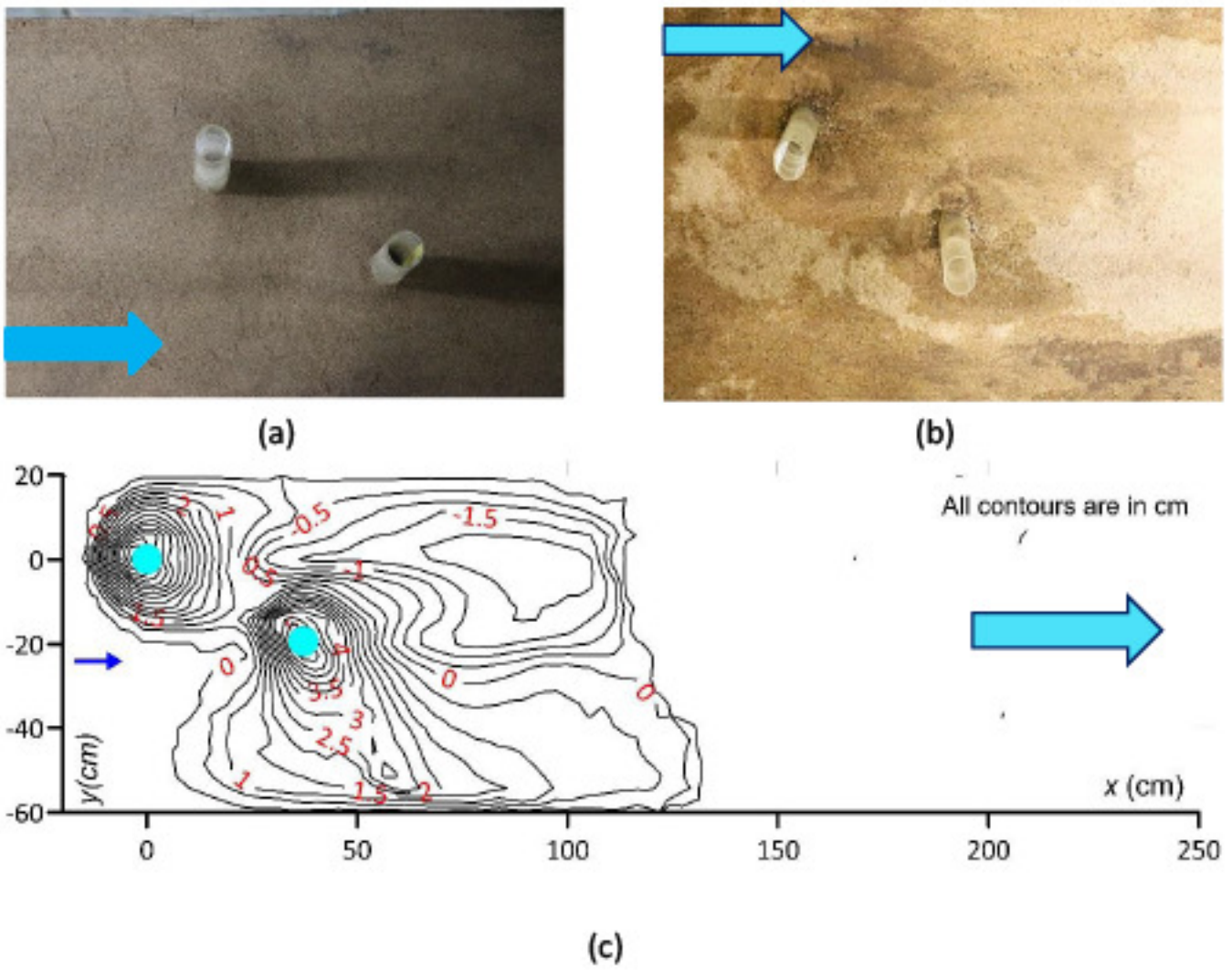
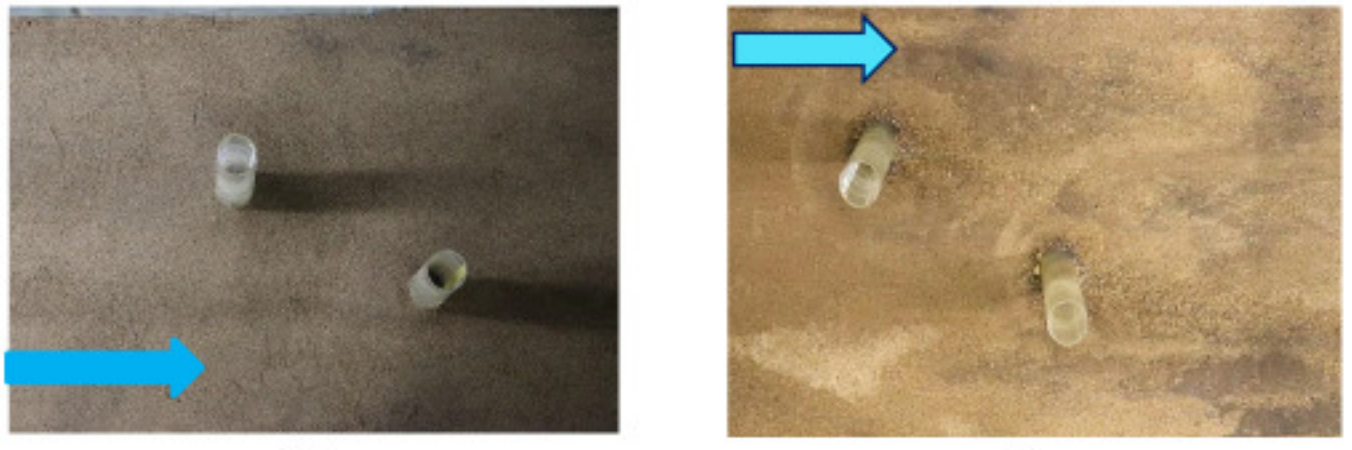



**Fig. 6.16** Experimental condition for experiment 16, $e = 2.75b$, (a) Level bed, (b) Scour bed, (c) Contour Map.

The frequency of recording the scour depths was increased with the passing of each hour. The scour depth observed at the front pier was **7.5 cm** and that at the eccentric pier was **6.75 cm**, after the completion of the experiment.

### 6.1.17 Experiment No. 17

This experiment was conducted for an eccentricity of $3b$ for 4 hours. The values of subsequent scour depths were recorded with the help of the laser distance meter.



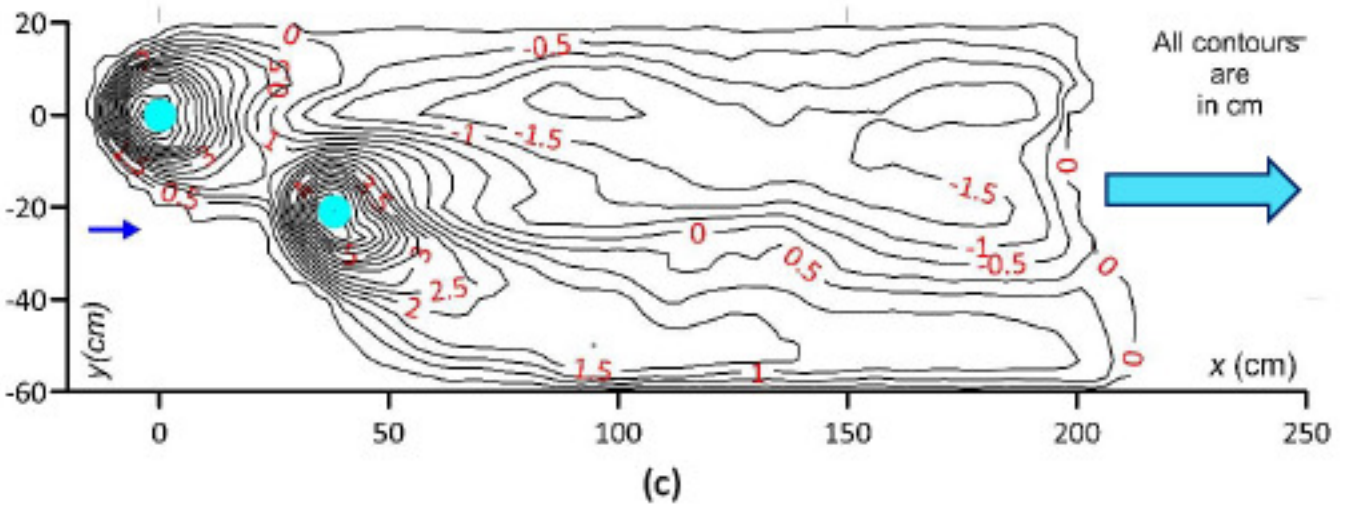



**Fig. 6.17** Experimental condition for experiment 17, $e = 3b$, (a) Level bed, (b) Scour bed, (c) Contour Map.

The frequency of recording the scour depths was increased with the passing of each hour. The scour depth observed at the front pier was **7.81 cm** and that at the eccentric pier was **7.55 cm**, after the completion of the experiment.

### 6.1.18 Experiment No. 18

This experiment was conducted for an eccentricity of $3b$ for 6 hours. The values of subsequent scour depths were recorded with the help of the laser distance meter.

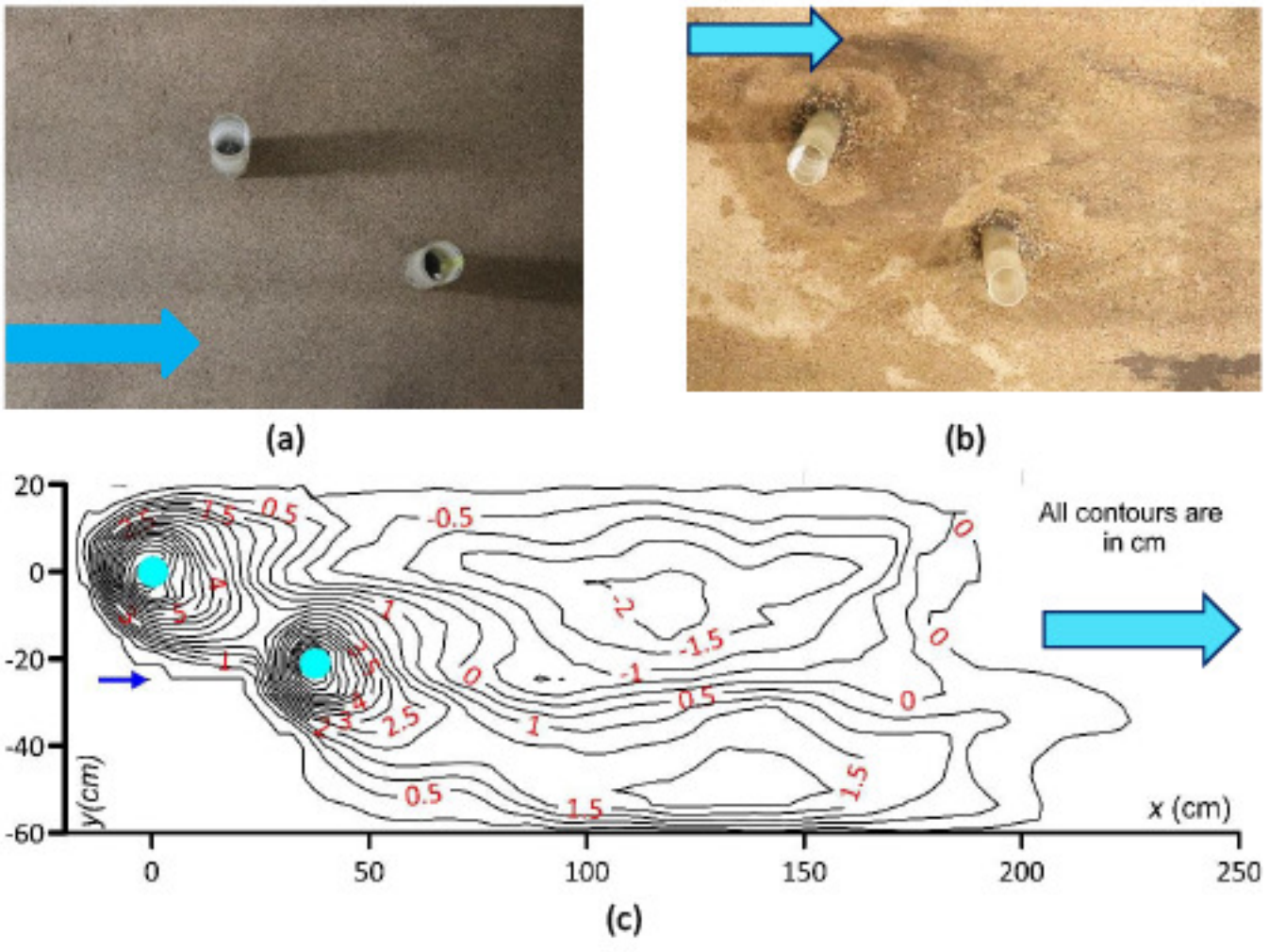



**Fig. 6.18** Experimental condition for experiment 18, $e = 3b$, (a) Level bed, (b) Scour bed, (c) Contour Map.

The frequency of recording the scour depths was increased with the passing of each hour. The scour depth observed at the front pier was **7.53 cm** and that at the eccentric pier was **7.41 cm**, after the completion of the experiment.

### 6.1.19 Experiment No. 19

This experiment was conducted for an eccentricity of 3*b* for 5 hours. The values of subsequent scour depths were recorded with the help of the laser distance meter.

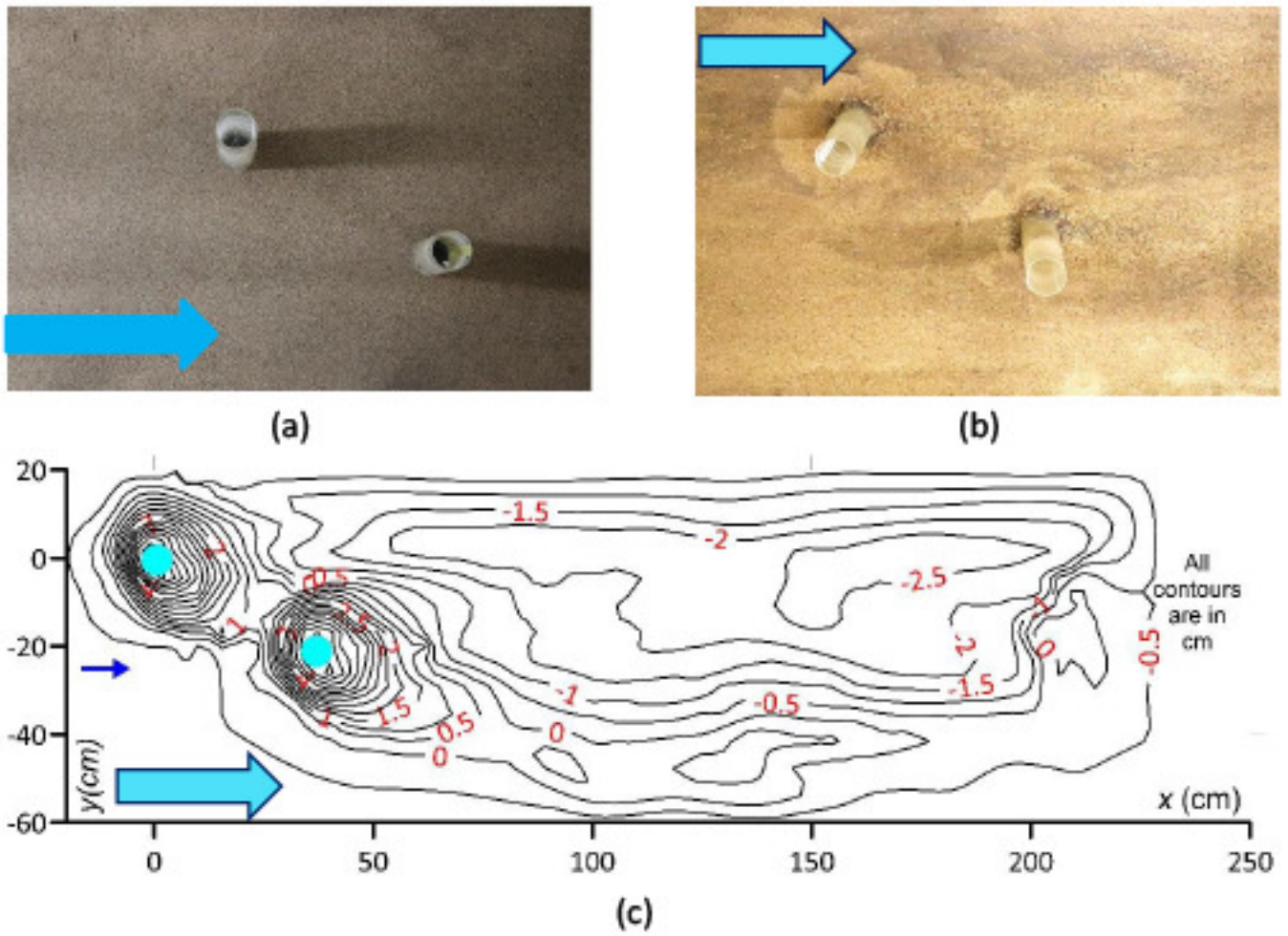



**Fig. 6.19** Experimental condition for experiment 19, $e = 3b$, (a) Level bed, (b) Scour bed, (c) Contour Map.

The frequency of recording the scour depths was increased with the passing of each hour. The scour depth observed at the front pier was **7.09 cm** and that at the eccentric pier was **6.95 cm**, after the completion of the experiment.

### 6.1.20 Experiment No. 20

This experiment was conducted for an eccentricity of 3*b* for 7 hours. The values of subsequent scour depths were recorded with the help of the laser distance meter.

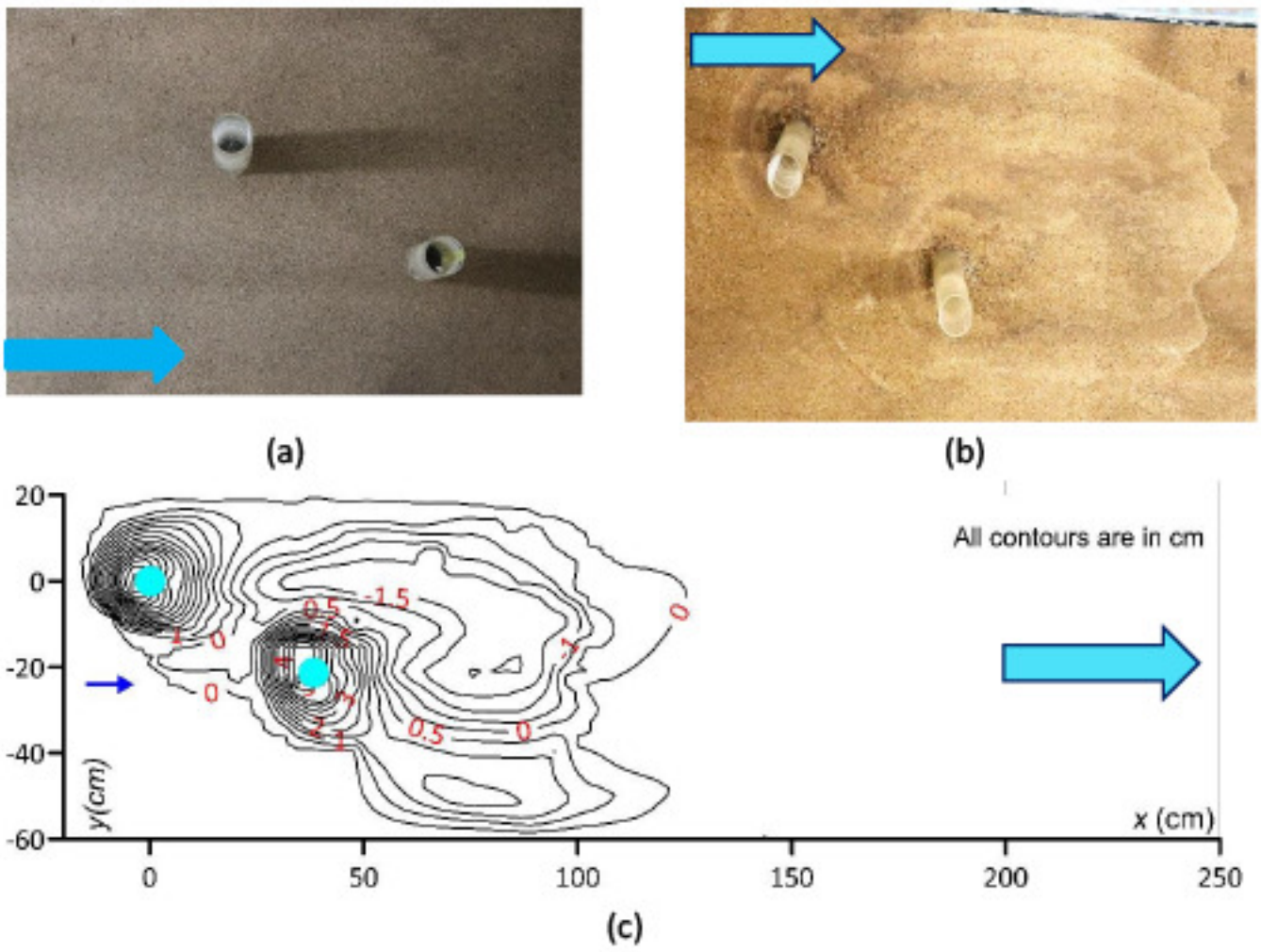
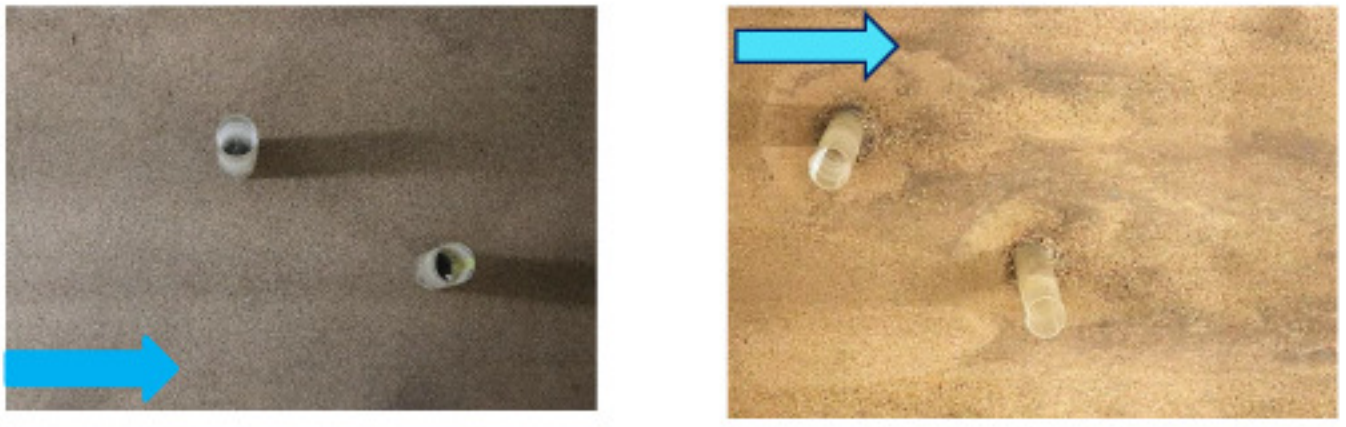



**Fig. 6.20** Experimental condition for experiment 19, $e = 3b$, (a) Level bed, (b) Scour bed, (c) Contour Map.

The frequency of recording the scour depths was increased with the passing of each hour. The scour depth observed at the front pier was **6.71 cm** and that at the eccentric pier was **5.01 cm**, after the completion of the experiment.

### 6.1.21 Experiment No. 21

This experiment was conducted for an eccentricity of $3.5b$ for 5 hours. The values of subsequent scour depths were recorded with the help of the laser distance meter.



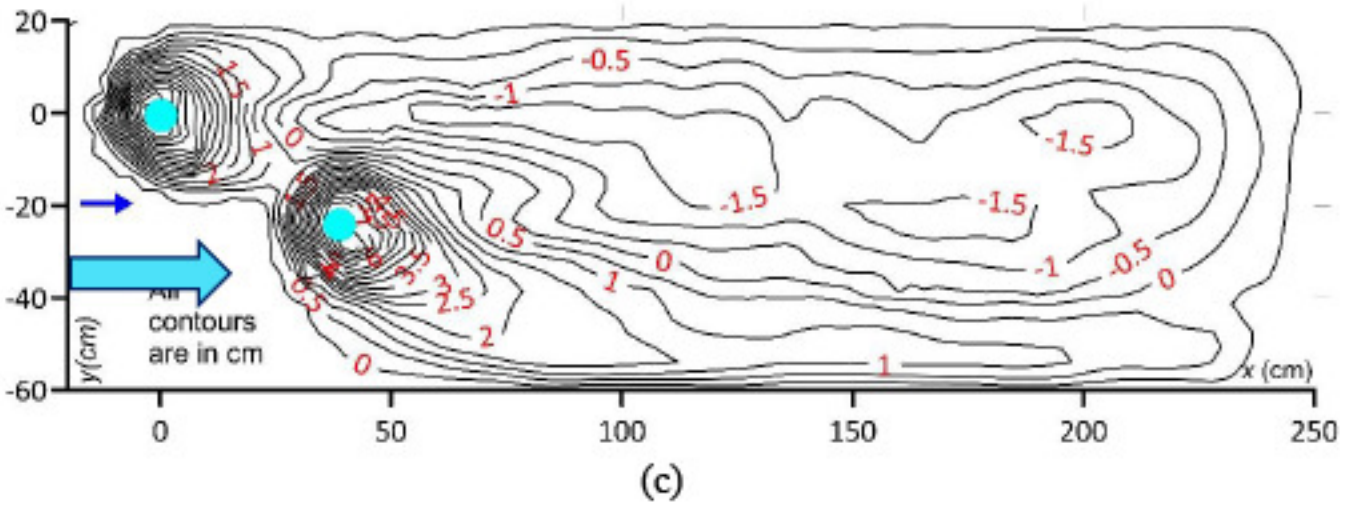



**Fig. 6.21** Experimental condition for experiment 19, $e = 3.5b$, (a) Level bed, (b) Scour bed, (c) Contour Map.

The frequency of recording the scour depths was increased with the passing of each hour. The scour depth observed at the front pier was **7.54 cm** and that at the eccentric pier was **7.19 cm**, after the completion of the experiment.

### 6.1.22 Experiment No. 22

This experiment was conducted for an eccentricity of $3.5b$ for 2.5 hours. The values of subsequent scour depths were recorded with the help of the laser distance meter.

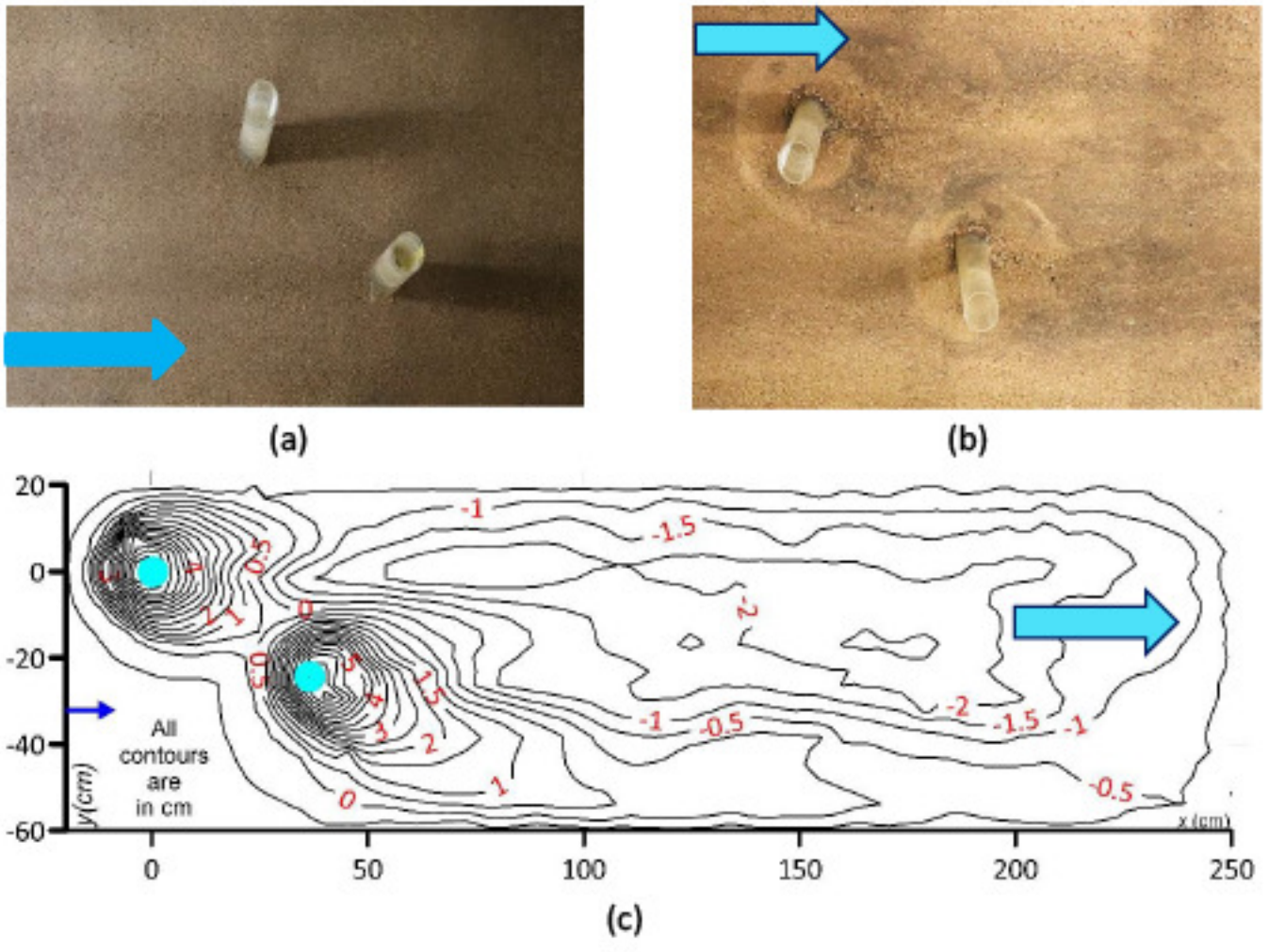



**Fig. 6.22** Experimental condition for experiment 22, $e = 3.5b$, (a) Level bed, (b) Scour bed, (c) Contour Map.

The frequency of recording the scour depths was increased with the passing of each hour. The scour depth observed at the front pier was **7.47 cm** and that at the eccentric pier was **7.38 cm**, after the completion of the experiment.

### 6.1.23 Experiment No. 23

This experiment was conducted for an eccentricity of 3.5*b* for 8 hours. The values of subsequent scour depths were recorded with the help of the laser distance meter.

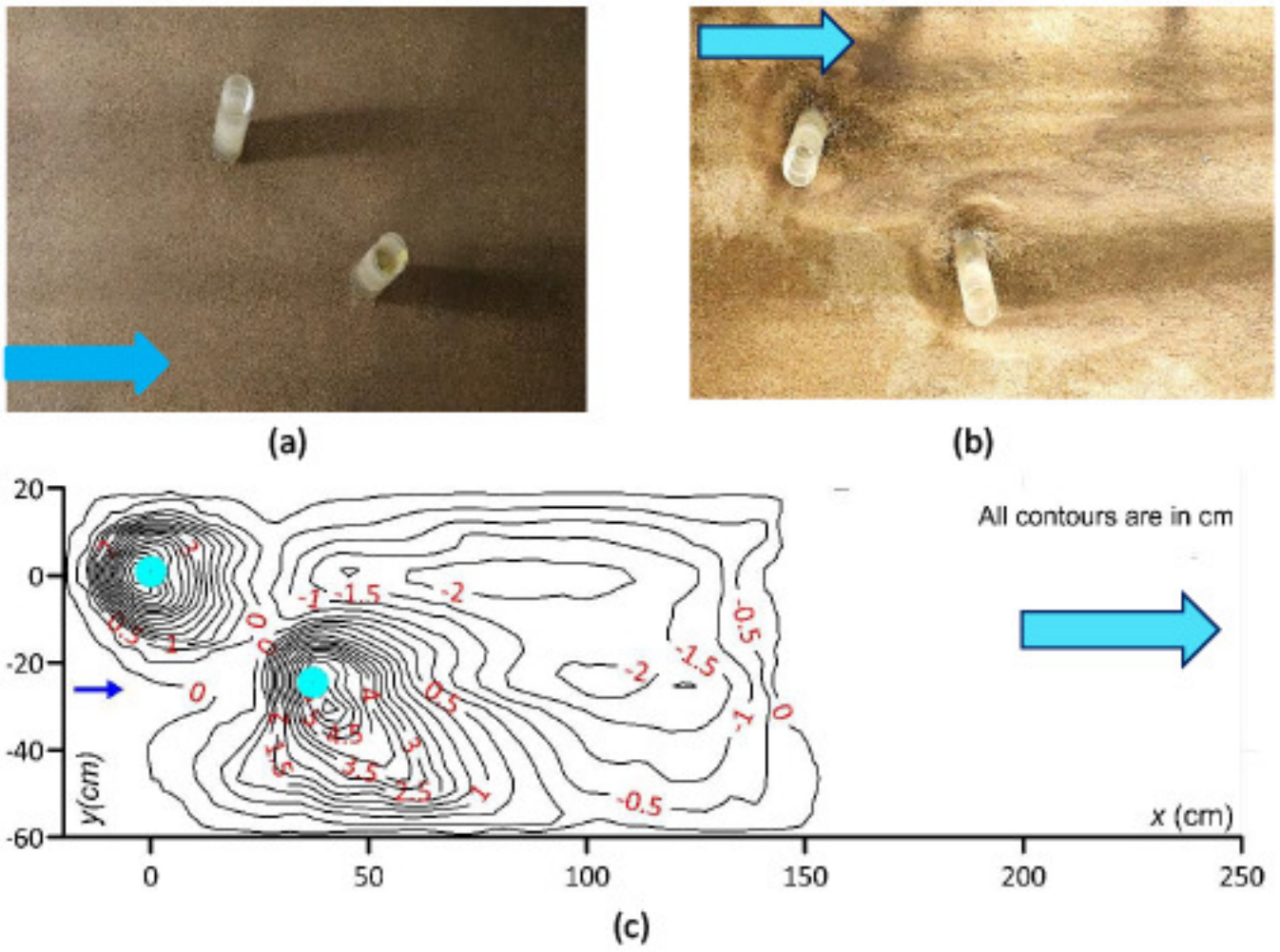



**Fig. 6.23** Experimental condition for experiment 23, $e = 3.5b$, (a) Level bed, (b) Scour bed, (c) Contour Map.

The frequency of recording the scour depths was increased with the passing of each hour. The scour depth observed at the front pier was **7.22 cm** and that at the eccentric pier was **6.09 cm**, after the completion of the experiment.

### 6.1.24 Experiment No. 24

This experiment was conducted for an eccentricity of 3.5*b* for 7 hours. The values of subsequent scour depths were recorded with the help of the laser distance meter.

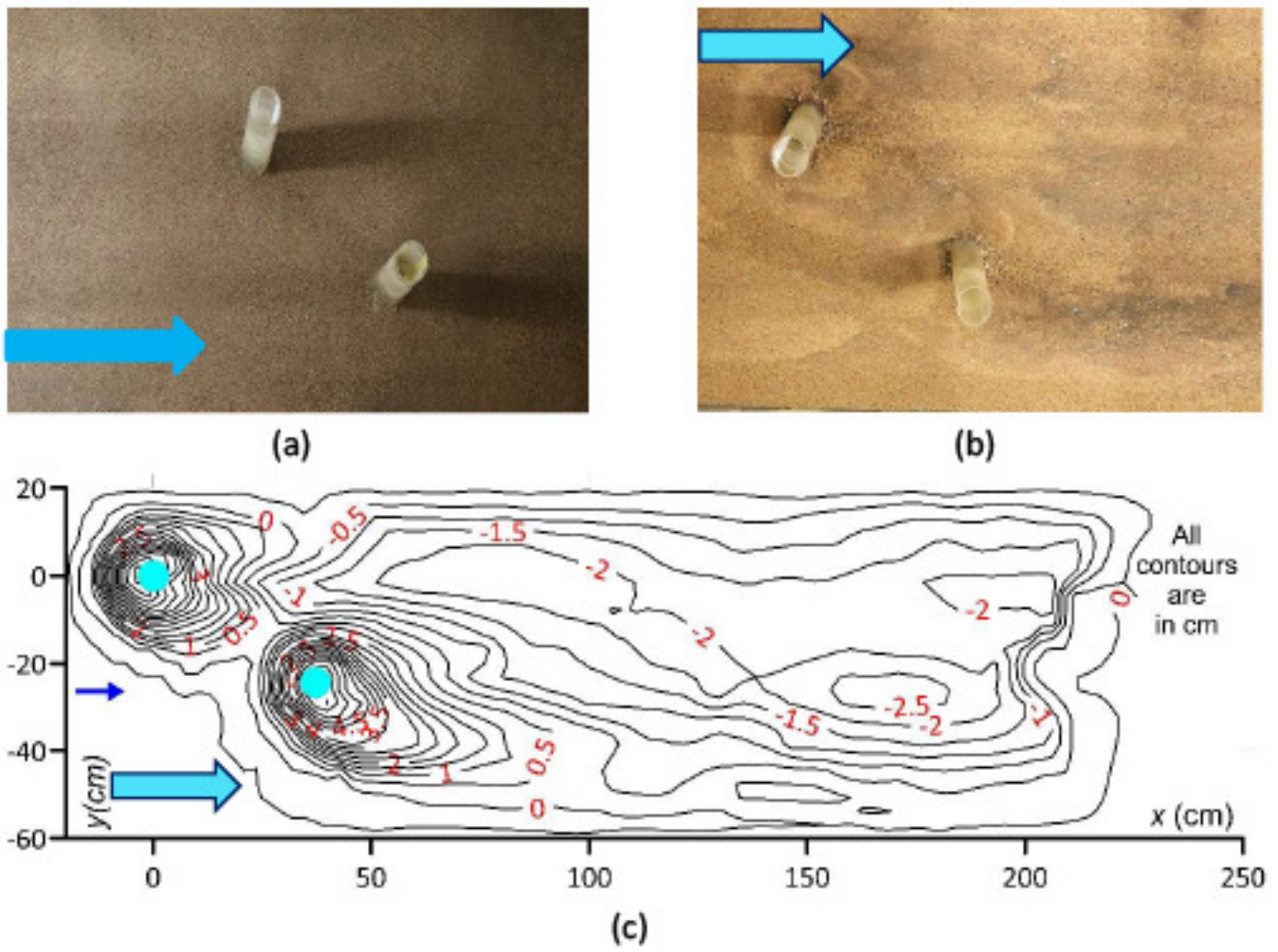



**Fig. 6.24** Experimental condition for experiment 24, $e = 3.5b$, (a) Level bed, (b) Scour bed, (c) Contour Map.

The frequency of recording the scour depths was increased with the passing of each hour. The scour depth observed at the front pier was **7.16 cm** and that at the eccentric pier was **7.2 cm**, after the completion of the experiment.

### 6.1.25. Experimental outcomes

Total 24 nos experimental outcomes are given in Table 6.2.

**Table 6.2:** Experimental outcomes

| Exp. No. | $e$ | b (cm) | $d_{sf}$ (cm) | $d_{se}$ (cm) | $l_s$ (cm) | $w_s$ (cm) | $a_{ps}$ ($cm^2$) | $a_{ss}$ ($cm^2$) | $V_s$ ($cm^3$) |
|---|---|---|---|---|---|---|---|---|---|
| 1 | 2*b* | 7 | 6.65 | 6.41 | 218 | 42 | 8252.34 | 8418.33 | 5727.39 |
| 2 | 2*b* | 7 | 7.44 | 6.66 | 165 | 48 | 9990.55 | 10195.56 | 10172.08 |
| 3 | 2*b* | 7 | 7.03 | 6.78 | 152 | 51 | 3800.94 | 3973.99 | 4788.54 |
| 4 | 2*b* | 7 | 3.91 | 3.37 | 81 | 39 | 6004.72 | 6076.55 | 1599.37 |
| 5 | 2.25*b* | 7 | 6.7 | 6.71 | 190 | 48 | 9491.16 | 9491.16 | 7680.39 |
| 6 | 2.25*b* | 7 | 6.92 | 6.74 | 150 | 48 | 7223.02 | 7412.43 | 7486.13 |
| 7 | 2.25*b* | 7 | 7.12 | 6.4 | 124 | 48 | 7901.09 | 8098.93 | 6307.96 |
| 8 | 2.25*b* | 7 | 4.84 | 4.65 | 136 | 42 | 8008.75 | 8115.60 | 3113.44 |
| 9 | 2.5*b* | 7 | 6.48 | 6.37 | 123 | 48 | 9114.67 | 9304.51 | 6747.34 |
| 10 | 2.5*b* | 7 | 5.38 | 4.72 | 115 | 45 | 7183.83 | 7307.38 | 2957.47 |
| 11 | 2.5*b* | 7 | 4.14 | 3.56 | 92 | 42 | 5677.48 | 5755.58 | 1720.48 |

| | | | | | | | | | |
|---|---|---|---|---|---|---|---|---|---|
| 12 | 2.5*b* | 7 | 2.22 | 2.39 | 66 | 36 | 6610.46 | 6645.19 | 862.73 |
| 13 | 2.75*b* | 7 | 7.17 | 7.71 | 222 | 54 | 9925.33 | 10171.63 | 6877.98 |
| 14 | 2.75*b* | 7 | 7.81 | 7.12 | 227 | 54 | 8977.32 | 9253.45 | 10914.28 |
| 15 | 2.75*b* | 7 | 7.34 | 6.86 | 187 | 54 | 7863.91 | 8098.82 | 8511.05 |
| 16 | 2.75*b* | 7 | 7.5 | 6.75 | 148 | 51 | 12847.12 | 13072.10 | 9916.03 |
| 17 | 3*b* | 7 | 7.81 | 7.55 | 220 | 54 | 11158.82 | 11447.88 | 12998.70 |
| 18 | 3*b* | 7 | 7.53 | 7.41 | 213 | 54 | 9153.30 | 9449.76 | 14327.87 |
| 19 | 3*b* | 7 | 7.09 | 6.95 | 227 | 60 | 4060.54 | 4249.34 | 5677.03 |
| 20 | 3*b* | 7 | 6.71 | 5.01 | 120 | 57 | 4554.09 | 4760.33 | 5615.80 |
| 21 | 3.5*b* | 7 | 7.54 | 7.19 | 227 | 60 | 12793.74 | 9803.89 | 10067.11 |
| 22 | 3.5*b* | 7 | 7.47 | 7.38 | 227 | 60 | 6827.46 | 7051.00 | 8492.55 |
| 23 | 3.5*b* | 7 | 7.22 | 6.09 | 168 | 60 | 9434.35 | 9633.96 | 10004.08 |
| 24 | 3.5*b* | 7 | 7.16 | 7.2 | 227 | 60 | 9539.31 | 9777.70 | 9205.75 |

Note: $e$ = eccentricity; $d_{sf}$- front pier scour depth; $d_{se}$- eccentric pier scour depth; $l_s$- scour lengh; $w_s$- scour width; $a_{ps}$- planer surface area of scour hole; $a_{ss}$-surface area of scour hole; $V_s$- volume of scour hole.

### 6.1.26 Comparison of maximum scour depths

The maximum scour depth, which differs from the equilibrium scour depth, occurs after the experimental run. Our major goal is to examine the impacts of eccentricity on scour, hence experimental duration was reduced to 2.5 to 10 hours for the experiments depending their condition. Equilibrium scour depth occurs asymptotically with time, but theoretically, it will require infinite time to reach the equilibrium state.

For all the experiments, the maximum scour depth was recorded after the experimental stipulated duration mentioned above. The inflow depth varies from 12.60 to 15.75 cm. The variation of scour depth for the front and eccentric pier is shown in Fig. 6.25.

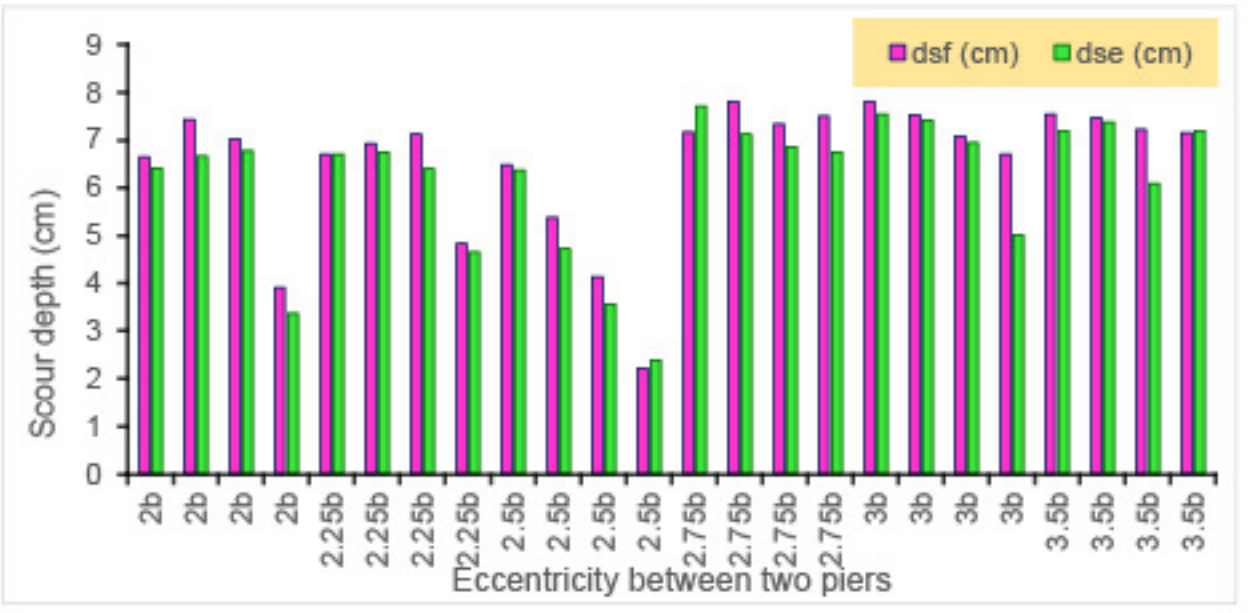



**Fig. 6.25** Maximum scour depth for all experiments

The experiment with the eccentricity of 2.5*b* had the lowest maximum scour depth with respect to other experiments, whereas the experiment with the eccentricity of 2.75*b* and *3b* had the highest maximum scour depth.

### 6.1.27 Temporal evolution of scour depth

The evolution of instantons scour depth was measured physically with the help of a laser distance meter, after applying the refraction correction factor. It was observed that the 70-80 % scour occurred in the first 2-4 hours, which can be seen from the time versus depth graph. For all the experiments, it was clearly seen that the rate of scour development is higher for eccentric piers due to the combined effect of the wake vortex of the upstream pier and the horseshoe vortex of the downstream pier generally known as the interference effect. The time-dependent scour depth for experimental run no 1 and 24 has shown in Figs 6.26 and 6.27.

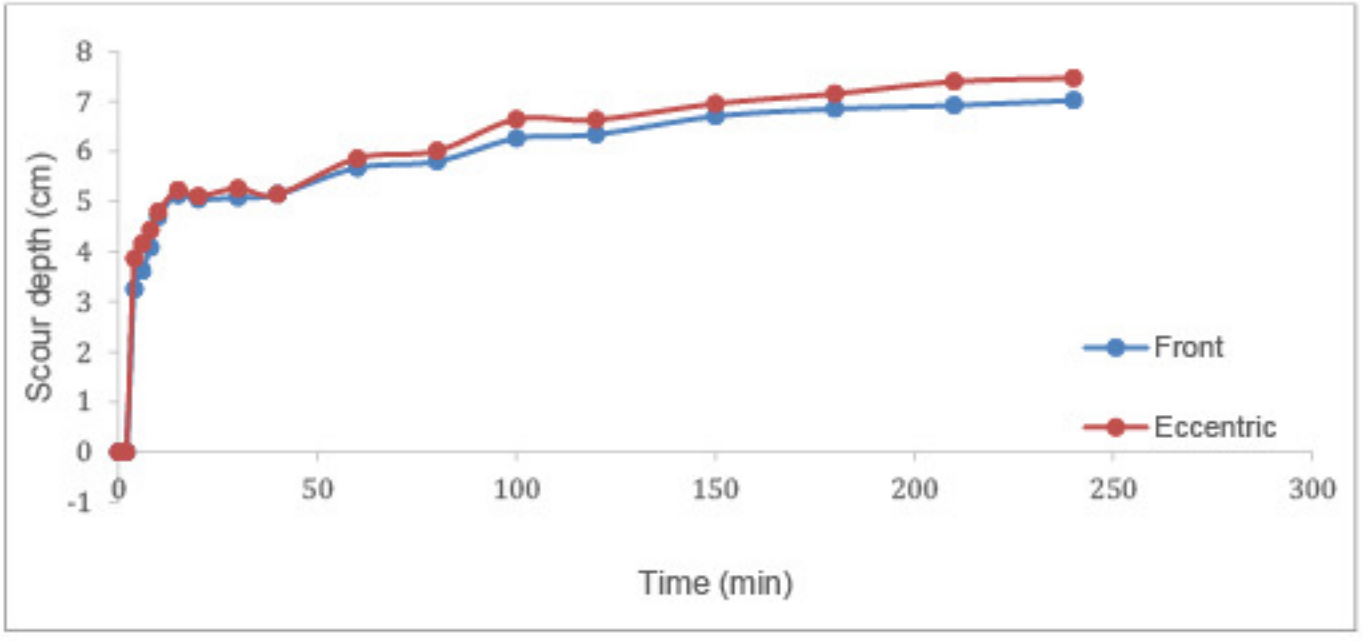



**Fig. 6.26** Temporal evolution of scour during experiment -1

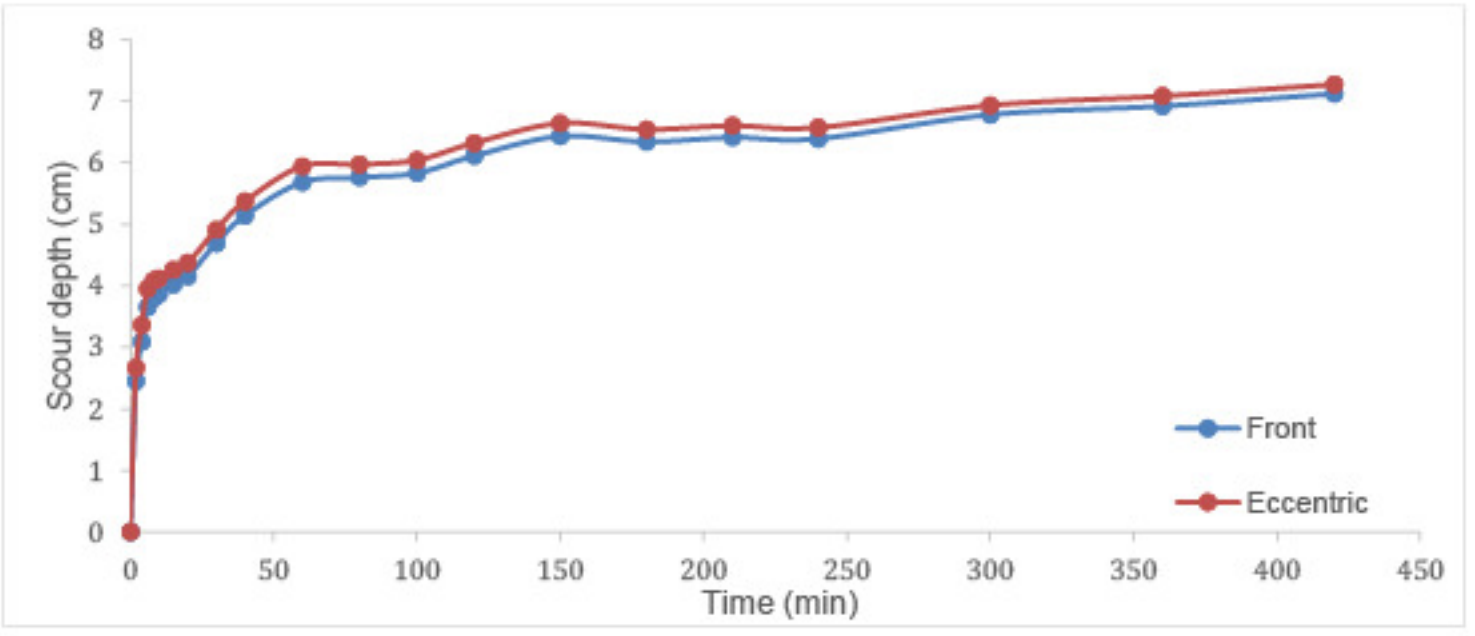



**Fig. 6.27** Temporal evolution of scour during experiment -24

### 6.1.28 Comparison of surface area with eccentricity

During the experimental run for the first six experiments, inflow depth varied from 12.6 to 15.75cm. And after completing the procedure, from the experimental data, the plane surface area ($a_{ps}$) and surface area of scour ($a_{ss}$) for each eccentricity was calculated with the help of Surfer software. From Fig. 6.28, we can observe that the plane surface area is found to be the highest for the eccentricity $e$=3.5$b$ and the lowest for the eccentricity $e$=2$b$ for both cases.

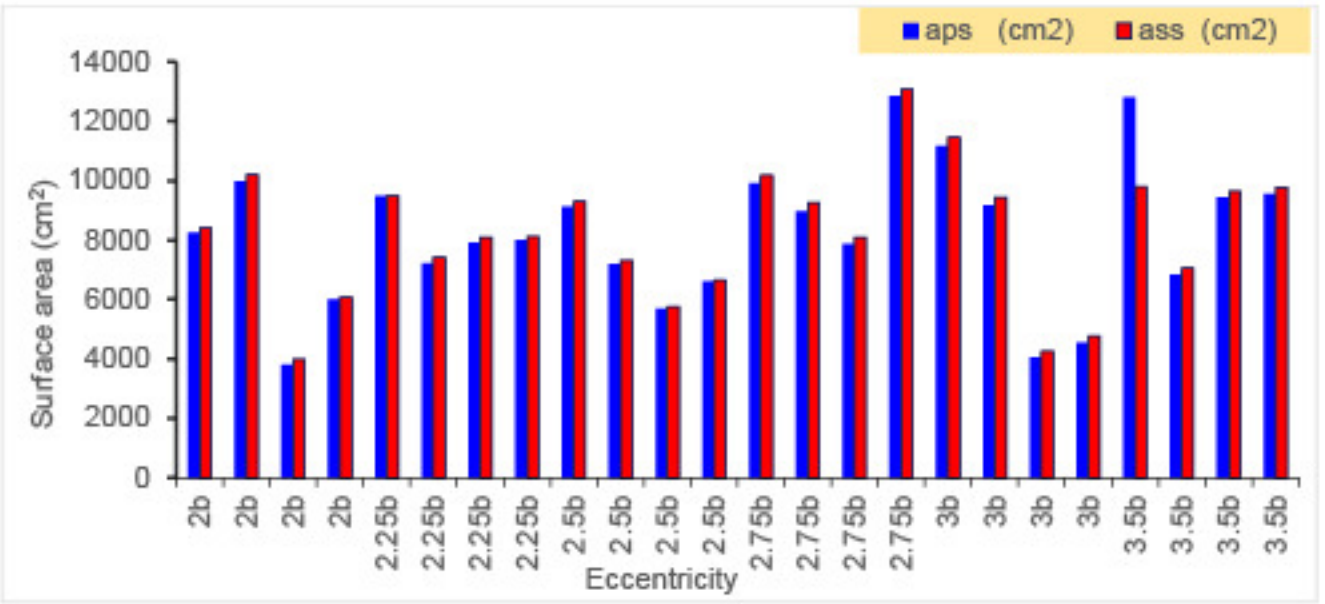



**Fig. 6.28** Variation of plane surface area ($a_{ps}$) and surface area of scour ($a_{ss}$) with varying eccentricity.

### 6.1.29 Comparison of volume with eccentricity

During the experimental run for all the experiments inflow depth was varying from 12.6 to 15.75 cm. After completing the procedure from the experimental data volume of scour ($v_s$) for each eccentricity was calculated with the help of surfer software. From Fig. 6.29, we can see that the volume of scour ($v_s$) is found to be highest for eccentricity $e$=3$b$ and lowest for eccentricity $e$=2.5$b$.

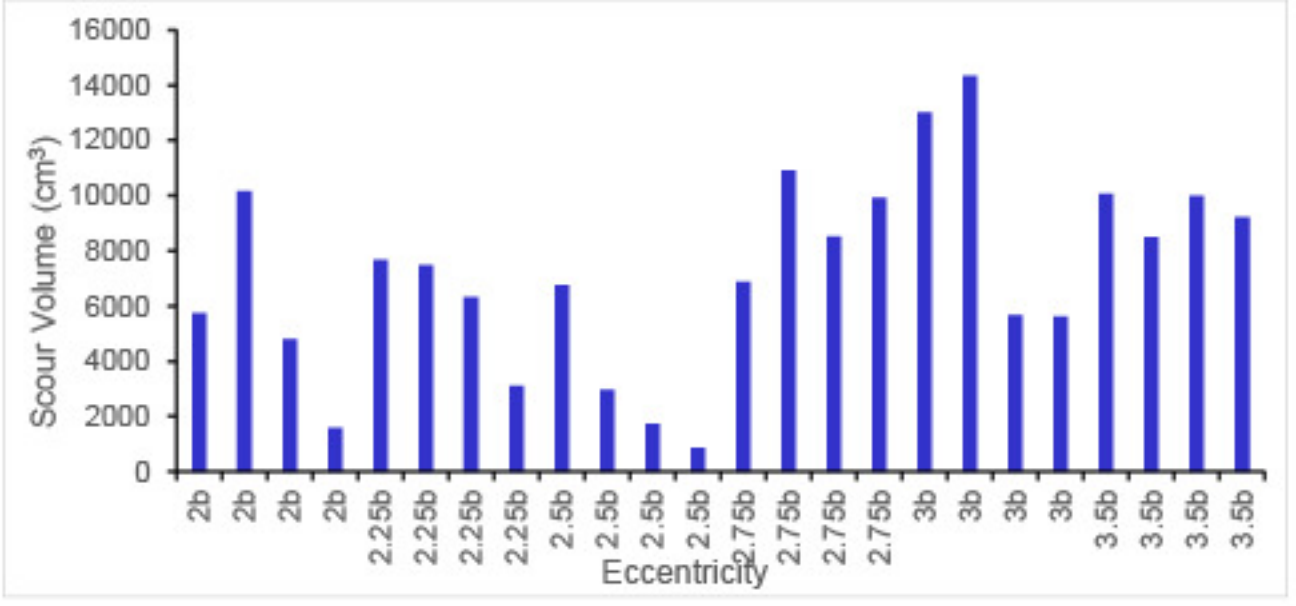



**Fig. 6.29** Change of scour volume at different eccentricities

### 6.1.30 Comparison of width with eccentricity

During the experimental run for all the experiments. After completing the procedure, from the experimental data, contour diagrams for each eccentricity were generated with the help of Surfer software. After getting all the contour diagrams with the help of surfer tools the width of scour ($w_s$) for each eccentricity was calculated. From Fig. 6.30, we can observe that the width of scour ($w_s$) was found to be highest for eccentricity $e$=3.5$b$ and lowest for eccentricity $e$=2.5$b$.

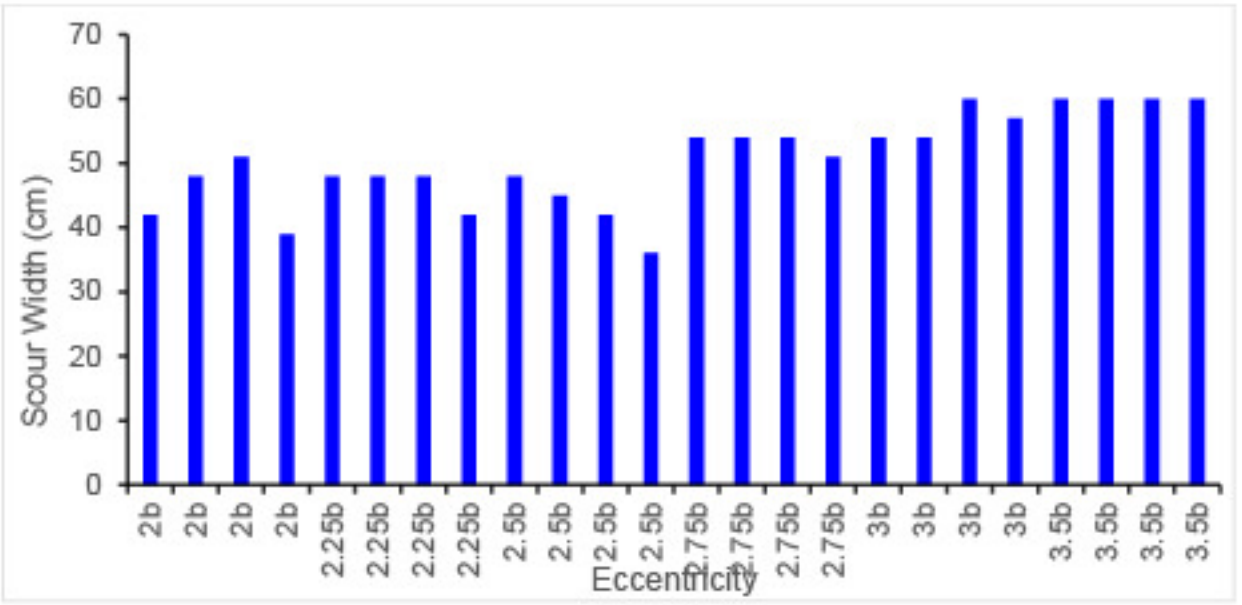



**Fig. 6.30** Change of scour width at different eccentricities.

### 6.1.31 Comparison of length with eccentricity

During the experimental run for all the experiments. After completing the procedure, from the experimental data, contour diagrams for each eccentricity were generated with the help of Surfer software. After getting all the contour diagrams with the help of Surfer tools the length of scour ($l_s$) for each eccentricity was calculated. From Fig.6.31, we can see that the length of scour ($l_s$) was found to be highest for eccentricity $e$=3.5$b$ &2.75$b$ and lowest for eccentricity $e$=2.5$b$.

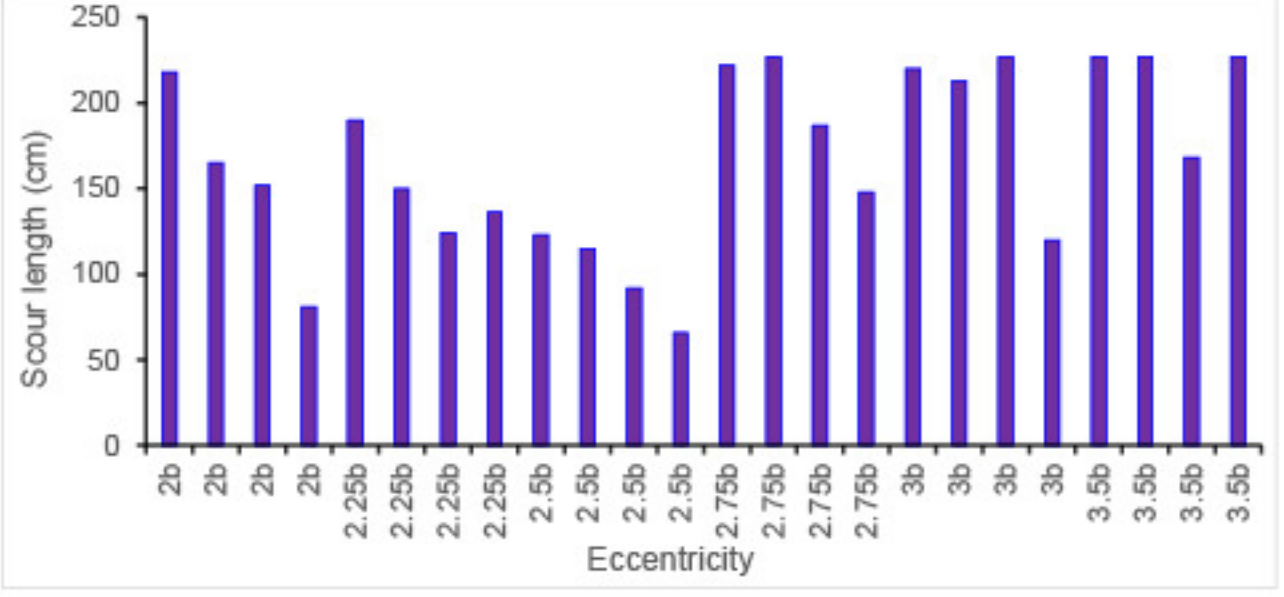



**Fig. 6.31** Measured scour length at different eccentricities

# Chapter 7

## 7.1 Conclusions

Local scour around eccentric circular piers in alluvial channels is a difficult challenge. Attempts to model it computationally have had limited success. As a result, physical modelling remains the most reliable approach of calculating local scour depth. In this study, an experimental analysis is performed for circular piers positioned at varying eccentricities to observe the interference of piers with one another. The study is conducted to evaluate the parametric fluctuation of scour depth throughout time. Additionally, the parametric variation of the maximum scour depth is investigated. To examine the aforementioned variation, two piers were placed with a constant longitudinal spacing of 5.185 of pier diameter ($b$) c/c. The front pier remained stationary. Another pier is positioned at a different eccentric ($e$) distance ($2b$, $2.25b$, $2.5b$, $2.75b$, $3b$, $3.5b$ c/c). The investigation is carried out in clear water condition. The experiments were carried out at different depth of flow (12.6cm, 13.65cm, 14.7cm, 15.75cm). At various depths, the flow response of the sand bed was examined. We also observed the temporal scour w.r.t time. We concluded that depth and length of scour increased as depth of flow decreased and width of the scour increased as the eccentricity of piers increased. The following important findings are noted from the present study.

- The front pier has a maximum scour depth of 7.54 cm at $e = 3.5b$ for the approaching flow depth of 12.6 cm, and a minimum scour depth of 2.22 cm at $e = 2.5b$ for the approaching flow level of 15.75cm.
- The eccentric rear pier has a maximum scour depth of 7.71 cm at $e = 2.75b$ for the flow depth of 12.6 cm, and a minimum scour depth of 2.39 at $e = 2.5b$ for the approaching flow depth of 15.75 cm.
- The greatest scour width is 60 cm for $e = 3.5b$ when approaching a flow depth of 15.75 cm, while the minimum scour width is 30.2 cm for $e = 2b$ when approaching a flow depth of 15.75 cm.
- The maximum scour length for $e = 3.5b$ is 227 cm for an approaching flow depth of 12.6 cm, 13.65 cm and 15.75 cm whereas the lowest scour length for $e = 2.5b$ is 66 cm for an approaching flow depth of 15.75 cm.
- For $e = 3b$, the maximum plane surface area and surface area are 11138.815cm$^2$ and 11447.88 cm$^2$, respectively, for an approaching flow depth of 12.6 cm, while the minimum plane surface area and surface area are 3800.94cm$^2$ and 3973 cm$^2$, respectively, for an approaching flow depth of 13.65 cm.
- The greatest volume of scour is 143278.87cm$^3$ for $e = 3b$ when approaching a flow depth of 12.6 cm, and the minimum volume of scour is 862.73cm$^3$ when approaching a flow depth of 15.75 cm.

Maximum scour occurrences, as described by various scour features, shed light on the ability of controlling sediment migration to channel banks in real-world circumstances. Adopting criteria associated with minimal scour incidence, on the other hand, becomes crucial for designing bridge piers that are both cost effective and safe. However, one limitation of this study is that it was carried out on a small scale in a laboratory. As a result, the findings may not accurately reflect real-world situations.

## 7.2 Future scopes of the study

In the present study, we conducted an analysis of scour depth data while maintaining a varying inflow depth and varying eccentricity. Exploring the impact of longitudinal inline spacing in conjunction with eccentricity warrants attention, as this parameter can significantly influence scour dynamics. Moreover, it is important to consider that bridge piers may be constructed on soil types other than cohesion-less soil. To gain valuable insights, into performance and the temporal evolution of scour in cohesive soil conditions, a comprehensive analysis should be conducted. Furthermore, as the spacing between piers increases, the unprotected region between them is prone to erosion, resulting in more pronounced scour holes around the rear piers.

## REFERENCES


Abed, L., and Gasser, M. M., (1993). Model study of local scour downstream bridge piers. *Proceedings National Conf. on Hydraulic Engineering*, San Francisco, pp. 1738–1743.

Ahmed, F., and Rajaratnam, N., (1998). Flow around bridge piers. *Journal of Hydraulic Engineering*, Vol. 124, Issue 3, pp. 288-300.

Ashtiani, B. A., and Kordkandi, A. A., (2012). Flow field side-by-side piers with and scour without hole. *European Journal of Mechanics B/Fluilds*, Vol. 36, pp.152-166.

Barbhuiya, A.K., Dey, S., (2004). Measurement of turbulent flow field at a vertical semi-circular cylinder attached to the sidewall of a rectangular channel Flow *Measurement and Instrumentation*, Vol. 15, Issue 2, pp. 87-96.

Barbhuiya, A.K., and Dey, S., (2004). Local scour at abutments: a review, Sadhana. *Proc. Indian Acad. Sci.*, 29(Oct.), pp. 449-476.

Barman, G. (2023), Scour Geometry Evaluation around Eccentric Pier in Clear Water Condition. ME Thesis. School of Water Resources Engineering, Jadavpur University.

Breusers, H. N. C., Nicollet, G., and Shen, H. W., (1977). Local scour around cylindrical piers. *Journal of Hydraulic Research*, Vol. 15, Issue 3, pp. 211-252.

Breusers, H.N.C., and Raudkivi, A.J., (1991). *Scouring*. IAHR hydraulic structures design manual, Rotterdam, The Netherlands, 2.

Cheremisinoff, N. P., and Cheremisinoff, P. N., (1987). *Flow Measurement for Engineers and Scientists* (Vol. 32). CRC Press.

Chiew, Y. M., and Lim, F. H., (2001). Parametric study of riprap failure around bridge piers. *Journal of hydraulic research*, Vol. 39, Issue 1, pp. 61-72.

Dargahi, B., (1990). Controlling Mechanism of local scouring. *Journal of Hydraulic Engineering*, Vol. 116, Issue 10, pp. 1197-1214.

Das, R., Das, S., Jaman, H., and Mazumdar, A., (2019). Impact of Upstream Bridge Pier on the Scouring Around Adjacent Downstream Bridge Pier. *Arabian Journal for Science and Engineering*, 44(5), pp. 4359–4372.

Das, S., and Mazumdar, A., (2015). Turbulence flow field around two eccentric circular piers in scour hole. *International Journal of River Basin Management*, Vol. 13, Issue 3, pp. 343-361.

Das, S., Das, R., and Mazumdar, A. (2016). Comparison of local scour characteristics around two eccentric piers of different shapes. *Arabian Journal for Science and Engineering*, Vol. 41, pp. 1199-1213.

Das, S., Das, R., and Mazumdar, A., (2013). Comparison of characteristics of horseshoe vortex at circular and square piers. *Research Journal of Applied Sciences, Engineering and Technology*, Vol. 5, Issue 17, pp. 4373-4387.

Das, S., Das, R., and Mazumdar, A., (2015, June). Velocity profile measurement technique for scour using ADV. In *Proceedings of the 2015 International Conference on Testing and Measurement: Techniques and Applications, TMTA*, pp. 249-252.

Das, S., Ghosh, S., and Mazumdar, A., (2014*a*). Kinematics of Horseshoe Vortex in a Scour Hole around Two Eccentric Triangular Piers. *International Journal of Fluid Mechanics Research*, Vol. 41, Issue 4, pp. 296-317.

Dey, S., (1999). Time-variation of scour in the vicinity of circular piers. *Proceedings of the Institution of Civil Engineers-Water Maritime and Energy*, Vol. 136, Issue 2, pp. 67-75.

Dey, S., (2003). Incipient Motion of Bivalve Shells on Sand Beds. *Journal of Engineering Mechanics*, Vol. 129, Issue 2, pp. 232-240.

Dey, S., and Barbhuiya, A.K., (2005). Turbulent flow field in a scour hole at a semicircular abutment. *Canadian Journal of Civil Engineering*, Vol. 32, Issue 1, pp. 213-232.

Dey, S., and Raikar, R. V., (2007). Characteristics of horseshoe vortex in developing scour holes at piers. *Journal of Hydraulic Engineering*, Vol. 133, Issue 4, pp. 399-413.

Dey, S., Bose, S. K., and Sastry, G.L.N., (1995). Clear Water Scour at Circular Piers. *Journal of Hydraulic Engineering*, Vol. 121, Issue 12, pp. 869-876.

Graf, W.H., and Istiarto, I., (2002). Flow pattern in the scour hole around a cylinder. *Journal of Hydraulic Research*, Vol. 40, Issue 1, pp. 13-20.

Hoffmans, G. J., and Verheij, H. J., (1997). *Scour manual*. Routledge.

Jain, S.C., and Fischer, E.E., (1979). Scour around bridge piers at high Froude numbers. *Report. No. FHWA- RD-79-104, Federal Highway Administration. Washington D.C.*

Jaman, H, Das, S., Kuila, A., and Mazumdar, A., (2017*a*). Hydrodynamic flow patterns around three inline eccentrically arranged circular piers. *Arabian Journal for Science and Engineering*, Vol. 42, Issue 9, pp. 3973-3990.

Jaman, H., Das, S., Das, R., and Mazumdar, A., (2017*b*). Hydrodynamics of flow obstructed by inline and eccentrically-arranged circular piers on a horizontal bed surface. *Journal of The Institution of Engineers (India): Series A*, Vol. 98(1-2), pp. 77-83.

*Journal of Hydraulic Engineering*, Vol. 109, Issue 3, pp. 338-350.

Khaple, S., Hanmaiahgari, P. R., Gaudio, R., and Dey, S., (2017). Interference of an upstream pier on local scour at downstream piers. *Acta Geophysica*,Vol. 65, Issue 1, pp. 29-46.

Kothyari U. C. and Ranga Raju K. G. (2001) Scour around spur dikes and bridge abutments, *Journal of Hydraulic Research*, 39:4, pp. 367-374,

Kothyari, U.C., Raju, K.G.R. and Garde, R.J. (1992*a*). Live-bed scour around cylindrical bridge piers. *Journal of Hydraulic Research*, Vol. 30, Issue 5, pp. 701-715.

Kothyari, U.C., Raju, K.G.R. and Garde, R.J. (1992*b*). Temporal variation of scour around circular bridge piers. *Journal of Hydraulic Engineering*, 118(8), pp.1091-1106.

Kuila, A., Jaman, H., Das, S., & Mazumdar, A. (2020). Computing equilibrium flow structures at three interfering square piers causing relative scour. *Topics in intelligent computing and industry design (ICID)*, Vol. 1, pp. 20-24.

Laursen, E.M. and Toch, A. (1956). Scour around bridge piers and abutments.

Link, O., & Zanke, U. (2004). On the time-dependent scour-hole volume evolution at a circular pier in uniform coarse sand. In *Proceedings 2nd International Conference on Scour and Erosion (ICSE-2). November 14.–17., 2004, Singapore.*

Liu, H. K., Chang, F. M. and Skinner, M. M. (1961). Effect of bridge constriction on scour and backwater. *Report No. CER60HKL22, Civil Engineering Section, Colorado State Univ. Fort Collins, Colo.*

Malik, R. A. H. U. L., and Setia, B. A. L. D. E. V. (2014). Experimental study on behaviour of closely placed bridge pier models. In *Proceedings of the National Conference in Department of Civil Engineering, National Institute of Technology Kurukshetra, Kurukshetra, India*.

Malik, R., and Setia, B. (2020). Interference between pier models and its effects on scour depth. *SN Applied Sciences*, Vol. 2, pp. 1-12.

Malik, R., and Setia, B. (2021). Local scour around closely placed bridge piers. *ISH Journal of Hydraulic Engineering*, Vol. 27, Issue 4, pp. 396-403.

Marsh, N.K., Western, A.W. and Grayson, R.B. (2004). Comparison of methods for predicting incipient motion for sand beds. *Journal of Hydraulic Engineering*, Vol. 130, Isssue 7, pp. 616-621.

Melville, B. and Sutherland, A. (1988). Design method of time Dependent Local Scour at Circular Bridge Pier. *Journal of Hydraulic Engineering,* Vol. 114, Issue 10, pp. 1210-1226.

Melville, B.W. (1975). *Local scour at bridge sites*. Rep. No. 117, School of Engineering, University of Auckland, Auckland, New Zealand.

Melville, B.W. (1975). *Local scour at bridge sites*. Rep. No. 117, School of Engineering, University of Auckland, Auckland, New Zealand.

Melville, B.W. (1992). Local scour at bridge abutments. *Journal of Hydraulic Engineering,* Vol. 118, Issue 4, pp. 615–631.

Melville, B.W. and Chiew, Y.M. (1999). Time scale for local scour at bridge piers. *Journal Hydraulic Engineering,* Vol. 125, Issue 1, pp. 59-65.

Melville, B.W. and Chiew, Y.M. (1999). Time scale for local scour at bridge piers. *Journal Hydraulic Engineering,* Vol. 125, Issue 1, pp. 59-65.

Melville, B.W. and Coleman, S.E. (2000). Bridge scour. *Water Resources Publications*, Fort Collins, Colorado, USA.

Mia, M. F., and Nago, H. (2003). Design method of time-dependent local scour at circular bridge pier. *Journal of Hydraulic Engineering*, Vol. 129, Issue 6, pp. 420-427.

Muzzammil, M. and Gangadhariah, T. (2003). The mean characteristics of horseshoe vortex at a cylindrical pier. *Journal of Hydraulic Research*, Vol. 41, Issue 3, pp. 285-297.

Nandi, B. and Das, S. (2023). Identify most promising temporal scour depth formula for circular piers proposed over last six decades, *Ocean Engineering*, Vol. 286, Issue 2, Art. No. 115639.

Oliveto, G. and Hager, W.H. (2002). Temporal evolution of clear-water pier and abutment scour. *Journal of Hydraulic Engineering*, Vol. 128, Issue 9, pp. 811-820.

Raeisi, N., and Ghomeshi, M. (2020). Effect of bridge pier diameter on maximum depth of scour impacts on the environment. *SN Applied Sciences*, Vol. 2, pp. 1-12.

Raudkivi, A. J., & Ettema, R. (1977). Effect of sediment gradation on clear water scour. *Journal of the Hydraulics Division*, Vol. 103, Issue 10, pp. 1209-1213.

Raudkivi, A.J. (1986). Functional trends of scour at bridge piers. *Journal of Hydraulic Engineering*, Vol. 112, Issue 1, pp. 1-13.

Raudkivi, A.J. and Ettema, R. (1983). Clear water scour at cylindrical piers.

Richardson, J.R. and Richardson, E.V. (1994). Practical method for scour prediction at bridge piers. *Proceedings, ASCE National Conference on Hydraulic Engineering*, Buffalo, N.Y. pp. 1–5.

Shen, H.W., Schneider, V R. and Karaki, S. (1969). Local scour around bridge piers. *Journal of Hydraulic Division,* 95(6), HY6, pp. 1919–1940.

Shields, A. (1936). Application of similarity principles and turbulence research to bed-load movement. Mitteilunger der Preussischen Versuchsanstaltfür Wasserbau und Schiffbau, Berlin, Germany, Vol. 26, pp. 5-24.

Tseng, M. H., Yen, C. L., & Song, C. C. (2000). Computation of three-dimensional flow around square and circular piers. *International journal for numerical methods in fluids*, Vol. 34, Issue 3, pp. 207-227.

Van Rijn, L. C. (1984). Sediment transport, part I: bed load transport. *Journal of hydraulic engineering*, Vol. 110, Issue 10, pp. 1431-1456.

Vol. 4. Iowa Highway Research Board. Ames, Iowa.

Wang, H., Tang, H., Liu, Q., and Wang, Y. (2016). Local scouring around twin bridge piers in open-channel flows. Journal of Hydraulic Engineering, Vol. 142, Issue 9, Art. No. 06016008.

Yang, Y., Qi, M., Wang, X., & Li, J. (2020). Experimental study of scour around pile groups in steady flows. *Ocean Engineering*, Vol. 195, Art. No. 106651.

Yilmaz, M., Yanmaz, A. M., and Koken, M. (2017). Clear-water scour evolution at dual bridge piers. *Canadian Journal of Civil Engineering*, Vol. 44, Issue 4, pp. 298-307.

Zhou, K., Duan, J. G., and Bombardelli, F. A. (2020). Experimental and theoretical study of local scour around three-pier group. *Journal of Hydraulic Engineering*, Vol. 146, Issue 10, Art. No. 04020069.